UNIVERSIDAD DE GRANADA

ANALYSIS OF NIGHTTIME STREAMER CORONA DISCHARGES IN STORM CLOUDS WITH ASIM DATA

Sergio Soler
Department of Solar System
Instituto de Astrofísica de Andalucía

Thesis Supervisors
Dr. Francisco José Gordillo Vázquez
Dr. Francisco Javier Pérez Invernón

A thesis submitted for the Physics and Space Science Doctorate Program

January 2023

Contents

List of Figures

List of Tables

List of Acronyms

AGRI Advanced Geosynchronous Radiation Imager

ASIM Atmospheric Space Interaction Monitor

CAPE Convective Available Potential Energy

CC Cloud to Cloud

CEPA Columbus External Payloads Adaptor

CG Cloud to Ground

CHU Camera Head Unit

CID Compact Intracloud Discharges

CLWC Cloud Liquid Water Content

CR Cosmic Rays

CTH Cloud Top Height

DE Detection Efficiency

DPU Data Processing Unit

ELF Extreme Low Frequency

ESA European Space Agency

EMP ElectroMagnetic Pulses

FHT First Hitting Time

FNS First Negative System

FORTE Fast On-orbit Recording of Transient Events

FOV Field Of View

FPS First Positive System

GLD360 Global Lightning Detection 360

HF High Frequency

IC Intra Cloud

ISUAL Imager of Sprites / Upper Atmospheric Lightning

ISS International Space Station

LASA Los Alamos Spheric waveform Array

LBH Lyman Birge Hopfield

LF Low Frequency

LIS Lightning Imager Sensor

MMIA Modular Multispectral Imaging Array

MXGS Modular X-ray and Gamma-ray Sensor

NBE Narrow Bipolar Events

OTD Optical Transient Detector

PDD Photo Diode Detector

PPD Peak Power Density

RPB Radiation Belt Particles

SAA South Atlantic Anomaly

SM Supplementary Material

SPS Second Positive System

STEPS Severe Thunderstorm Electification and Precipitation Study

TGF Terrestrial Gamma-ray Flash

TIPP TransIonospheric Pulse Pairs

TLE Transient Luminous Events

TP Total Precipitation

TRMM Tropical Rainfall Measuring Mission

VHF Very High Frequency

VLF Very Low Frequency

Resumen

El objetivo de esta tesis doctoral es estudiar de forma exhaustiva las descargas eléctricas de tipo corona que tienen lugar en las nubes de tormenta. Las descargas corona se caracterizan, entre otras cosas, por emitir luz en el rango ultravioleta cercano y azul (280 - 450 nm). Es por esto por lo que se las ha llamado Blue LUminous Events (BLUEs). Esta tesis presenta la primera climatología nocturna de descargas de corona en las nubes de tormenta combinando dos años de datos de BLUEs recogidos por el instrumento MMIA de ASIM a bordo de la ISS (Neubert et al., 2019).

La tesis se centra en, por un lado, investigar la física de los BLUEs, esto es, en descifrar su naturaleza y en determinar cuáles son los mecanismos que los producen. Por otra lado, se aborda el análisis detallado de la distribución geográfica y estacional de los BLUEs a partir de dos años de datos obtenidos por el Modular Multispectral Imaging Array (MMIA) del instrumento Atmosphere Space Interaction Monitor (ASIM) de la Agencia Espacial Europea (ESA) que fue lanzado al espacio el 18 de abril de 2018 y que está operativo en la Estación Espacial Internacional (ISS) desde entonces. MMIA está formado por tres fotómetros rápidos (100 kHz) y dos cámaras. Los fotómetros disponen de filtros interferenciales centrados en las longitudes de onda 337.0 nm (con una anchura de banda de 4 nm), 777.4 nm (con una anchura de banda de 5 nm) y un filtro ancho entre 180 nm y 230 nm. Las dos cámaras disponibles usan filtros centrados en 337.0 nm y 777.4 nm con las mismas características que los filtros de los fotómetros.

La tesis doctoral se presenta como una colección de tres artículos científicos en los que soy primer autor. Estos artículos sobre electricidad atmosférica han sido publicados en revistas de alto impacto en el campo de las ciencias atmosféricas. Los artículos vienen precedidos por un índice de la tesis, un resumen (en español e inglés), una introducción, la motivación de los estudios realizados, una breve descripción de la metodología que se ha seguido y una descripción concisa de los BLUEs.

En mi primer artículo (publicado en *Journal of Geophysical Research - Atmospheres*, 2020, y destacado por su editor) se describe la estructura de los BLUEs apoyándose en las observaciones de una tormenta registrada por ASIM el 14 de Mayo de 2019 sobre Indonesia. Los eventos fueron observados con el fotómetro 337.0 nm, sin actividad concurrente, o despreciable en el fotómetro centrado en la banda 777.4 nm (emisiones típicas de rayos). A través de mediciones de radio efectuadas desde el suelo, se concluyó que 7

de los 10 casos analizados correspondían a eventos bipolares estrechos positivos o *positive narrow bipolar events* (NBE) en inglés. Los NBEs se caracterizan por ser pulsos muy fuertes de radiofrecuencia (RF) con tres rasgos importantes: (1) su muy corta duración (apenas 20 microsegundos), (2) un aspecto bipolar (muy rápida subida y bajada de dos pulsos de radio de polaridad positiva y negativa o viceversa) de la forma de onda en el rango de frecuencias VLF / LF (10 - 400 kHz) y (3) por venir habitualmente seguidos de potentísimos estallidos de radiación VHF / HF (3 - 300 MHz).

Los NBE detectados en el rango VLF / LF son por lo general diez veces más intensos que las emisiones de radio en el rango de alta frecuencia (HF) procedentes de rayos normales intranube o entre nubes. Además, observaciones recientes (2016 y 2017) parecen sugerir que los NBEs son el resultado de procesos muy rápidos de ruptura eléctrica del aire típicos de descargas eléctricas frías, esto es, aquellas que no calientan el aire circundante (al contrario que los rayos normales) y en las que la temperatura de los electrones ambientales alcanzan valores muy elevados de hasta 80000 °C (unos 7 eV [electrón voltios]). El hecho de que los electrones tengan una masa muy pequeña (2000 veces más ligeros que el átomo más liviano) impide que, aún siendo muy energéticos, puedan calentar el aire circundante.

En este primer trabajo se desarrolló un nuevo y novedoso método para determinar la altura de los BLUEs en las nubes de tormenta a partir del análisis de sus señales ópticas. En particular, el método se basa en ajustar las curvas de luz captadas por el fotómetro centrado en 337.0 nm de MMIA a un modelo de difusión de luz en las nubes de tormenta. La altura obtenida concuerda bien con medidas realizadas con métodos basados en radio detección.

La altitud a la que ocurren estos NBEs se sitúa aproximadamente entre 8.5 y 14 km. Las observaciones indican que los flashes azules con un solo pulso son originados por streamers (dardos de plasma de aire con fuerte ionización en la cabeza) que, como se ha mencionado, no calientan el aire, esto es, son descargas frías, la luz emitida por streamers es pues la manifestación óptica de dichos NBEs. Los hallazgos que se discuten en el primer trabajo nos llevaron a concluir que los NBEs positivos son descargas corona formadas por cientos de millones de streamers positivos (la cabeza del streamer transporta carga eléctrica positiva) que se forman en las nubes de tormenta y que los BLUEs son la manisfestación óptica de dichos NBEs.

Mi segundo artículo (publicado en *Geophysical Research Letters*, 2021), se centra en el análisis a nivel global de los pulsos azules observados en las nubes de tormenta, deteniéndose en estudiar la relación de los BLUEs con los rayos, tanto anual como estacionalmente. Para ello se ha desarrollado y utilizado un novedoso algoritmo para poder filtrar la información en bruto de MMIA, y obtener sistemáticamente sólo la actividad

de BLUEs excluyendo el resto de interacciones eléctricas en las nubes de tormenta. El resultado de este completo trabajo es la primera, y hasta ahora la única, climatología nocturna de BLUEs (coronas en nubes de tormenta) obtenida a partir de datos del instrumento MMIA de ASIM. En nuestra investigación se concluyó que, aproximadamente, tienen lugar unos 11 BLUEs a nivel global cada segundo en la media noche local, y que el promedio de BLUEs en tierra / mar es de 7 a 4. Geográficamente, el pico de la distribución de BLUEs está localizado en una región al noroeste de Colombia. En esta distribución se muestran tres zonas principales de actividad eléctrica atmosférica: América, Europa/África, y Asia/Australia. También se ha encontrado una zona de actividad eléctrica más débil en el Pacífico.

Mi tercer trabajo (publicado en *Journal of Geophysical Research - Atmospheres*, 2022) profundiza en los resultados del segundo, y se centra en distinguir distintos tipos de pulsos azules en función de la bondad de su ajuste con el "first hitting model" ó FHM (modelo de difusión de luz en las nubes) y en obtener sus principales características tales como densidad de potencia óptica (μW m^{-2}) del máximo del pulso 337.0 nm, tiempo de subida del máximo, duración total, brillo, etc, con base al ajuste y a los datos en bruto. Además, también encontramos dos tipos de distribuciones globales de BLUEs, dependiendo de si se aplica (o no) un criterio extra al algoritmo del anterior trabajo en la anomalía magnética del Atlantico Sur (SAA). Este criterio adicional se incluye debido que se observó una clara sobredetección de rayos cósmicos con ASIM en la zona de la SAA. El criterio extra pretende limitar el número de rayos cósmicos detectados poniendo un límite en la duración de los eventos detectados en la SAA. Se estima que la cifra real de BLUEs se hallará entre las dos distribuciones encontradas en este último trabajo. El análisis de las características de los BLUEs nos indica que alrededor del 10% de los eventos son claramente BLUEs con un máximo claro. La mayoría de ellos tiene una densidad de potencia óptica por unidad de superficie de pico por debajo de 25 $\mu W/m^2$, ocurren a una distancia de hasta 4 km por debajo del límite superior de la nube y están formados por cientos de millones de streamers (hasta 3×10^9).

Abstract

The main objective of this doctoral thesis is to exhaustively study the corona-type electrical discharges that take place in storm clouds. Corona discharges are characterized, among other things, by transient optical emissions in the near ultraviolet and visible blue range (280 - 450 nm). This is why they have been called Blue LUminous Events (BLUEs). This thesis presents the first worldwide nighttime climatology of corona discharges in storm clouds by combining two years of BLUEs data recorded by MMIA instrument of ASIM on-board the ISS (Neubert et al., 2019).

This doctoral thesis focuses on investigating the physics of BLUEs, with the aim of understanding their nature and determining the mechanisms that produce them. Additionally, the thesis addresses the detailed analysis of the geographic and seasonal distribution of BLUEs is addressed from two years of unique data obtained by the Modular Multispectral Imaging Array (MMIA) of the European Space Agency's (ESA) Atmosphere Space Interaction Monitor (ASIM) instrument that was launched into space on April 18, 2018 and has been operational at the International Space Station (ISS) since then. MMIA has three fast photometers (100 kHz) and two cameras. The photometers have interferential filters centered on the wavelengths 337.0 nm (with a width of 4 nm), 777.4 nm (with a width of 5 nm) and a wide filter between 180 nm and 230 nm. The two available cameras use filters centered at 337.0 nm and 777.4 nm with the same characteristics as the light meter filters.

The doctoral thesis is presented as a collection of three scientific articles in which I am the first author. These articles have been published in high-impact journals in the field of atmospheric sciences (atmospheric electricity). The articles are preceded by a thesis index, a summary (in Spanish and English), an introduction, the motivation of the studies carried out, a brief description of the methodology that has been followed and a concise presentation of the BLUEs.

In my first article (published in *Journal of Geophysical Research - Atmospheres*, 2020, and highlighted by the editor) the structure of the BLUEs is described based on the observations of a storm recorded by ASIM on May 14, 2019 over Indonesia. The events were observed using the 337.0 nm photometer, during periods of little or no concurrent activity in the photometer centered on the 777.4 nm band (which is typical for lightning optical emissions). Through radio measurements made from the ground, it was concluded

that 7 of the 10 cases analyzed corresponded to positive narrow bipolar events (NBE). NBEs are characterized by being very strong radio frequency (RF) pulses with three important features: (1) their very short duration (about 20 microseconds), (2) a bipolar appearance (very fast rise and fall of two radio pulses of positive and negative polarity or vice versa) of the waveform in the VLF / LF frequency range (10 - 400 kHz) and (3) followed by extremely powerful bursts of radiation. on VHF / HF (3 - 300 MHz).

NBEs, when detected in the VLF/LF range, are typically ten times more intense than radio emissions in the high frequency (HF) range typically emitted by normal intracloud and/or intercloud lightning.. In addition, recent observations (2016 and 2017) suggest that NBEs are the result of very fast processes of electrical breakdown in air. Fast breakdown is associated to cold electrical discharges, that is, those that do not heat the surrounding air (unlike normal lightning) and in which the temperature of the ambient electrons reaches very high values of up to 80000 °C (about 7 eV) (electron volts). The fact that electrons have a small mass (2000 times lighter than the lightest atom) prevents them from heating the surrounding air.

In this first work, a new and innovative method was developed to determine the height of BLUEs in storm clouds from the analysis of their optical signals. In particular, the method is based on fitting the 337.0 nm light curves captured by the MMIA 337.0 nm photometer to a model of light diffusion in storm clouds. The height obtained agrees well with measurements carried out with methods based on ground-based radio detection.

The altitude at which these NBEs occur ranges between 8.5 km and 14 km. Observations indicate that single-pulse blue flashes are caused by streamers (air plasma darts with strong head ionization) which, as discussed above, do not heat the air (they are cold discharges). The findings discussed in the first paper led us to conclude that positive NBEs are corona discharges made up of hundreds of millions of positive streamers (the head of the streamer carries positive electrical charge) that form in thunderclouds and that the BLUEs are the optical manifestation of the NBEs.

My second article (published in *Geophysical Research Letters*, 2021), focuses on the global analysis of the blue pulses observed in storm clouds, focusing on studying the relationship of the BLUEs with lightning, both annually and seasonally. For this, a new algorithm has been developed and used to be able to filter the raw information from MMIA, and systematically obtain only the activity of BLUEs, excluding the rest of electrical interactions in storm clouds. The result of this comprehensive work is the first, and so far the only, nocturnal climatology of BLUEs (corona discharge activity in storm clouds) obtained from data from the ASIM MMIA instrument. Our research concluded that approximately 11 BLUEs occur globally every second at local midnight, and the average number of BLUEs on land/sea is 7 to 4. Geographically, the peak of

the distribution of BLUEs is located in a region in northwestern Colombia. Three main zones of atmospheric electrical activity are shown in this distribution: America, Europe / Africa, and Asia / Australia. A zone of weaker BLUE electrical activity has also been found in the Pacific.

My third paper (published in *Journal of Geophysical Research - Atmospheres*, 2022) delves into the results of the second, and focuses on distinguishing different types of blue pulses based on the goodness of their fit with the "first hitting model" or FHM (model of diffusion of light in storm clouds) and in extracting its main characteristics such as optical power density (μW m^{-2}) of the 337.0 nm pulse maximum, rise time of maximum, total duration, brightness, etc, based on the fit and raw data. In addition, we also found two types of global distributions of BLUEs, depending on whether an extra criteria is applied (or not) to the algorithm of the previous work (paper two) on the South Atlantic Magnetic Anomaly (SAA). This additional criteria is included because a clear oversensing of cosmic rays was observed with ASIM in the SAA region. The extra criteria aims to limit the number of cosmic rays detected by putting a limit on the duration of the events detected in the SAA. It is concluded that the real number of BLUEs would range between the two distributions found in this third work. The analysis of the characteristics of the BLUEs indicates that around 10% of the events are clearly BLUEs with a clear maximum. Most of them have a peak optical power density below 25 $\mu W/m^2$, occur up to 4 km below the upper cloud boundary and are made up of hundreds of millions of streamers (up to 3×10^9).

Acknowledgements

En primer lugar he de agredecer sinceramente a Paco la oportunidad de embarcarme en este proyecto y de ser mi director de tesis. Además de ser un buen investigador, me ha demostrado durante todos estos años que es también una buena persona, siempre está ahí cuando hay algún problema, disponible para ayudar, comentar los avances y proponer ideas.

También agradezco a Javier que haya sido mi codirector de tesis ayudándome mucho, sobre todo en los inicios cuando aún no sabía muy bien cómo funcionaban muchas cosas.

Quisiera agradecer también al CSIC, al Instituto de Astrofísica de Andalucía y a la Universidad de Granada la posibilidad de hacer la tesis trabajando en el centro con un contrato remunerado.

Finalmente, me acuerdo de mis años anteriores en Santander donde me formé inicialmente en la Universidad de Cantabria y el Instituto de Física de Cantabria dándome una sólida base científica para abordar esta tesis.

I would also like to acknowledge the collaboration with the ASIM team and the access to the MMIA data without which I could not have done all the analysis and papers that I publish in this thesis.

This thesis was supported by the Spanish Ministry of Science and Innovation, Ministerio de Ciencia e Innovación (AEI) under project ESP2017-86263-C4-4-R, PID2019-109269RB-C43 and the FEDER program. I acknowledge a PhD research contract through the project ESP2017-86263-C4-4-R and I also acknowledge financial support from the State Agency for Research of the Spanish MCIU through the "Center of Excellence Severo Ochoa" award for the Instituto de Astrofísica de Andalucía (SEV-2017-0709). ASIM is a mission of The European Space Agency (ESA). The project is funded by ESA and by national grants of Denmark, Norway and Spain.

Chapter 1

Introduction to electrical discharges

1.1 Brief historical perspective

Around 1756 Benjamin Franklin described the similarities between lightning and arc (so-called spark) discharges he created (Dwyer and Uman, 2014). Following Franklin's work, there was little advancement in the field of lightning science until the late 19th century. At that time, the relative accessibility of photography and spectroscopy led to an increase in research, as some scientists began to utilize these new techniques to study and record electrical discharges. The start of the modern era in lightning research can be dated to the days of the Nobel Prize winner C. T. R. during the 1920s in England. He applied remote, ground-based electric field measurements to study the electrical charge structure in thunderstorms and the charge flow inside lightning strokes. The following decades were more productive in lightning research because of the development of new techniques for the analysis of data using high-speed tape recording and direct 10 ns-scale digitization and storage analog electromagnetic signals (from the extremely low frequency (ELF) radio signals to optical and gamma radiation). Also the damage caused by lightning led the research in these field in order to keep safe critical structures such computers, spacecrafts or aircrafts.

1.2 Introduction to lightning

The most important mechanism for electric charge separation in thunderclouds is the collisions between graupel particles and ice crystals or other smaller hydrometeors. Graupel particles are created when supercooled liquid droplets join to ice crystals and then freeze (Cooray, 2003). The transfer of negative charge to graupel particles in collisions with smaller ice particles leads to gravitational separation of oppositely charged particles until the electric field is enough for dielectric breakdown. Depending on how electric charges are distributed in thunderclouds we can distinguish between three different types

of positive or negative polarity lightning: intracloud (IC), cloud-to-ground (CG) and cloud to cloud (CC).

Thunderstorms can occur worldwide and they are still difficult to predict. However, there are some parameters that can help us to predict their occurrence. The presence of water vapor in the atmosphere provides energy to thunderstorms from the released latent heat when water vapor change to its liquid and solid phases. Also, atmospheric instability generates vertical motion of air masses due to temperature, pressure and / or vapor concentration differences. Another important factor affecting the formation of thunderstorms is the vertical extent of cloud buoyancy, that is, the ability of thunderclouds to reach up to the local tropopause, that can reach up to 17 km in the tropical regions of the planet. Mixed-phase water microphysics is primordial to electric charge separation, with the mixed-phase region being located between 0° C and - 40°C isotherms (Cooray, 2003).

1.3 Spark development

Electric breakdown in a gas initiates with a leading (seed) electron creating an electron avalanche through electron ionization collisions with ambient atoms and molecules. The avalanche itself modifies the electric field in the vicinity of the avalanche's front so that, when the space charge electric field reaches a critical value, it becomes a streamer discharge. If the inter-electrode gap is sufficiently large, many streamers can originate from a common stem. Streamer currents generate heat and this raises the temperature of the streamer stem. When the temperature reaches a threshold value thermal ionization dominates in the stem and its electrical conductivity increases so that it transforms the collection of streamers into a leader discharge. Because of the good electrical conductivity of the leader channel, the electrode electric potential is transferred to the head of the leader. This induces a high electric field that makes streamers grow from the leader front. When the leader reaches the grounded electrode there is a current increase, and the voltage collapses, generating a spark (Cooray, 2003).

1.4 Electrical breakdown

Electrical breakdown is a self-sustaining discharge that produces a quick increase in the electrical conductivity, resulting in the collapse of the electric field (Dwyer and Uman, 2014). Electrical breakdown is an internal state of the system and it is invariant to external actions like ionizing radiation sources. Air normally breaks down at electric fields higher than $E_k = 3{\times}10^6$ V/m $\times$ N_{air}. When the air gap is non uniform it may not be necessary to exceed $3{\times}10^6$ V/m $\times$ N_{air} in all places, but only in one so that the process starts. When air breaks down, a hot channel is created where current flows. This

is necessary for kilometric scale discharges like lightning, because the quick attachment of free electrons in the air produces a sharp decrease of the electrical conductivity so that further current flow through long distances is difficult.

Lightning propagates by creating a hot leader channel. Leaders posses high electrical conductivity and can transfer electric charge between different parts of the cloud. When a leader reaches the ground, a large current flows, heating the channel and creating an extremely bright arc. Also, when the leader touches the ground it creates a short circuit between the cloud and the ground. Then, there appears a high current flow going upwards (typically tens of thousands of amperes) called return stroke, which is the brightest part of the flash.

1.5 Thunderstorm charge structure

One way to illustrate the charge structure in thunderclouds is the standard tripole model (Dwyer and Uman, 2014). This model contains a main middle level negative charge layer, a main positive charge layer and a small lower positive charge central region. The representative charge values are -40 C, $+40$ C, and $+3$ C, respectively.

The core of the main negative charge layer is located in a range of temperatures between -10° C and -25° C, regardless of the distance to the ground below the storm. In this region the clouds have ice and super-cooled water, which its collisions initiate the non-inductive charging mechanism (Takahashi, 1978). The altitude above sea level where these temperatures occur varies between 2 km and 8 km depending on the world region and season. The main positive charge layer is generally more diffuse than the main negative layer, and it is located above it, in a range between 8 km and 15 km in summer thunderstorms but in a lower range during winter thunderstorms. The small positive charge region is located below the main negative charge region, at the bottom of the cloud.

1.6 Transient Luminous Events (TLEs)

TLEs produce bursts of optical emissions from above thunderclouds in the stratosphere, mesosphere and lower ionosphere initiated by upward discharges (Blue Starters (Wescott et al., 1996; Lyons et al., 2003; Edens, 2011) and Blue Jets (Wescott et al., 1995; Krehbiel et al., 2008)) or in response to in-cloud and / or cloud-to-ground lightning leading to Halos, Sprites, Elves and Gigantic Blue jets (Dwyer and Uman, 2014).

1.6.1 Sprites and Halos

Sprites and Halos occur between 40 km and 90 km above the Earth surface and their appearance is caused by the electric breakdown of the high-altitude rarified air due to the action of the dipolar electric field originated in thunderclouds. This electric breakdown is the cause of the high altitude optical emissions (Passas et al., 2014). Halos appear as flattened diffuse flashes of light at an altitude around 80-85 km. Sprites show a sharp transition between an upper diffuse region and their lower plasma streamer region.

1.6.2 Elves

Elves are fast expanding rings of light in the lower ionosphere ($\sim$ 88 km - 95 km) that can expand up to 300 km horizontally. These events are generated by the electromagnetic pulse (EMP) from lightning return strokes (RS). The EMP propagates in spherical waves from the base of the lightning channel, then it intersects the lower ionosphere in a ring that expands outwards. The radiation electric field component of the EMP heats up free ionospheric electrons, enhancing their collisions with ambient gas (atomic and molecular) species and, consequently, promoting their excitations, ionization and light emissions (Dwyer and Uman, 2014). Elves are more commonly seen over the oceans (than over land) because they need large peak current lightning (Blaes, Marshall, and Inan, 2016), and this type of lightning is more frequent over oceanic regions than over the continents (Said, Cohen, and Inan, 2013).

1.6.3 Blue starters, Blue jets and Gigantic jets

Blue starters (Wescott et al., 1996; Edens, 2011) and blue jets (Wescott et al., 1995; Krehbiel et al., 2008)) are upward moving electrical discharges that exit the upper part of thunderclouds and finish in the lower and upper stratosphere, reaching approximately 25 km and 45 km altitudes, respectively. Blue jets are upward-propagating atmospheric discharges composed of streamers and a leader. They propagate at speeds of approximately 10^5 m/s and have a lifetime of around 300 ms. The leader of a blue jet can emit light at the 777.4 nm wavelength (Neubert et al., 2021). Gigantic jets can be considered as analogous to cloud to ground (CG) lightning but propagating upward to the conductive lower ionosphere up to about 90 km.

1.7 Terrestrial Gamma-ray Flashes (TGFs)

Terrestrial Gamma-ray Flashes are bursts of energetic gamma rays with single photon energies up to 40 MeV and with a duration from tens to hundreds of microseconds (Köhn et al., 2020) that are related with the presence of some type of lightning in thunderclouds.

TGFs seem to be produced through energetic electrons by bremsstrahlung process. Electrons in air are accelerated in an ambient electric field gaining energy, there is also a lost of energy through inelastic collisions caused by the air molecules, which results in a friction force that confines most of electrons at an energy level where the friction force equilibrates with the local electric force. Electron and molecule collisions are stochastic processes, so it is difficult that electrons can reach energies above the equilibrium level. If electrons can exceed energies above 150-200 MeV, where the friction force in air is maximum, the further acceleration becomes systematic instead of stochastic and it initiates a significant multiplication of energetic electrons named runaway electrons.

There are currently two possible theories that can explain the generation of energetic electrons at time scales of microseconds: the leader-streamer process where low-energy electrons are accelerated in the high-field regions in the vicinity of lightning leader tips (Dwyer et al., 2005; Kutsyk, Babich, and Donskoi, 2011; Babich et al., 2013; Celestin and Pasko, 2011), or the constant acceleration and multiplication of high-energetic electrons as a surplus of cosmic rays in the large-scale electric fields of thunderstorms (Wilson, 1925; Gurevich, Milikh, and Roussel-Dupre, 1992; Babich, 2005; Dwyer, 2003; Dwyer, 2007; Dwyer, 2012; Gurevich and Zybin, 2001).

Recent measurements by the Atmosphere-Space Interactions Monitor (ASIM) launched in April 2018 suggest that the production of TGFs is related to the leader step and associated streamer coronae when upward moving intracloud lightning illuminates (Köhn et al., 2020). However, the final inception mechanism of TGFs is not yet completely understood and more research is needed.

1.8 Corona discharges

Sometimes the electric field in air surrounding sharp objects or electrodes at high voltages or exposed to high external electric fields may overwhelm the threshold electric field needed for the development of electron avalanches in air. When the air volume where the electric field exists is a very small region around the object it will not lead to an electrical breakdown with another object in its surroundings but to a corona discharge characterized by concentrating the electrical activity in a small volume around the high voltage electrode.

In general, for any form of corona discharges, the inter-electrode gap can be divided into a narrow ($\sim$ 0.1 - 1 mm) visible ionization region and a dark low field drift region connecting the ionization region with the low-field passive electrode.

When a corona discharge occurs, the ionic space charge polarities accumulate around the high voltage electrode, changing the distribution of the electric field. The balance between accumulation and removal of the space charges start different modes of the corona discharge.

1.9 Negative coronas

The electron avalanche in negative coronas starts at the cathode (with negative voltage) and develops towards the anode following the attenuation of the electric field. Electrons with high mobility move fast from the cathode into the low electric field region, leaving a positive space charge in the cathode's surrounding region. The electron avalanche stops when the electric field goes below the ionization threshold. On the other hand, in the area where the electron avalanche stops, electrons are captured by oxygen molecules (through either dissociative attachment forming O^- and / or the direct attachment mechanism forming $O_2{}^-$) that generate a negative space charge. The difference of space charge polarities (positive near cathode, negative when avalanche ends) modifies the electric field in the inter-electrode gap, increasing it near the cathode and decreasing it around the anode. This results in three forms of corona modes: Trichel streamers, negative pulseless glow and negative streamers (Giao and Jordan, 1970).

1.9.1 Trichel pulse streamers

When a sufficiently high negative voltage is applied to the point electrode of a point (cathode)-to-plane electrode (anode) system at pressures above 10 kPa (0.1 atm), a negative corona discharge appears at the point cathode, where the discharge current consists of the negative corona Trichel pulses (TP). Each TP is discerned by a peaked signal where the current rises within several nanoseoonds to a maximum of ($\sim 1 - 10^2$ mA) before decreasing to a subsequent transient glow discharge stage that can last some hundreds of nanoseconds (Halanda et al., 2012).

Recent investigations have suggested that the basic aspects of TP formation can be explained on the basis of the streamer theory (Halanda et al., 2012). According to this, the sequence of events leading to the TP formation would be as follows (Černák and Hosokawa, 1991; Cernak, Hosokawa, and Odrobina, 1993; Černák et al., 1998):

An initial stage of the development of a sequence of avalanches linked by the secondary emission from the cathode, the space charge created can shield itself from the external electric field, creating a streamer initiating plasma. If some electrons are presented just in front of the plasma, the avalanche of electrons in the locally enhanced field cause

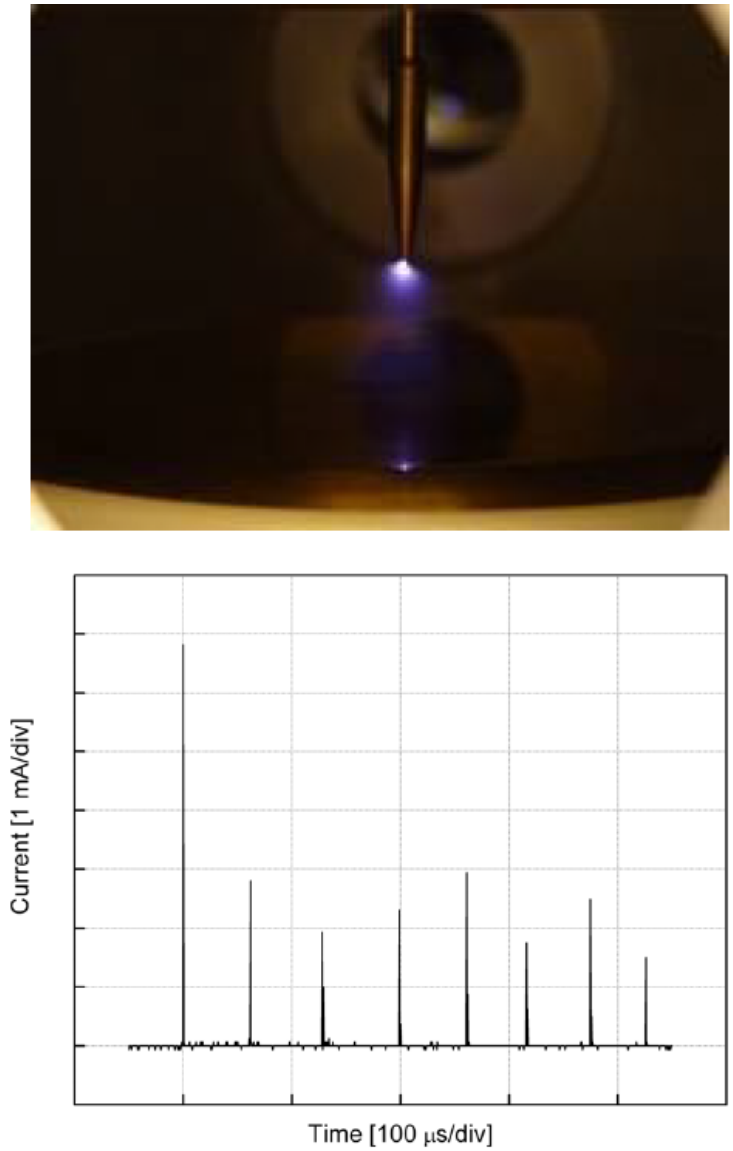

Figure 1.1. Negative corona in a short point-to-plane inter-electrode gap (top panel), and train of Trichel pulses (bottom panel) measured in ambient air (Halanda et al., 2012).

primary cathode- and anode-directed streamers to propagate. Thus, the feedback-to-cathode Townsend ionization mechanism (free electrons are accelerated by an electric field, collide with gas molecules, and consequently release additional electrons) fed by secondary electron emission from the cathode is supplanted by a faster feed-forward-to-gas streamer mechanism, where secondary electrons are created by photoionization in the gas. After an initial acceleration lasting ~ 1 nanosecond, the velocity of the cathode directed streamer increases exponentially to the order of 10^8 cm s^{-1} resulting in the TP rise due to the displacement current induced by the streamer movement in the cathode. The TP current rise is finished by the streamer arrival to the cathode and, subsequently, a low-current abnormal glow-discharge cathode spot is formed.

Contrary to the previous interpretations on the formation of TPs, the streamer-based model explanation for TPs admits the existence of a significant free electron current in negative corona discharges burning in ambient air even at distances from the cathode on the order of 1-10 mm (Černák et al., 1998) as indicated in Goldman, Goldman, and Sigmond (1985) and Černák and Skalnỳ (1984).

Trichel pulses exhibit a regular repetition pattern frequency, the duration of each TP and the subsequent transient glow discharge stage can range from a few tens of nanoseconds to some hundreds of nanoseconds in ambient air. The pulse frequency depends on the geometry of the electrode and pressure, and it raises when voltage increases (Giao and Jordan, 1970). Available results indicates that the rise time and magnitude of TPs are independent of the cathode material.

1.9.2 Negative pulseless glow

In short gaps, Trichel streamer pulses develop continuously until electric breakdown of the gap occurs. In long gaps however, the discharge turns over to a pulseless glow at higher cathode potentials ($>$ 130 kV at 1 atm and 19 cm inter-electrode point-to-plate gap). In this regime the negative ion space charge is no longer able to temporarily suppress the ionization at the cathode which then reaches a steady state corresponding to the pulseless corona current characteristic of a uniform (glow) discharge activity without pulse bursts. Thus, the discharge becomes particularly stable and exhibits well-defined features of a tiny glow discharge with a spherical negative glow region followed by a conical positive column, and with the whole discharge detached from the cathode by a dark space (Giao and Jordan, 1970).

1.9.3 Negative streamers

An additional increase of the cathode potential may cause the positive column of the negative glow region (see previous section) to constrict itself to form a streamer

channel which advances and retreats into the inter-electrode gap. The discharge current recovers (as in the Trichel Pulses) a pulse-like shape but with a low-frequency rate. The appearance of negative streamers can be prevented by the shape of the cathode. Thus, stable development of negative streamers can be limited to the case of spherical cathode protrusions. With point-ended electrodes (conical shape), the development of negative streamers can immediately lead to electric breakdown of the gap (Giao and Jordan, 1970).

1.10 Positive coronas

In positive coronas the first (seed) electrons create avalanches which grow towards the point anode (with positive voltage) inside the volume of gas where the electric field is higher than the threshold needed for electrical breakdown. As the avalanche develops in the direction of increasing electric field, the drift velocity of electrons raises as the avalanche increases, decreasing the probability of attachment to electronegative gases and giving rise to negative ions. When the electrons reach the anode they have such a high kinetic energy that they need to loose it before they are absorbed by the anode. This leads electrons to release their energy in ionization collisions that induces discharge activity nearby the surface of the anode. Finally, electron avalanches and the electrical activity at the anode leave a trace of positive space charge in front of the anode. When the density of the positive space charge in a volume of about 50 μm radius exceeds certain threshold the streamers that propagate towards the anode are generated.

With the same geometry and voltages, positive coronas appear a little smaller than the corresponding negative coronas. In addition, positive coronas have a much lower density of free electrons compared to negative coronas and much less total number of electrons. However, as mentioned above, electrons in a positive corona are concentrated close to the surface of the point conductor (with positive voltage), in a region of high electric potential gradient (and therefore electrons have high energy), whereas in a negative corona many of the electrons are in the outer, lower-field regions. Therefore, if electrons are to be used in an application which requires high activation energy, positive coronas may support a greater reaction constant than corresponding negative coronas; though the total number of electrons may be lower, the number of very high energy electrons may be larger. Coronas are efficient producers of ozone in air. A DC positive corona generates much less ozone than the corresponding DC negative corona, as the reactions which produce ozone are relatively low-energy. However, more ozone is produced in positive pulse corona than in positive DC coronas (Hu and Yang, 2020). Therefore, in general, the greater number of electrons of a negative corona leads to increased production of ozone.

For positive point-to-plane coronas in air, the sequence of phenomena has generally been accepted to be as follows (Loeb, 1965): At the corona threshold voltage the discharge starts with burst pulses, which probably are just trains of avalanches coupled through the gas photoionization. At a little higher applied voltage onset streamers occur together with these pulses. With increasing voltage the rate of onset streamers increases, and then decreases to zero at the onset of the positive glow. At still higher overvoltages, streamers appear again, concurrent with a background of steady positive glow. In this case they are called pre-breakdown streamers. These are more powerful (energetic) than onset streamers, and their length and number per unit time increase with the voltage. If some of them reach the plane electrode, a spark breakdown may follow (Kudu, Lågstad, and Sigmond, 1998). Avalanches and streamers are filamentary, while the glows are more diffusely spread out over the high-field electrode surface.

This positive corona sequence in air can be modified by changing the geometry of the discharge gap, the externally generated ionization, the air humidity, or the content of electronegative impurities.

1.10.1 Burst pulses

Burst pulses are trains of electron avalanches, initiated by electrons from external radiation or detached from negative ions formed in the corona drift region. The electrons from each avalanche disappear rapidly into the point anode, leaving a cloud of much slower positive ions just outside the metal. The ion space charge acts as a small expansion of the point, increasing the field in the ionization region outside it. Electrons liberated in the drift region by gas photoionization or at the cathode by photons from the first avalanche, will create new and larger avalanches, provided they reach the ionization region while the positive space charge is still inside it. This cumulative process stops when the bulk of the positive ions reach the outer border of the ionization region, reducing the field in this critical region. Increasing the applied voltage will increase both the number and the size of the burst pulses. If the lateral diffusion of the burst avalanches dominates, then they will spread over the anode point surface and form a positive glow. If the secondary avalanches and their positive ions are formed close to the primary avalanche, then the concentrated positive space charge will act as a needle-like elongation of the anode and push the ionization region ahead of it, and a streamer is formed (Kudu, Lågstad, and Sigmond, 1998).

1.10.2 Positive glow

In gases where the mean free path for gas ionizing photons is long, or photoelectrons from the cathode can cross the gap without being attached, secondary avalanches will spread over the anode surface. When the voltage is raised above the burst pulse level

a self-sustained positive glow corona will form, where the average current is stabilized by the reduction of the ionization region field by the positive ions drifting towards the cathode. However, as shown by Sigmond (1997), this glow may be oscillatory unstable by the same mechanism as that responsible for the burst pulse formation. A stochastic increase in the current will form a positive space charge increase close to the anode and increase the ionization region field, and also create extra secondary electrons outside the ionization region. If these electrons reach the ionization region well before the positive space charge perturbation has drifted out of it, a positive feedback results (Kudu, Lågstad, and Sigmond, 1998).

1.10.3 Breakdown streamers

When large avalanches, burst pulses or positive glow oscillations concentrate enough positive ions in a spot just outside the surface of the anode, the field between this positive space charge and the anode may be brought nearly to zero. Electrons from the secondary avalanches will then form a plasma with the positive ions there, and the ionization region will be pushed out to the tip of this plasma channel. New avalanches and plasma will be formed outside this tip, and the streamer channel will grow as long as plasma is formed faster than it can be recombined or absorbed at the anode. Streamers formation is thus favored by large avalanches and by short-range photoionization (Kudu, Lågstad, and Sigmond, 1998).

1.11 The long spark

In small gaps the streamer-to-spark transition occurs right after the streamer has crossed the inter-electrode gap and arrived to the grounded electrode. In the case of long sparks the process is the following: the first stage of the discharge development consists in the formation of a corona discharge (usually named first corona) that exhibits the shape of burst filamentary channels emerging from the high-voltage electrode. The next step continues with the formation of a highly conducting discharge channel. After this, the leader extends, with the aid of corona discharges emanating from its head, towards the grounded electrode. The final phase begins when the corona streamers emanating from the leader tip reach the grounded electrode.

1.12 The first corona

The initiation of the first corona needs two conditions to be accomplished. First, the availability of free electrons and, second, that those free electrons are placed in a volume of gas located in such a way that the electrons can initiate the rise of the avalanche that will become a streamer discharge. The natural production rate of electrons in air

due to natural background radiation is of about 10 electrons cm^{-3} s^{-1} (Cooray, 2003). These electrons attach to electronegative oxygen species (atoms and molecules) forming negative ions. Therefore, natural ambient radiation provides a supply of negative ions. Electrons can detach from the negative ions under the action of the electric field, which is the main process that provides seed electrons. In order to create an avalanche able to lead to a streamer, seed electrons in the inter-electrode gap should appear in a volume of the gas where the electric field is higher than the critical electric field needed for electric breakdown. The probability of finding an electron able to initiate the breakdown process increases with increasing applied voltage.

Chapter 2

Corona electrical discharges in storm clouds

2.1 Narrow Bipolar Events (NBEs)

In 1980, Le Vine (1980) was the first detecting strong radio-frequency (RF) sources from intra-cloud (IC) electrical discharges characterized by short duration (10 - 30 μs) bipolar sferic waveforms detected in very low frequency (VLF) / low frequency (LF) (10 kHz - 400 kHz) and commonly accompanied by strong very high frequency (VHF) (30 - 300 MHz) radiation bursts called Compact Intracloud Discharges (CIDs) or Narrow Bipolar Events (NBEs) (Smith et al., 1999). Because of the NBE sferic strength, they can be radio detected at hundreds of kilometers distance (Rison et al., 2016). CIDs are also named strong TransIonospheric Pulse Pairs (TIPPs) as they were originally recorded by the VHF receivers aboard the ALEXIS satellite (Holden, Munson, and Devenport, 1995). The acronym TIPPs is based purely on the appearance of the VHF pulse recorded on a satellite above the ionosphere containing a distinct double pulse which indicates an elevated intracloud source. TIPPs are common in-cloud events, being approximately half of all VHF events collected by the Fast On-orbit Recording of Transient Events (FORTE) satellite launched in 1997 (Light and Jacobson, 2002). The impulsive NBE events (or weak TIPPs) seen in the VLF / LF range are still typically 10 times more powerful than the emissions from normal lightning discharges at high frequencies (HF) (3 - 30 MHz) (Smith et al., 1999). The extensive FORTE VHF recordings distinguished between impulsive events (TIPPs) and non-impulsive events, the so-called "non-TIPPs", that include both cloud-to-ground (CG) and in-cloud lightning signals such as IC events (Light and Jacobson, 2002). Fast positive and negative breakdown cause NBEs and NBEs can initiate normal IC lightning (Rison et al., 2016; Tilles et al., 2019). Fast breakdown (Rison et al., 2016; Tilles et al., 2019) suggests streamer coronas to be the origin of narrow bipolar events. Recent results suggest that $\sim$ 10 % of IC lightning are initiated by NBEs and the rest are triggered by very fast (typically less than 0.5 μs) VHF pulses with no obvious spatial development (Lyu et al., 2019). Note that the terms

regular or normal lightning are used hereinafter with the meaning of lightning flashes with durations of a few tens of milliseconds to several seconds with hot leader channels rather than such processes as isolated NBEs which last a few tens of microseconds or the continuous breakdown in overshooting tops.

Jacobson et al. (2013) reported dim optical detections from NBEs by a wideband (0.4 - 1.1 μm) photodiode detector (PDD) sampling at 66 kHz (15 μs) on-board the FORTE satellite. These dim satellite-based NBE optical recordings produced a peak optical radiance (at 825 km altitude) above the effective trigger threshold of 350 μW m^{-2} corresponding to $\sim 3 \times 10^8$ W of peak optical isotropic power at the top of the cloud (Jacobson and Light, 2012). Because of the wideband (700 nm) filter used, Jacobson et al. (2013) were not able to distinguish the characteristic color of NBE optical emissions. More recently, Chanrion et al. (2016) reported profuse activity of blue electrical discharges at the top of a thunderstorm observed from the International Space Station (ISS) during the THOR experiment in 2015 aimed to investigate electrical activity from thunderstorms and convection related to water vapor transport. Blue starters and a pulsating blue jet propagating into the stratosphere were color photographed from the ISS as a result of the THOR mission (Chanrion et al., 2016).

In terms of light emissions, both impulsive and continuous streamer corona discharges in air are distinctly characterized by spectra strongly dominated by near-ultraviolet blue emissions (280 - 450 nm) corresponding to the Second Positive System (SPS) of molecular nitrogen (N_2) (Gallimberti, Hepworth, and Klewe, 1974; Grum and Costa, 1976; Ebert et al., 2010) with its strongest transition in 337.0 nm (Gordillo-Vázquez, Luque, and Simek, 2012a; Hoder et al., 2016; Malagón-Romero and Luque, 2019; Hoder et al., 2020). Available laboratory measurements also show that red and near-infrared optical features from the First Positive System (FPS) of N_2 and the spectral contribution from oxygen atoms is negligibly small (0.5 % - 4 %) compared to N_2 SPS in both leader and leaderless streamer coronas (Gallimberti, Hepworth, and Klewe, 1974; Grum and Costa, 1976; Ebert et al., 2010). Finally, leader coronas spectra exhibit larger (double) intensity of N_2^+ First Negative System (FNS) at 391.4 nm than leaderless corona discharges (Gallimberti, Hepworth, and Klewe, 1974).

2.2 Blue LUminous Events (BLUEs)

Transient (from a few to hundreds of milliseconds) bluish optical emissions from thunderstorm cloud tops were originally identified from aircraft by Wescott et al. (1995) and Wescott et al. (1996). They distinguished two types, fast upward moving jets named blue jets reaching terminal heights of 45 km - 50 km (Wescott et al., 1995), and blue starters that come out upward from the cloud top to a maximum of $\sim$ 25 km and that were

not coincident with negative or positive cloud to ground (CG) lightning strokes (Wescott et al., 1996). Multispectral video recordings show evidence that a small fraction of bluish optical emissions from both blue jets and starters are due to N_2^+ FNS (Wescott et al., 2001).

The term Blue LUminous Events (BLUEs) has been recently applied to in-cloud and to partially emerged transient electrical discharges that emit pulses of light mostly blue, that is, they could include a small fraction of red (from the First Positive System of molecular nitrogen (N_2)) and infrared optical emissions (777.4 nm from atomic oxygen). This definition includes blue jets and starters, but also positive and negative NBEs, which are the VLF/LF radio manifestation of in-cloud leaderless streamer coronas (Kuo, Su, and Hsu, 2015; Rison et al., 2016; Liu et al., 2018; Tilles et al., 2019; Liu et al., 2019; Cooray et al., 2020; Soler et al., 2020; Neubert et al., 2021; Liu et al., 2021b)

Optical detection of BLUEs has been increasingly efficient since the beginning of the XXI century. During the Severe Thunderstorm Electrification and Precipitation Study (STEPS) ground-based campaign in 2000 (Lyons et al., 2003), brief (33−136 ms) upward−propagating discharges called *gnomes* were filmed slightly ($\sim$ 1 km) rising out of the convective dome of a supercell storm in the Great Plains of the United States. In 2011, also from the ground, Edens (2011) reported a real color image with associated in-cloud VHF sources of a small blue starter that occurred on 4 August 2010 over an active thunderstorm in west central New Mexico. The event exhibited three diffuse streamer regions attached to leader-like channels, which appeared more white in the color image than the blue streamers emerging from the cloud top at $\sim$ 15 km and reaching a terminal altitude of $\sim$ 17 km (Edens, 2011).

Optical BLUE detections from space have been reported from the limb-pointing Imager of Sprites/Upper Atmospheric Lightning (ISUAL) onboard FORMOSAT-2 (Kuo et al., 2005; Chou et al., 2011; Kuo, Su, and Hsu, 2015; Chou et al., 2018; Liu et al., 2018). Chou et al. (2018) reported dim red emissions (623-754 nm) at the lower edge of some ISUAL detected BLUEs. A variety of BLUEs including kilometer-scale blue discharges at the cloud top layer at $\sim$ 18 km altitude BLUEs have also been recently observed by the nadir-pointing MMIA instrument onboard ASIM in the ISS since April 2018 (Soler et al., 2020; Neubert et al., 2021; Li et al., 2021).

2.3 Atmosphere Space Interaction Monitor (ASIM)

The Atmosphere Space Interaction Monitor (ASIM) is an instrument set in the International Spatial Station (ISS) and originally designed to measure lightning, Transient Luminous Events (TLEs) and Terrestrial Gamma-ray Flashes (TGFs) generated

in thunderstorms (Neubert et al., 2019). TLEs are light phenomena that occur in the stratosphere and mesosphere in response to lightning occurring in storm clouds. TGFs are bursts of gamma radiation probably caused by the deceleration of charged particles in thunderstorms (however, the production mechanism of TGFs is not yet completely clear).

ASIM is formed by two modules: the Modular X-ray and Gamma-ray Sensor (MXGS), created to detect TGFs by observing the associated emissions in the UV, near-infrared, X-ray and Gamma-ray spectral bands, and the Modular Multi-spectral Imaging Array (MMIA) designed to detect optical signals from lightning, corona discharges and TLEs. MMIA includes three high-speed photometers to measure at different spectral bands: 180-230 nm (UV), 337.0 nm (Near Ultraviolet), and 777.4 nm (Infrared). The sampling rate of the photometers is 100 kHz, which is much better than the 10 kHz provided by ISUAL or the 20 kHz provided by GLIMS. MMIA also includes two cameras at 337.0 nm and 777.4 nm bands taking up to 12 frames per second and their spatial resolution is $\sim$ 400 m (Chanrion et al., 2019). MXGS and MMIA take synchronized observations and trigger when flashes are detected. Also, the ISS share the field of view at the same nadir position with the Lightning Imaging Sensor (LIS), allowing simultaneous observations with ASIM. From January 2022 the field of view of ASIM changed to limb orientation.

Figure 2.1. Photograph of the blue starter event above the cloud top. The frame is a crop of the full-size photograph and represents a transverse area of approximately 5.35 km wide by 4.11 km high; the resolution of the photograph is 9.2 m/pixel. The hardly visible light band across the base of the event and to either side is scattered light from the cloud (Edens, 2011).

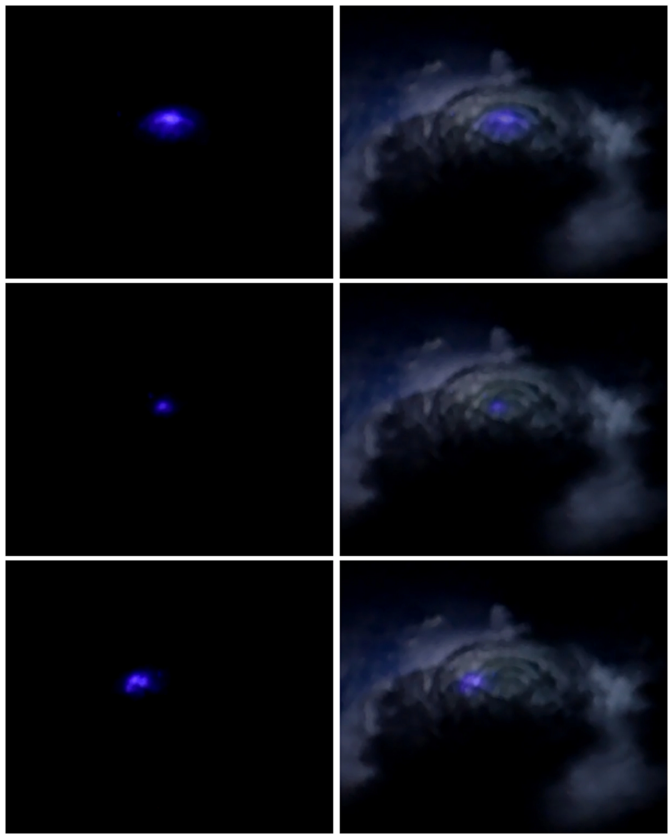

Figure 2.2. BLUE (corona) electrical discharges on the top of storm clouds (left column). Observed corona discharges from the ISS over-imposed on an image of the storm cloud (right column).

Figure 2.3. Real image of the ASIM module on the Columbus Externals Payloads Adaptor (CEPA) of the ISS.

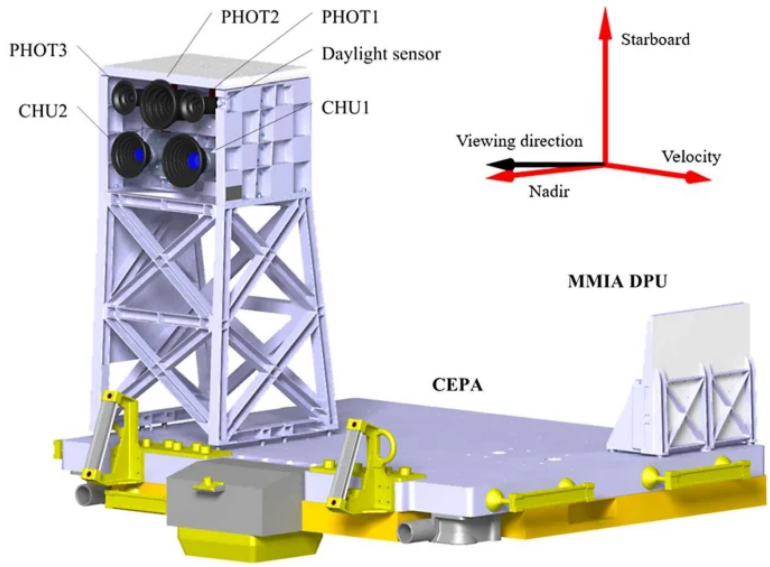

Figure 2.4. MMIA on the Columbus Externals Payloads Adaptor (CEPA). The Camera Head Units (CHUs) and the photometers (PHOTs) are mounted on an optical bench that sits on top of a support structure to avoid having the payload on the nadir-directed platform in the field of view. The instrument computer, the Data Processing Unit (DPU), is placed directly on the CEPA and is clad with a radiating shield for thermal control. The viewing direction is indicated by a black arrow in the ISS frame given by the velocity vector, the nadir and starboard direction (Chanrion et al., 2019).

Chapter 3

Motivation

Research results and observational evidences over the last 40 years indicate that, in addition to lightning, kilometer scale corona electrical discharges formed by hundreds of millions of streamers (Liu et al., 2019; Cooray et al., 2020) are common in thunderclouds around the globe but their inception process (Le Vine, 1980; Smith et al., 1999; Rison et al., 2016; Tilles et al., 2019; Soler et al., 2020; Neubert et al., 2021), dynamics (Jacobson and Heavner, 2005; Wiens et al., 2008) and probable atmospheric chemistry impact (Shlanta and Moore, 1972; Zahn et al., 2002; Simek, 2002; Minschwaner et al., 2008; Bozem et al., 2014) remain to be well understood.

By combining two years of Blue LUminous Events (BLUEs) data recorded by the MMIA instrument of ASIM on-board the ISS (Neubert et al., 2019) this thesis presents the first worldwide nighttime climatology of BLUEs (corona discharges) in storm clouds. Key aspects are discussed such as the average annual and seasonal distribution of BLUEs, regional differences, land/ocean variability, zonal/meridional distributions, and the global rate of BLUEs in local time. Therefore, ASIM-MMIA analysis and nighttime climatology of BLUEs presented in this thesis is the first of its kind and complements the global frequency and 24 h lightning distribution (within $\pm$ 70° latitude) first available since 2003 (Christian et al., 2003). This was generated with data from the Optical Transient Detector (OTD), a prototype of the Lightning Imaging Sensor (LIS), in operation from May 1995 to March 2000. LIS was later onboard the Tropical Rainfall Measuring Mission (TRMM) also providing full day global lightning data within $\pm$ 38° latitude from early 1998 to April 2015 when TRMM was deorbited (Cecil, Buechler, and Blakeslee, 2014). More recently, since 1 March 2017, LIS is onboard the ISS providing high latitude (up to $\pm$ 52°) all-day (24 h) lightning data (Blakeslee, 2019; Blakeslee et al., 2020).

While the hot and thermal lightning plasma mostly excites atomic species like oxygen atoms released from thermal dissociation of O_2 leading to 777.4 nm optical emissions typical of lightning, streamer corona discharges are cold non-thermal plasmas where only heavy particles are cold and electrons are very hot. Thus corona discharges are able to activate molecular species like N_2, O_2 and H_2O by non-equilibrium electron-impact

collisions (Gordillo-Vázquez et al., 2018). This underlies their different efficiencies in producing key chemical species. For instance, lightning is a key direct source of tropospheric nitride oxide (NO) that, when oxidized, produces NO_2 leading to the known lightning NO_x (LNO_x) with significant impact on tropospheric chemistry (Schumann and Huntrieser, 2007; Finney et al., 2016; Gordillo-Vázquez et al., 2019). In contrast, laboratory produced streamer coronas generate only small amounts of NO but considerable greenhouse gases such as ozone (O_3) and nitrous oxide (N_2O) (Donohoe, Shair, and Wulf, 1977; Brandvold, Martinez, and Hipsh, 1996), which is an ozone depleting gas and the third strongest greenhouse gas after carbon dioxide and methane. N_2O has the largest ($\sim$ 300 times that of CO_2 for a 100-year timescale) global warming potential of these gases (Myhre, Shindell, and Pongratz, 2014). Perturbations to concentrations of greenhouse gases affect more the radiation balance when the altitude of the sources are higher. In this respect ASIM can facilitate their detection since it is more sensitive to discharges higher in the clouds.

The results obtained in this thesis suggest that streamer corona discharges in thunderclouds are relatively common as observed by ASIM-MMIA. Thus, thundercloud streamer corona discharges, which can occur continuously in the vicinity of ordinary lightning strokes, but also in isolation, may be a critical upper troposphere source of greenhouse gases such as N_2O and O_3, and of oxidant gases like OH and HO_2, in convectively active areas that deserves further detailed studies.

Once achieved the challenge of building up the first climatology of BLUEs in storm clouds, it is possible to use the data (ASIM observations of BLUEs and meteorological variables) to develop parameterizations of BLUEs to simulate global distributions of thundercloud corona discharges occurring during nighttime.

This thesis intends to increase the knowledge on corona electrical discharges occurring daily in storm clouds and I hope this work can be useful for atmospheric electricity related scientific communities like atmospheric sciences in general.

Finally, despite the possible interest of this work, there are a number of limitations to consider. First of all, BLUE observations by ASIM are only possible during nighttime. However, lightning observation by LIS is possible during all day (the full 24 h). We solved this by comparing our BLUE geographical (and seasonal) distribution with the geographical (and seasonal) distribution of nighttime only LIS lightning detections. It is also important to mention that the ASIM field of view (FOV) (also the FOV of LIS) covers a small fraction of the Earth area at any time, thus ASIM (and LIS) only observes a very small fraction of the total number of BLUEs (or lightning) that occur worldwide at any moment.

Chapter 4

Methodology and Data Analysis

All MMIA data used in this thesis has been obtained from a private server at DTU (Denmark), and it is required to have a credentials to access it. Inside the server we can explore all MMIA recordings processed at level 1 stored in .cdf files. The data is stored chronologically from 2018 till the present. Image data and photometer data are located in different .cdf files, and not all photometer data has its correspondent image file. All .cdf files contain a lot of important parameters (peak power density of the photometer analysed, latitude and longitude of the ISS, time array, timestamp, etc) to each frame of the event of study. We have used Python 3.7 to develop our algorithms, data analysis and create plots.

4.1 Why Python?

Python is a modern, interpreted, object-oriented, open.source programming language that can be used in all kinds of software engineering (Lin, 2012). Python comes with many packages very useful to work with science, data, statistics, mathematics, plotting, geographical information systems, etc. Besides, Python have an easy and concise natural syntax that makes it very friendly for people that are not pure software engineers. Also, the modern data structures and the object-oriented nature makes the code more robust. One of the most important positive points of Python is that nowadays is one of the favourite programming language in the scientific community. This makes it support easier and it is also easier to find help for eventual troubles in the process of coding, because almost always it is possible to find another person with the same problem. Personally, GitHub and StackOverflow helped me a lot in understanding code and enhance my own ideas to find a better solution.

4.2 Optical signal fitting procedure

The temporal profile of optical emissions emanating from deep within a cloud is dominated by the time of multiple photon scattering by cloud droplets and ice crystals (Light et al., 2001; Thomason and Krider, 1982). Under the assumptions that the optical pulse is impulsive and localized, that the cloud is homogeneous and bounded above by a plane, and that the photons exit the cloud isotropically, with scattering outside the cloud being negligible, one can derive a simple expression for the signal registered by a photometer above the cloud top. As we see below, this expression provides a rough estimate of event altitudes.

If the source is far from the cloud boundary, the photons experience so many scattering events before exiting the cloud that their transport is well approximated by a diffusive process with a diffusion coefficient $D = \Lambda c/(3(1-g\omega_0))$ (Koshak et al., 1994), where Λ is the photon mean free path, c is the speed of light, g is the scattering assymetry parameter and ω_0 is the single-scattering albedo. Since the radius of the cloud droplets is much larger than the optical wavelengths of interest, one can assume an extinction efficiency of two (Van der Hulst, 1981) and express the mean free path as $\Lambda = (2\pi r^2 n)^{-1}$ with r being the radius of scatterers and n their concentration. The single-scattering albedo ω_0 denotes the probability that a photon is re-emitted after a scattering event, and under our conditions it is close to unity. Nevertheless, over the course of many collisions a photon may accumulate a nonnegligible probability of being absorbed. We express this by means of an absorption rate $\nu = c(1-\omega_0)/\Lambda$. However, the signal decay is not only determined by absorption in scattering events but also by photons leaving the cloud from the lower and lateral boundaries. Hence, we consider an effective decay rate ν which is a model parameter derived from the photometer curve.

The time profile of the signal is then determined by the probability distribution of the time that it takes a diffusing and weakly absorbed particle to reach a plane at a distance L from its starting point. In our case L is the distance from the event to the cloud top. This problem belongs to the family of first-passage (or first-hitting-time) problems and can be solved by standard methods of statistical physics (see e.g. Krapivsky, Redner, and Ben-Naim (2010)). The solution reads

$$f(t) = \frac{\theta(t-t_0)e^{2\sqrt{\nu\tau}}}{\tau\sqrt{\pi}} \left(\frac{\tau}{t-t_0}\right)^{3/2} e^{-\tau/(t-t_0)-\nu(t-t_0)}, with \int_{-\infty}^{\infty} f(t)dt = 1 \qquad (4.1)$$

where θ is the step function, t_0 is the emission time and $\tau = L^2/4D$ is the characteristic time of the process. Given a photometer signal, one can fit it to (8.1) and obtain values for the parameters t_0, τ and ν. Then the depth of the event can be estimated as $L = (4D\tau)^{1/2} \approx (4\Lambda c\tau/(3(1-g)))^{1/2}$. In this work we used $g = 0.87$ (Thomason and

Krider, 1982) and $\Lambda = 4$ m to 16 m, corresponding to a droplet concentration $n = 10^8$ m^{-3} and radii $r = 10$ μm to 20 μm (Thomason and Krider, 1982), which correspond to a range of the diffusion coefficient D from 3×10^9 to 12×10^9 m^2 s^{-1}.

The above analytic equation is consistent with a full scattering model of lightning optical emissions (Luque et al., 2020) that simulates how a satellite observes optical radiation emitted by a lightning flash after it is scattered within an intervening cloud. This model is specifically tailored to modern instruments such as the MMIA component of the ASIM that operates from the ISS but can also be used in a wider context of lightning scattering.

4.3 Algorithm for BLUE search

One of the most relevant point of this thesis is the implementation of a new algorithm that filter BLUE events from lightning activity, the algorithm is described in the papers below. The importance if this is that in the data server we have hundreds of thousands of many different events and we just want to analyze a small portion of this, this task is almost impossible do it manually. The steps of the algorithm are the following:

1. Consider only frames of photometer events where the trigger of the 337.0 nm equals 1, regardless of other MMIA photometer triggers.

2. Given a photometer event, calculate the blue and red median values in each frame. Then calculate the blue and red threshold by adding 3 σ to the respective means.

3. In most of the cases the threshold values are below 1 $\mu W/m^2$, so we replace the threshold by 1 $\mu W/m^2$.

4. Create groups defined by five or more consecutive blue counts (10 μs each) above the blue threshold. Groups separated by more than 10 milliseconds are considered different BLUE events.

5. Given groups of blue counts, find the maximum in each group and keep only events with red signal below threshold 15 and 5 milliseconds before and after the blue peak, respectively.

6. Disregard very weak BLUEs by requesting that the maximum blue signal is at least 3 times the blue threshold.

7. Given groups of blue counts with red signal, keep only the events which: (a) red peak is above 2.5 $\mu W/m^2$ and the blue maximum is at least 10 times the red peak, or (b) the red peak is below or equal 2.5 $\mu W/m^2$ and the blue maximum is at least 2 times the red peak.

8. This is a final optional step to delete cosmics rays or high energy particles. Delete those events where its rise time is below or equal 40 μs and its total time is below or equal 150 μs.

4.4 ASIM Organization

The ASIM Science Data Center (ASDC) receives raw data from ESA's Belgian User Support and Operation Center (B.USOC), which contains all ASIM instrument and payload data, and some parameters from ISS (Neubert et al., 2019). All data is calibrated and classified depending on the event type, also there is a control of the performance of the instrument.

ASDC is distributed between the University of Bergen, Norway, the University of Valencia, Spain, and DTU Space, Denmark, where is located the main node. The University of Bergen controls the operations and calibrations of the MXGS high-energy and low-energy detectors. The University of Valencia supports instrument operations and estimate imaging parameters for angle-of-arrival of TGF photons. Finally, DTU space is the organisation responsible for MMIA commisioning, operations and calibration.

Chapter 5

Conclusions

The main conclusions of the three articles that form this PhD thesis are:

5.1 First article

1. A succession of up to 30 blue flashes forming a cluster during about 33 seconds (almost one flash per second) were recorded by the 337.0 nm-filtered camera and photometer of the MMIA instrument on board ASIM. The detected blue events exhibit one, two or multiple optical pulses (as seen from photometric signals) lasting 1.60-3.60 ms (single) and beyond 14 and 8 ms (double, multiple).

2. The seven identified +NBEs (in coincidence with single pulse blue flashes) occur simultaneously (within error, see Table 2) with five ICs and two CGs lightning as labeled by GLD360. However no concurrent 777.4 nm optical emissions were detected by MMIA in any of the seven cases. Out of these seven +NBEs, the one occurring at 13:09:34.8905 UTC (fourth blue dashed line from the left, see Figure 6.2) precedes 7 successive IC lightning (out of a total of 79 strokes detected by GLD360 in the area of study), probably initiating a seven-stroke lightning flash in agreement with recent results suggesting that $\sim$ 10 % of IC lightning flashes are initiated by NBEs.

3. None of the recorded (single, double or multiple pulse) blue flashes exhibit concurrent near infrared (777.4 nm) optical emissions typical of ordinary lightning. It was found that the 777.4 nm peak intensity in the single-pulse blue events is at least a factor 50 (or 25) below the 777.4 nm maximum (or mean) peak emissions of other discharges in the same flash.

4. A new method based on the fitting of single blue optical flashes detected by ASIM has allowed us to estimate the depth below cloud top of the events occurring inside thunderstorm clouds. The optically derived event altitudes - ranging between $\sim$ 1.7 km and $\sim$ 6.5 km below a CTH of $\sim$ 14-15 km as recorded by the FY-4A satellite - are found to be consistent with heights (11 - 14 km) resulting from the analysis

of VLF / LF signals of concurrent positive NBEs detected by ground-based VLF stations. The method developed here is generally valid for single optical pulses (no matter the color) associated to events occurring inside (or almost) the clouds so that photons are affected by scattering and absorption in the cloud.

5. The consistent source altitudes derived by optical and radio signal analysis indicate that the detected single blue flashes are due to optical emissions of streamers occurring in corona discharges forming positive NBEs as suggested from simultaneous (within error) VLF / LF sferics detected by ground-based stations. Double and multi-pulse blue flashes might also be due to deep in the cloud pure (with no lightning leader) cloud coronas or lightning leaders and corona streamers with the 777.4 nm optical emission being absorbed in its way to the detector through the cloud water droplets and ice.

5.2 Second article

1. Streamer corona discharges in thunderclouds are relatively common as observed by ASIM-MMIA. Thus, thundercloud streamer corona discharges, which can occur continuously in the vicinity of ordinary lightning strokes, but also in isolation, may be a critical upper troposphere source of greenhouse gases such as N_2O and O_3, and of oxidant gases like OH and HO_2, in convectively active areas that deserves further detailed studies.

2. Our global and seasonal nighttime thundercloud streamer corona distributions, zonal and meridional averages, and nighttime variability provide the first worldwide view of coronas occurring in thunderstorms.

5.3 Third article

1. We have found in this study that approximately ~ 10 % to ~ 12 % of all BLUEs detected globally are impulsive single pulse ones. However, there can still be ambiguous (mostly not impulsive) single pulse events with $R^2 < 0.75$. A systematic analysis has been undertaken to determine the geographical (zonal and meridional) distribution of key properties of BLUEs including impulsive single pulse ones. In particular, our analysis focussed on quantifying their altitudes and depths below thundercloud tops, characteristic rise and total duration times, peak power density, total brightness, vertical extension and number of streamers.

2. Our study concludes that the over detection (concentrated between 1 September 2018 and 31 March 2019) of BLUEs shown in Soler et al. (2021) in the high latitudes of the northern and southern hemispheres was caused by a combined effect of (i)

an update in the ASIM-MMIA cosmic rejection algorithm software (ON only over the SAA before March 2019, ON everywhere after March 2019), (ii) cosmic rays and the particle flux from the inner radiation belts detectable in the SAA and in the high latitudes of the northern and southern hemispheres.

3. As a consequence of this, two new worldwide annual average (and seasonal) distributions of nighttime BLUEs were generated and presented here using global ASIM-MMIA level 1 (calibrated) data in a different two-year period (1 April 2019 - 31 March 2021) shifted seven months ahead with respect to the earlier two-year period explored in Soler et al. (2021). While the first global average distribution (GD-1) of BLUEs is derived using exactly the same algorithm described in Soler et al. (2021), the second distribution (GD-2) removes events in all planet (including the SAA) with rise time (τ_{rise}) $\leq$ 40 μs and total duration (τ_{total}) $\leq$ 150 μs. This remarkably removes the SAA shadow in GD-1 but can also underestimate the number of BLUEs in South America and, consequently, the total number of BLUEs that could range between the $\sim$ 26,500 obtained for GD-2 and the $\sim$ 46,000 counted for GD-1.

4. Two distinct populations of BLUEs with peak power density $<$ 25 μWm^{-2} (common) and $\geq$ 25 μWm^{-2} (rare) are observed. While BLUEs with small to moderate ($<$ 25 μWm^{-2}) peak power can occur over land and the maritime regions, BLUEs with large ($>$ 50 μW/m^2) peak power occur scattered across all latitudes and longitudes mainly over land.

5. BLUEs are globally found between the cloud tops and $\sim$ 4 km below cloud tops in the tropics and $\leq$ 1 km in mid and higher latitudes. Fast rise time ($<$ 0.05 ms) BLUEs with short ($<$ 0.5-0.6 ms) total times occur (across all latitudes and longitudes) very superficially ($<$ 1 km) near cloud tops with high power density $\geq$ 100 μWm^{-2}. BLUEs with peak powers below 50 μWm^{-2} have longer ($>$ 50 μs) rise times and longer ($>$ 0.5 ms) durations.

6. Zonal distributions show that BLUEs concentrated within the tropics exhibit rise and total times ranging from 50 μs up to 0.5 ms, and from 0.8 ms up to $\sim$ 4 ms, respectively. Complementarily, meridional distributions show that BLUEs in the three chimneys exhibit roughly the same rise and total duration times with the Europe/Africa chimney being the one with slightly faster rise times and shorter durations.

7. The vertical length of BLUEs as well as their number of streamers are two interesting features of in-cloud corona discharges that have also been characterizated and geographically analysed in this work. The vertical extension of most impulsive single pulse BLUEs changes between $\sim$ 100 m and $\sim$ 1500 m with a group of longer (up to $\sim$ 4-5 km) BLUEs located within the tropics in the three main BLUE chimneys especially visible in GD-2.

8. The obtained climatology for the features of BLUEs opens the door to investigate the relationship between characteristics of BLUEs and meteorological parameters. The observed variability in some features of BLUEs, such as their depth, number of streamers, the rise time and the total duration of their optical pulses, indicates that they can be influenced by some meteorological parameters like the convective available potential energy (CAPE)(see Figure 7.17 in the supplementary material of Soler et al. (2021), and Husbjerg et al. (2022)). These findings suggest that monitoring the occurrence and the features of BLUEs could serve as an indicator to characterize severe weather (deep convection episodes) (Liu et al., 2018; Soler et al., 2021; Husbjerg et al., 2022). In particular, Husbjerg et al. (2022) show difference in convection levels for lightning producing storms and BLUE producing storms.

9. Recent airborne observations (Brune et al., 2021) and laboratory experimental results (Jenkins, Brune, and Miller, 2021) indicate that considerable amounts of oxidant species (OH, HO_2) could be directly produced by visible and subvisible (corona) electrical discharges in thunderstorm anvils and not only be the indirect result of atmospheric chemical processes after the injection of lightning NO_x (Schumann and Huntrieser, 2007; Finney et al., 2016; Gordillo-Vázquez et al., 2019). The production of OH and HO_2 recently reported by Jenkins, Brune, and Miller (2021) could also be due to air plasma streamers in corona discharges occurring in thunderstorm anvils (Zahn et al., 2002; Minschwaner et al., 2008; Bozem et al., 2014; Pérez-Invernón et al., 2019; Gordillo-Vázquez and Pérez-Invernón, 2021) since thundercloud coronas (Soler et al., 2020; Li et al., 2021; Liu et al., 2021a) are now known to be more frequent (about 10 per second worldwide) (Soler et al., 2021) than previously suspected. Corona discharges in thunderclouds are especially frequent in the Tornado alley in North America (Soler et al., 2021) where airborne observations by Brune et al. (2021) have recently reported significant regional transient enhancements of OH and HO_2 concentrations during thundercloud electrical activity.

10. In summary, the geographical (and seasonal) distributions of BLUEs and all their characteristics presented here (including the knowledge of the altitude distribution of impulsive single pulse BLUEs and their number of streamers) can be critical parameters to explore how corona discharges in thunderclouds could contribute to the global chemical budget of important oxidant species like OH and HO_2, and key greenhouse gases such as ozone (O_3) and nitrous oxide (N_2O) in the climate sensitive region of the upper troposphere and lower stratosphere region.

Chapter 6

First article: "Blue optical observations of narrow bipolar events by ASIM suggest corona streamer activity in thunderstorms"

Published in *Journal of Geophysical Research - Atmospheres*, 2020

DOI: https://doi.org/10.1029/2020JD032708

Authors

S. Soler[1],F. J. Pérez-Invernón[1,2],F. J. Gordillo-Vázquez[1],A. Luque[1],D. Li[1], A. Malagón-Romero[1],T. Neubert[3],O. Chanrion[3],V. Reglero[4],J. Navarro-González[4],G. Lu[5],H. Zhang[6],A. Huang[7],N. Østgaard[8]

Affiliations

[1] Instituto de Astrofísica de Andalucía (IAA-CSIC), Glorieta de la Astronomía s/n, 18008 Granada, Spain [2]Deutsches Zentrum für Luft- und Raumfahrt, Institut für Physik der Atmosphäre, Oberpfaffenhofen, Germany [3]National Space Institute, Technical University of Denmark (DTU Space), Kongens Lyngby, Denmark [4]Image Processing Laboratory, University of Valencia, Valencia, Spain [5]Key Laboratory of Geospace Environment, Chinese Academy of Sciences, University of Science and Technology of China, Hefei, China [6]Key Laboratory for Middle Atmosphere and Global Environment Observation, Institute of Atmospheric Physics, Chinese Academy of Sciences, Beijing, China [7]Duke University, Electrical and Computer Engineering Department, Durham, NC, United States [8]Birkeland Centre for Space Science, Department of Physics and Technology, University of Bergen, Bergen, Norway

Key Points

- ASIM has detected blue flashes associated with positive Narrow Bipolar Events. No simultaneous lightning 777.4 nm emission was recorded
- Source altitudes derived from optical and radio signals agree and locate blue flash sources between 8.5 km and 14 km inside the cloud
- Observations suggest that blue flashes are due to streamers, and that positive Narrow Bipolar Events are cloud coronas with many streamers

6.1 Abstract

While narrow bipolar events (NBEs) could be related with lightning initiation, their intrinsic physics remains in question. Here we report on optical measurements by the Atmosphere-Space Interactions Monitor (ASIM) on the International Space Station (ISS), of blue flashes associated with NBEs. They are observed in a narrow blue band centred at 337.0 nm, with no simultaneous activity at 777.4 nm, considered a strong lightning emission line. From radio waves measured from the ground, we find that 7 of 10 single pulse blue events can be identified as positive NBEs. The source altitudes estimated from optical and radio signals agree and indicate that the sources of the blue flashes are located between $\sim$ 8.5 and $\sim$ 14 km, in a cloud reaching 14-15 km altitude. The observations suggest that single pulse blue flashes are from cold ionization waves, so-called streamers, and that positive NBEs are corona discharges formed by many streamers.

Plain Language Summary

A special type of cloud electrical discharges called narrow bipolar events (NBEs) could be related with lightning initiation but their intrinsic physics remains in question. Here we report on optical measurements by the Atmosphere-Space Interactions Monitor (ASIM) on the International Space Station (ISS), of blue flashes associated with NBEs. They are observed with no simultaneous optical emissions from regular lightning. From radio waves measured from the ground, we find that 70 % of the detected single pulse blue events can be identified as positive NBEs. The source altitudes estimated from optical and radio signals agree and indicate that the sources of the blue events are located between $\sim$ 8.5 and $\sim$ 14 km inside the thundercloud. The observations suggest that single pulse blue flashes are from cold ionization waves, so-called streamers, and that positive NBEs are corona discharges formed by many streamers.

6.2 Introduction

In 1980, Le Vine (1980) first detected strong radio-frequency (RF) sources from intracloud (IC) electrical discharge processes characterized by short-duration (10 - 30 μs) bipolar sferic waveforms detected in very low frequency (VLF) / low frequency (LF) (10 kHz-400 kHz) and usually accompanied by strong very high frequency (VHF) (30 - 300 MHz) radiation bursts called compact intracloud discharges (CIDs) or Narrow bipolar events (NBEs) (Smith et al., 1999). Because of the substantial NBE sferic strength, they can be radio detected at hundreds of km distance (Rison et al., 2016). CIDs are also named strong transionospheric pulse pairs (TIPPs) as they were originally recorded by the VHF receivers aboard the ALEXIS satellite (Holden, Munson, and Devenport, 1995). The acronym TIPPs is based purely on the appearance of the VHF pulse recorded on a

satellite above the ionosphere containing a distinct double pulse which indicates an elevated intracloud source. TIPPs are not uncommon in-cloud events, being approximately half of all VHF events collected by the Fast On-orbit Recording of Transient Events (FORTE) satellite launched in 1997 (Light and Jacobson, 2002). The impulsive NBE events (or weak TIPPs) seen in the VLF / LF range are still typically 10 times more powerful than the emissions from normal lightning discharges at high frequencies (HF) (3 - 30 MHz) (Smith et al., 1999). The extensive FORTE VHF recordings distinguished between impulsive events (TIPPs) and non-impulsive events, the so-called "non-TIPPs", that include both cloud-to-ground (CG) and in-cloud lightning signals such as IC events (Light and Jacobson, 2002). Fast positive and negative breakdown cause NBEs and NBEs can initiate normal IC lightning (Rison et al., 2016), (Tilles et al., 2019). Recent results suggest that $\sim$ 10 % of IC lightning are initiated by NBEs and the rest are triggered by very fast (typically less than 0.5 μs) VHF pulses with no obvious spatial development (Lyu et al., 2019). Note that the terms regular or normal lightning are used hereinafter with the meaning of lightning flashes with durations of a few tens of milliseconds to several seconds with hot leader channels rather than such processes as isolated NBEs which last a few tens of microseconds or the continuous breakdown in overshooting tops.

Jacobson et al. (2013) reported dim optical detections from NBEs by a wideband (0.4 - 1.1 μm) photodiode detector (PDD) sampling at 66 kHz (15 μs) on-board the FORTE satellite. These dim satellite-based NBE optical recordings produced a peak optical radiance (at 825 km altitude) above the effective trigger threshold of 350 μW m^{-2} corresponding to $\sim 3 \times 10^8$ W of peak optical isotropic power at the top of the cloud (Jacobson and Light, 2012). Because of the wideband (700 nm) filter used, Jacobson et al. (2013) were not able to distinguish the characteristic color of NBE optical emissions. More recently, Chanrion et al. (2016) reported profuse activity of blue electrical discharges at the top of a thunderstorm observed from the International Space Station (ISS).

In this paper, we present the first pure - only 337.0 nm (hereafter called blue for easiness) - pulse-like discharge observations recorded by the Modular Multispectral Imaging Array (MMIA) of the Atmosphere-Space Interactions Monitor (ASIM) aboard the ISS during its flyby over a very active thunderstorm on 14 May 2019 in Indonesia. We first show that the detected in-cloud optical flashes are only seen in the narrowband photometer centred at 337.0 nm with peak optical radiances below 25 μW m^{-2}, that is, between 14 and 15 times less than the 350 μW m^{-2} effective trigger threshold of the PDD on-board the FORTE satellite. We then go on to show VLF / LF radio detections (using a sampling frequency of 1 MHz) of positive NBEs that occur in coincidence with single pulse blue optical flashes recorded by ASIM. The source altitudes of NBEs associated with single pulse blue optical flashes are determined by analysis of ground and sky radio waves (Smith et al., 2004) and by a novel method based on the fitting and analysis of

the MMIA optical (photometric) signals. Finally, we conclude that the detected positive NBEs occurring inside thunderclouds are caused by fast (10 - 30 μs) positive breakdown (Rison et al., 2016) accompanied by distinct bluish optical emissions (337.0 nm) of corona discharges formed by many streamers with no measurable red (777.4 nm) light emissions typical of lightning. While double and multiple pulse blue flashes detected by MMIA are briefly discussed in this paper, we focus our discussion, analysis and conclusions on single pulse blue flashes.

6.3 Observation of blue flashes and lightning

The blue emissions occurred during a very active thunderstorm on 14 May 2019 over Indonesia. Figure 6.1 shows the cloud top height (CTH) - up to 14-15 km - derived from measurements by the Fengyun-4A (FY-4A) satellite launched on 11 December 2016 and located at 105° East longitude observing the Indian Ocean. The CTH retrieved by FY-4A has a vertical resolution of 1 km (Tan et al., 2019). FY-4A is the first of a new generation of Chinese geostationary meteorological satellites (Yang et al., 2017). FY-4A delivers imagery every 15 minutes from the 14 spectral channels of the Advanced Geosynchronous Radiation Imager (AGRI) (Zhang et al., 2018). A repeat cycle of 15 min for full-disk imaging provides multispectral observations of rapidly changing phenomena like, for instance, deep convection.

A total of 30 blue events of different types (single, double and multiple pulse) were recorded by MMIA in a relatively short period of time between 13.09.21.4903 and 13.09.54.8739 Coordinated Universal Time (UTC) on 14 May 2019 in a thunderstorm over the island of Sumatra (Indonesia). Figure 6.1 shows the cloud-to-ground (CG) lightning activity in the region of interest together with the single pulse (large squares), and double and multiple pulse (small squares) blue flashes forming a cluster and an isolated double pulse blue event appearing to the upper left of the cluster (see top panel of Figure 6.1). All blues occur in a region of cloud tops of $\simeq$ 14 - 15 km. The blue flashes recorded by MMIA exhibited an occurrence rate of $\sim$ 48 per minute (almost one per second).

The short time interval during which blue flashes were detected together with their spatial distribution based on clustering is in agreement with previous findings by Jacobson and Heavner (2005) in connection to the spatial relationship between CGs and NBEs and to the fact that the occurrence of NBEs tends to cover less of the spatial extent or temporal lifetime of the thunderstorm (Jacobson and Heavner, 2005). We found that there are no neighbor CG lightning discharges in the 10 ms preceding or following the blue flashes (Jacobson and Light, 2012). In addition, by looking at Figure 6.1 one can not consistently confirm the spatial correlation between blue flashes and CGs. In addition,

if we look at Figure 6.2 we cannot confirm that a sequence of CGs is the cause or the consequence of a blue event. This was also found by Jacobson and Heavner (2005) in the case of NBEs detected during the 4 year (1999 - 2002) operation of Los Alamos Sferic waveform Array (LASA) in Florida.

Some key features of the 10 single pulse blues recorded by ASIM are shown in Table 1. The illuminated cloud top area of the blue events ranges between $\sim$ 24 km^2 and $\sim$ 131 km^2 with a variable number of active pixels between 149 and 819. The number of pixels of the transient blue events are determined by choosing pixels (with an area of $\sim$ 0.16 km^2) with a threshold value of 20% of the maximum and 2 times the minimum pixel value (2×55 μW /(m^2 sr)). The total duration time of the photometer signal is obtained from the first-hitting model fit function (see next section) as the time since the fit starts until the value of the fit when it decays to 10 % of its maximum value or it is lower than the noise level value (0.5 μW/m^2). The rise time is the time since the fit function starts until it reaches its maximum. On the other hand, the single blue events rise time, defined as the time up to the maximum, changes between 0.14 ms and 0.48 ms. The peak brightnesses as seen by the 337.4 nm photometer in μW/m^2 varies by a factor of 2.8 (between 7.76 μW/m^2 and 21.67 μW/m^2). In the same period of time the peak brightnesses of regular lightning scale from about 1 μW/m^2 to about 64 μW/m^2. The cloud-top surface-averaged brightnesses change between 15.2 MR and 299 MR. Note however that for quantifying the peak brightness in Rayleighs we considered the illuminated cloud top area shown by the 337.0 nm camera, which will differ from the emitting area of the blue discharge.

The total duration of recorded single blue events changes between 1.60 ms and 3.60 ms while the duration of double and multi-pulse blue flashes can be of $\sim$ 14 and $\sim$ 8 ms, respectively. We have observed that the typical individual pulse contained in double- and multiple-pulse events lasts longer than the typical isolated pulse, suggesting that double- and/or multiple-pulse events either have a deeper source or are produced by discharge mechanisms with significantly longer time scales.

There were a total of 1360 lightning strokes reported by Vaisala GLD360 within a 5 minute interval (from 13.07 UTC to 13.12 UTC) in an area (from -1.6° latitude, 97° longitude to 3.4° latitude, 102° longitude) of the thunderstorm region within a square of 5° $\times$ 5° around the detected blue events. The ground-based Vaisala GLD360 global lightning network detected 1360 lightning strokes and classified 359 as CG and 1001 as IC.

Figure 6.2 shows a temporal sequence of single pulse blue events (vertical dashed lines) and the cumulative number of IC (green dots) and CG (red dots) lightning strokes as classified by GLD360 occurring in a square centered in the centroid of the detected blue

flashes (see caption of Figure 6.2 for details). Figure 6.2 also shows the cumulative number of 777.4 nm flashes detected by the MMIA 777.4 nm photometer between 5 seconds before the first single pulse blue flash and 5 seconds after the last single pulse blue flash.

As seen in Figure 6.2, most of the MMIA detected single blue events do not exhibit a clear predecessor or successor CG with most blue flashes being temporally isolated with respect to CG strokes. There are two single-pulse blue flashes classified as +NBE at 13:09:46.7538 UTC and 13:09:54.8739 UTC that seem to occur simultaneously (within error, see Table 2) with two CG lightning strokes as classified (possibly misclassified) by GLD360, but no concurrent 777.4 nm optical emissions were detected by MMIA.

The seven identified +NBEs (in coincidence with single-pulse blue flashes) occur simultaneously (within error, see Table 2) with five IC and two CG lightning strokes as classified by GLD360. However, no concurrent 777.4 nm optical emissions were detected by MMIA in any of the seven cases. Out of these seven +NBEs, only the one occurring at 13:09:34.8905 UTC (fourth vertical dashed line from the left, see Table 2) seems to initiate 7 successive IC lightning out of a total of 79 GLD360-detected IC strokes in this time interval and spatial area (see caption of Figure 6.2) in agreement with recent results suggesting that $\sim$ 10 % of IC lightning strokes are initiated by NBEs (Lyu et al., 2019).

As mentioned before from looking at the GLD360 data, there are eight GLD360 strokes (seven classified as IC and one classified - possibly mis-classified - as CG) within 15 km and up to 750 ms after the fourth blue flash. These strokes probably belonged to an IC flash which was initiated by the positive NBE associated with this fourth blue flash, which means the light emissions from these strokes were probably about the same location in the cloud as the blue flash. Figure 6.2 indicates that there were 777.4 nm emissions detected from these strokes. This suggests that 777.4 nm emissions from these strokes were able to get out of the cloud, but no 777.4 nm emission from the blue flash was able to get out of the cloud. This has allowed us to put limits on the 777.4 nm emissions from the blue flash compared to the other strokes in this flash. We found that the maximum 777.4 nm peak intensity in this period was $\sim 17\ \mu W/m^2$. Considering that the noise level of the red photometer is $\sim 0.35\ \mu W/m^2$, the 777.4 nm peak intensity in the blue event is at least a factor 50 (or 25) below the 777.4 nm maximum (or mean) peak emissions of other discharges in the same flash. The factor 25 is derived considering that the 777.4 nm optical emission peaks barely above ($2\ \mu W/m^2$) the noise. These factors 50 and 25 are in agreement with streamer spectra recorded at 25 mbar in air (equivalent to $\sim$25 km altitude) showing that the blue near-ultraviolet optical emissions of the second positive system (SPS) of N_2 dominates over a small (almost indistinguishable) trace of the 777.4 nm line that is less than 1% of the SPS of N_2 (Ebert et al., 2010) as we comment in section 5.

There is a continuous CG and IC lightning occurrence in the nearby (several milliseconds) times when single blue flashes are detected by ASIM. This is consistent with the findings by Wu et al. (2011) reporting that ± NBEs occur in relative temporal isolation with respect to normal lightning discharges.

The detected transient events in this study are pure blue events, that is, there was no detectable 777.4 nm optical emissions typical of ordinary lightning. As previously mentioned, the duration of the single-pulse blue optical emissions is between 1.60 ms and 3.60 ms. Figure 6.3 shows three representative examples of the types of blue events recorded with ASIM. An example of a single-pulse blue event lasting about 3.5 ms is shown in the top panel of Figure 6.3. The middle and bottom panels of Figure 6.3 illustrate the temporal durations (photometer), shape and appearance (image) of, respectively, a double and a multi-pulse blue event with "long" durations of 14 and 8 ms, respectively. The ASIM photometer signal of a single-pulse blue flash shown in the top panel of Figure 6.3 is fitted with a distribution function (orange line) resulting from considering the process of scattering and absorption (see next section) experienced by photons traveling through the cloud.

6.3.1 Derivation of altitudes from photometer signals

The temporal profile of optical emissions emanating from deep within a cloud is dominated by the time of multiple photon scattering by cloud droplets and ice crystals (Light et al., 2001; Thomason and Krider, 1982). Under the assumptions that the optical pulse is impulsive and localized, that the cloud is homogeneous and bounded above by a plane, and that the photons exit the cloud isotropically, with scattering outside the cloud being negligible, one can derive a simple expression for the signal registered by a photometer above the cloud top. As we see below, this expression provides a rough estimate of event altitudes.

If the source is far from the cloud boundary, the photons experience so many scattering events before exiting the cloud that their transport is well approximated by a diffusive process with a diffusion coefficient $D = \Lambda c/(3(1-g\omega_0))$ (Koshak et al., 1994), where Λ is the photon mean free path, c is the speed of light, g is the scattering assymetry parameter and ω_0 is the single-scattering albedo. Since the radius of the cloud droplets is much larger than the optical wavelengths of interest, one can assume an extinction efficiency of two (Van der Hulst, 1981) and express the mean free path as $\Lambda = (2\pi r^2 n)^{-1}$ with r being the radius of scatterers and n their concentration. The single-scattering albedo ω_0 denotes the probability that a photon is re-emitted after a scattering event, and under our conditions it is close to unity. Nevertheless, over the course of many collisions a photon may accumulate a nonnegligible probability of being absorbed. We express this by means of an absorption rate $\nu = c(1-\omega_0)/\Lambda$. However, the signal decay is not only

determined by absorption in scattering events but also by photons leaving the cloud from the lower and lateral boundaries. Hence, we consider an effective decay rate ν which is a model parameter derived from the photometer curve.

The time profile of the signal is then determined by the probability distribution of the time that it takes a diffusing and weakly absorbed particle to reach a plane at a distance L from its starting point. In our case L is the distance from the event to the cloud top. This problem belongs to the family of first-passage (or first-hitting-time) problems and can be solved by standard methods of statistical physics (see e.g. Krapivsky, Redner, and Ben-Naim (2010)). The solution reads

$$f(t) = \frac{\theta(t-t_0)e^{2\sqrt{\nu\tau}}}{\tau\sqrt{\pi}} \left(\frac{\tau}{t-t_0}\right)^{3/2} e^{-\tau/(t-t_0)-\nu(t-t_0)}, with \int_{-\infty}^{\infty} f(t)dt = 1 \qquad (6.1)$$

where θ is the step function, t_0 is the emission time and $\tau = L^2/4D$ is the characteristic time of the process. Given a photometer signal, one can fit it to (8.1) and obtain values for the parameters t_0, τ and ν. Then the depth of the event can be estimated as $L = (4D\tau)^{1/2} \approx (4\Lambda c\tau/(3(1-g)))^{1/2}$. In this work we used $g = 0.87$ (Thomason and Krider, 1982) and $\Lambda = 4$ m to 16 m, corresponding to a droplet concentration $n = 10^8$ m^{-3} and radii $r = 10$ μm to 20 μm (Thomason and Krider, 1982), which correspond to a range of the diffusion coefficient D from 3×10^9 to 12×10^9 m^2 s^{-1}. The resulting values of L are listed in Tables 1 and 2. Note that for our purposes the optical properties of water and ice are close enough to ignore their difference.

It is worth mentioning that the distribution shown in equation (8.1) could be applied to any type of single-pulse light emission sources inside clouds other than those only emitting in the near ultraviolet (337.0 nm). For example, it could be applied to lightning pulses usually recorded in the 777.4 nm optical range. This will allow an estimation of the altitude where different lightning sources are located in thunderclouds and a comparison with other procedures like the use of lightning mapping arrays (LMAs), interferometric or VLF techniques. In this study, we compare the relative to cloud top altitudes derived by optical fit with the altitude of associated positive NBEs detected by the Melaka VLF ground-based station (see Table 1).

The above analytic equation 8.1 is consistent with a full scattering model of lightning optical emissions (Luque et al., 2020) that simulates how a satellite observes optical radiation emitted by a lightning flash after it is scattered within an intervening cloud. This model is specifically tailored to modern instruments such as the MMIA component of the ASIM that operates from the ISS but can also be used in a wider context of lightning scattering.

6.4 Ground-based radio detection

For the comparison with VLF detections, we focus our analysis on single pulse blue flashes. While the time correlation between blue (337.0 nm) pulses, 777.4 nm pulses, and the GLD360 network is weak, the correlation between blue pulses and the Melaka NBE signature is excellent (about 100 μs), as shown in Table 2. Seven of the 10 single-pulse blue flashes detected by ASIM during its flyby over the Indonesian thunderstorm of 14 May 2019 occurred simultaneously (within error) to lightning detected by GLD360 and by the Melaka VLF/LF ground-based station. The analysis of the radio atmospheric signals (sferics) of IC lightning revealed that seven of them exhibited the typical fast (10 - 30 μs) bipolar shape of positive NBEs. We consider narrow single pulses having a duration of $\leq$ 4 ms. We hereafter distinguish between narrow single-pulse blue events likely associated to NBEs and regular single pulse blue events with no detected NBEs.

Table 2 shows all times at the source (referred to GLD360 lightning detections at the source) of narrow and regular single pulse blue flashes detected by MMIA and the associated +NBEs including their depths below cloud top (source altitude is determined by substracting depth from cloud top height) determined by (*i*) fitting the photometer narrow single-pulse (optical) blue flash and by (*ii*) analyzing the relative times of arrival of +NBE signal reflections (sky waves) from the ionosphere and ground waves with an uncertainty of $\pm$ 1 km (Li et al., 2019; Li et al., 2020). The table also shows the distance d of the events to the Melaka VLF / LF station derived by GLD360 location and the altitude of NBEs that was determined by calculating the time difference between the ground wave and two reflected sky waves in the VLF/LF radio signal (Smith et al., 2004). Note that d is the great-circle distance calculated by using haversine formula (Robusto, 1957) based on the position between the source provided by GLD360 and the VLF sensor.

The optical source altitudes are determined by subtracting the depth below cloud top derived by analysis of MMIA optical signals from the cloud top heights measured by FY-4A. Table 2 shows that the source altitudes derived by both methods (optical and radio) are consistent and point to source locations inside the clouds producing blue (337.0 nm) emissions with no traces of near infrared (777.4 nm) optical emissions typical of lightning.

Figure 6.4 (top panel) shows a comparison between the blue flash detected by MMIA at 13:09:54.8739 UTC (source) $\pm$ 0.1 ms and the VLF sferic waveforms - B_r (orange line) and B_ϕ (green line) magnetic field components - associated to the positive NBE detected at 13:09:54.87398350 UTC (source) $\pm$ 50 ns by the Melaka VLF / LF station. The blue flash and the positive NBE appear isolated from any other nearby cloud electrical activity. Details of the optical signal and VLF sferics of this positive NBE can be seen in

the three bottom panels of Figure 6.4 where it is shown the zoomed-in of the top panel region around the sferic of the NBE.

Both the total duration of the single-pulse blue flashes and the cloud-top illuminated area are related with the location (altitude) of the event in the cloud. In general, the larger the total duration and the illuminated area, the deeper in the cloud the events are located. On the contrary, the shorter the total duration, the higher an event is located in the cloud.

6.5 Interpretation and analysis

Energetic electrons in corona streamers occurring at upper tropospheric pressures can excite molecules, but also, depending on how high the gained energy is, electrons can dissociate and ionize ambient N_2 and/or O_2 molecules (Adachi et al., 2008; Gordillo-Vázquez, Luque, and Simek, 2011; Gordillo-Vázquez, Luque, and Simek, 2012a; Hiraki, 2010; Luque and Ebert, 2009; Luque and Gordillo-Vázquez, 2011; Parra-Rojas, Luque, and Gordillo-Vázquez, 2013; Parra-Rojas et al., 2013; Pérez-Invernón, Gordillo-Vázquez, and Luque, 2016; Williams et al., 2012).

Blue optical emissions due to, respectively, the Second Positive System (SPS) of N_2 and the First Negative System (FNS) of $N_2{}^+$ are typical of streamers and corona discharges formed by a large collection of streamers. The high reduced electric field (300 - 600 Td) in the head of streamers (Luque and Ebert, 2010; Pasko, Inan, and Bell, 1998; Stenbaek-Nielsen et al., 2010) acting during short times - from some nanoseconds (at ground pressure) to some milliseconds (at mesospheric pressure) - and the short (approximately milliseconds) glow that follows after the propagation of streamer heads can activate nonequilibrium electron-driven kinetics in the surrounding air (Gordillo-Vázquez, 2008; Gordillo-Vázquez and Donkó, 2009; Hoder et al., 2016; Parra-Rojas, Luque, and Gordillo-Vázquez, 2015; Pérez-Invernón, Luque, and Gordillo-Vázquez, 2018; Sentman et al., 2008). In particular, the production of the ^{5}P electronic state of O I, whose radiative decay produces the 777.4 nm line, can be activated by (i) electron impact dissociative excitation of O_2 ($e+O_2 \rightarrow O+O(^5P)+e$) generating ground state O I atoms and electronically excited $O(^5P)$ atoms in a non-equilibrium air plasma and (ii) direct electron impact excitation of ground state of ambient O I atoms producing electronically excited $O(^5P)$ atoms ($e + O \rightarrow O(^5P) + e$). The rate coefficients of mechanisms (i) and (ii) in air increase as the reduced electric field grows, but the production of $O(^5P)$ by dissociative excitation is always significantly higher than the one by direct electron impact excitation from ground state oxygen atoms. Therefore, depending on the ambient pressure, it could be possible that 777.4 nm optical emissions appear in well-resolved spectra of streamers. In this regard, it is worth mentioning that the recorded high-resolution spectra of sprites

at 74 km altitude ($\sim$ 0.023 mbar) only show spectroscopic features of neutral molecular nitrogen (Gordillo-Vázquez et al., 2018) with no traces of the strong 777.4 nm atomic oxygen (O I) triplet usually seen in lightning spectra in the troposphere. However, while streamer spectra recorded at 25 mbar in air (equivalent to $\simeq$ 25 km altitude) is dominated by the blue emissions of the SPS of N_2, it exhibits a small (almost indistinguishable) trace of the 777.4 nm line that is less than 1% of the SPS of N_2 (Ebert et al., 2010).

Streamers can appear in isolated corona discharges but also in the forefront of downward or upward propagating hot lightning leaders. Optical emissions of streamers in front of leaders should be accompanied by 777.4 nm emissions originated by thermal excitation of the ^{5}P electronic state of atomic oxygen in hot lightning channels. However, the single-pulse blue events reported in this paper lack a companion 777.4 nm emission. This could be due to (i) events occurring deep in the cloud so that accompanying 777.4 nm optical emissions from streamers and / or leaders are completely absorbed by cloud water droplets and / or ice since both liquid and ice water absorbtion is stronger in the near infrared (777.4 nm) than in the near ultraviolet (337.0 nm) (Hale and Querry, 1973; Warren and Brandt, 2008), (ii) the presence of low temperature (2000 K - 4000 K) leader channels that produce inefficient thermal excitation of O(^{5}P) that, consequently, produce negligible 777.4 nm emissions in comparison with prevailing blue emissions from corona streamers and / or (iii) the fact that the only source of the detected near ultraviolet (337.0 nm) optical emissions is a corona of many streamers inside the cloud and that, consequently, the 777.4 nm optical emissions are negligible.

Moreover, as shown in Figure 6.2 the NBE at 13:09:34.8905 apparently initiated seven IC strokes detected by GLD360. These strokes are almost certainly associated with hot leaders at about the same altitude as this +NBE. It is clear from Figure 6.2 that the cloud did not absorb the 777.4 nm emissions from these strokes since they were detected by MMIA. This strengthens the argument that there is little if any 777.4 nm emissions from the short-duration blue flashes. On the other hand, there is no evidence of low-temperature leaders channels which do not produce 777.4 nm optical emissions.

Having said the above, the fact that no 777.4 photometric signals are simultaneously detected with the recorded blue (337.0 nm) signal - or that the 337.0 nm and 777.4 nm cameras of MMIA show spatially separated structures - together with the derived altitudes of the discharge sources in the thunderclouds lead us to think that the recorded single-pulse blue events are the optical manifestation of corona discharges like positive NBEs occurring at different depths inside thunderclouds in the 8.5 km - 14 km range between the mid-level main negative and upper positive charge regions of thunderclouds (Bandara et al., 2019; Rison et al., 2016; Smith et al., 2004; Wu et al., 2011). Negative NBEs can occur at higher altitudes (16 - 20 km), between the upper positive charge cloud layer and the negative screening charge layer above the cloud where normal lightning

rarely occur (Smith et al., 2004; Wu et al., 2011), and might be connected to emerged blue starters (Chou et al., 2018; Liu et al., 2018) in regions with active deep convection.

6.6 Conclusions

The findings of this study are the following:

1. A succession of up to 30 blue flashes forming a cluster during about 33 seconds (almost one flash per second) were recorded by the 337.0 nm-filtered camera and photometer of the MMIA instrument on board ASIM. The detected blue events exhibit one, two or multiple optical pulses (as seen from photometric signals) lasting 1.60-3.60 ms (single) and beyond 14 and 8 ms (double, multiple).

2. The seven identified +NBEs (in coincidence with single pulse blue flashes) occur simultaneously (within error, see Table 2) with five ICs and two CGs lightning as labeled by GLD360. However no concurrent 777.4 nm optical emissions were detected by MMIA in any of the seven cases. Out of these seven +NBEs, the one occurring at 13:09:34.8905 UTC (fourth blue dashed line from the left, see Figure 6.2) precedes 7 successive IC lightning (out of a total of 79 strokes detected by GLD360 in the area of study), probably initiating a seven-stroke lightning flash in agreement with recent results suggesting that $\sim$ 10 % of IC lightning flashes are initiated by NBEs.

3. None of the recorded (single, double or multiple pulse) blue flashes exhibit concurrent near infrared (777.4 nm) optical emissions typical of ordinary lightning. It was found that the 777.4 nm peak intensity in the single-pulse blue events is at least a factor 50 (or 25) below the 777.4 nm maximum (or mean) peak emissions of other discharges in the same flash.

4. A new method based on the fitting of single blue optical flashes detected by ASIM has allowed us to estimate the depth below cloud top of the events occurring inside thunderstorm clouds. The optically derived event altitudes - ranging between $\sim$ 1.7 km and $\sim$ 6.5 km below a CTH of $\sim$ 14-15 km as recorded by the FY-4A satellite - are found to be consistent with heights (11 - 14 km) resulting from the analysis of VLF / LF signals of concurrent positive NBEs detected by ground-based VLF stations. The method developed here is generally valid for single optical pulses (no matter the color) associated to events occurring inside (or almost) the clouds so that photons are affected by scattering and absorption in the cloud.

5. The consistent source altitudes derived by optical and radio signal analysis indicate that the detected single blue flashes are due to optical emissions of streamers occurring in corona discharges forming positive NBEs as suggested from simultaneous (within error) VLF / LF sferics detected by ground-based stations. Double

and multi-pulse blue flashes might also be due to deep in the cloud pure (with no lightning leader) cloud coronas or lightning leaders and corona streamers with the 777.4 nm optical emission being absorbed in its way to the detector through the cloud water droplets and ice.

Acknowledgements

This work was supported by the Spanish Ministry of Science and Innovation, Ministerio de Ciencia e Innovación (AEI) under project ESP2017-86263-C4-4-R, PID2019-109269RB-C43 and the FEDER program. SS acknowledges a PhD research contract through the project ESP2017-86263-C4-4-R. FJPI, AL, DL and AM were supported by the European Research Council (ERC) under the European Union H2020 programme/ERC grant agreement 681257. Authors SS, FJPI, FJGV, AM and AL acknowledge financial support from the State Agency for Research of the Spanish MCIU through the "Center of Excellence Severo Ochoa" award for the Instituto de Astrofísica de Andalucía (SEV-2017-0709). ASIM is a mission of The European Space Agency (ESA). The project is funded by ESA and by national grants of Denmark, Norway and Spain. We acknowledge VAISALA for the granted access to the GLD360 global lightning dataset of great value for this work. The authors would like to thank Jiang Lingfeng of the National Satellite Meteorological Center, China Meteorological Administration, who helped preprocess related CTH data based on the data sharing proxy in Fengyun Satellite data center at `https://bit.ly/2ZxNYUT`. The authors would like to thank Mohd Riduan Ahamd of the Atmospheric and Lightning Research Lab, Centre for Telecommunication Research and Innovation (CeTRI), Fakulti Kejuruteraan Elektronik dan Kejuruteraan Komputer, Universiti Teknikal Malaysia Melaka, Hang Tuah 7 Jaya, 76100 Durian Tunggal, Melaka, Malaysia. The data that support the findings of this study are available through a persistent repository in `https://figshare.com/s/5ed963f0315dfe04f6b1`. FJPI acknowledges the sponsorship provided by the Federal Ministry for Education and Research of Germany through the Alexander von Humboldt Foundation. .

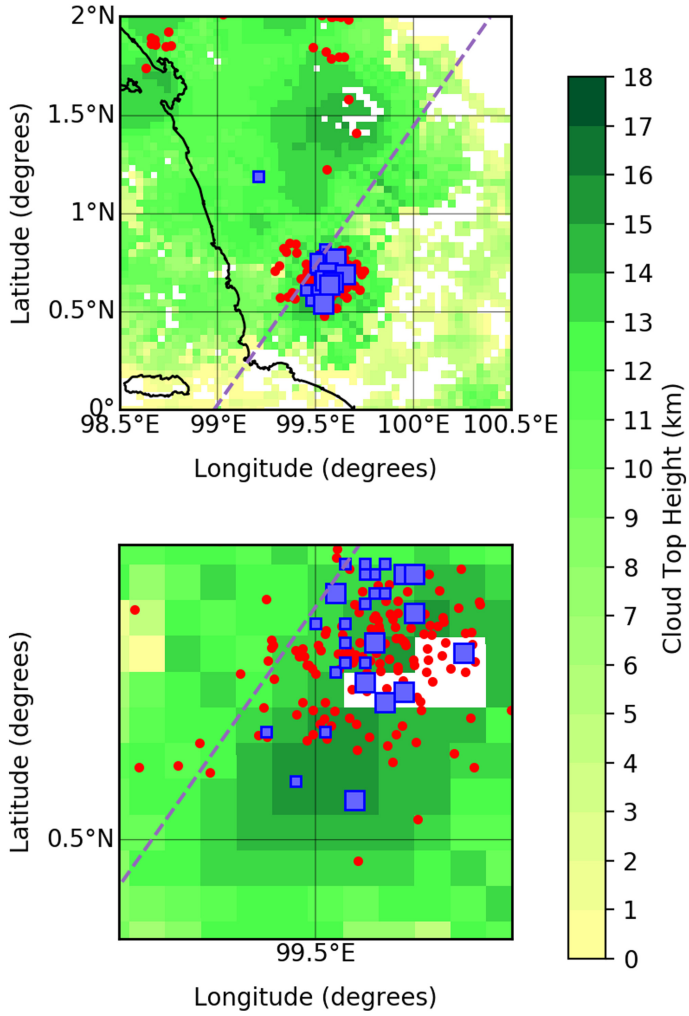

Figure 6.1. (Upper panel) Single (big blue squares), double and multiple pulse blue events (small blue squares) and cloud to ground (CG) lightning (small red dots) detected between 13:09 and 13:12 UTC by GLD360 represented over a cloud top height (CTH) map derived from (4 km × 4 km spatial resolution) measurements by the Chinese Fengyun-4A (FY-4A) geostationary meteorological satellite. (Bottom panel) zoom-in of the top panel where more details can be observed. Thundercloud CTHs between 14 km and 15 km close to the tropopause are visible. The white spots are missing values. The dashed line represents the ISS orbit.

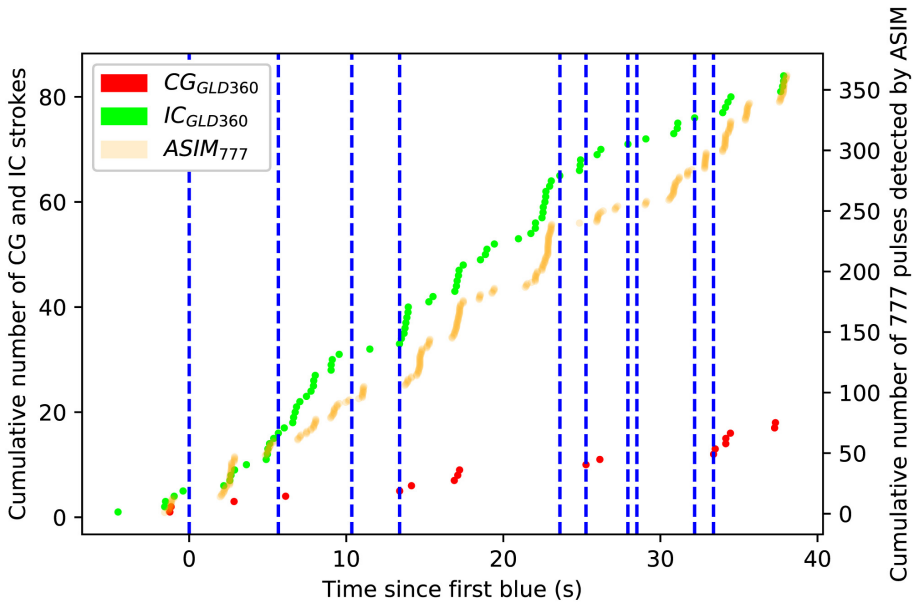

Figure 6.2. The vertical dashed lines indicate the temporal sequence of single pulse blue flashes detected by ASIM. The right axis marks the cumulative number of ASIM 777.4 nm flashes (orange dots) detected in its field of view between 5 seconds before the first single pulse blue flash and 5 seconds after the last single pulse blue event. The left axis indicates the cumulative number of cloud discharges classified by GLD360 as CG lightning strokes (red dots) and IC lightning strokes (green dots) occurring within a square of 1° side centered in the centroid of the blue events and counting between 5 seconds before the first single pulse blue flash and 5 seconds after the last single pulse blue event.

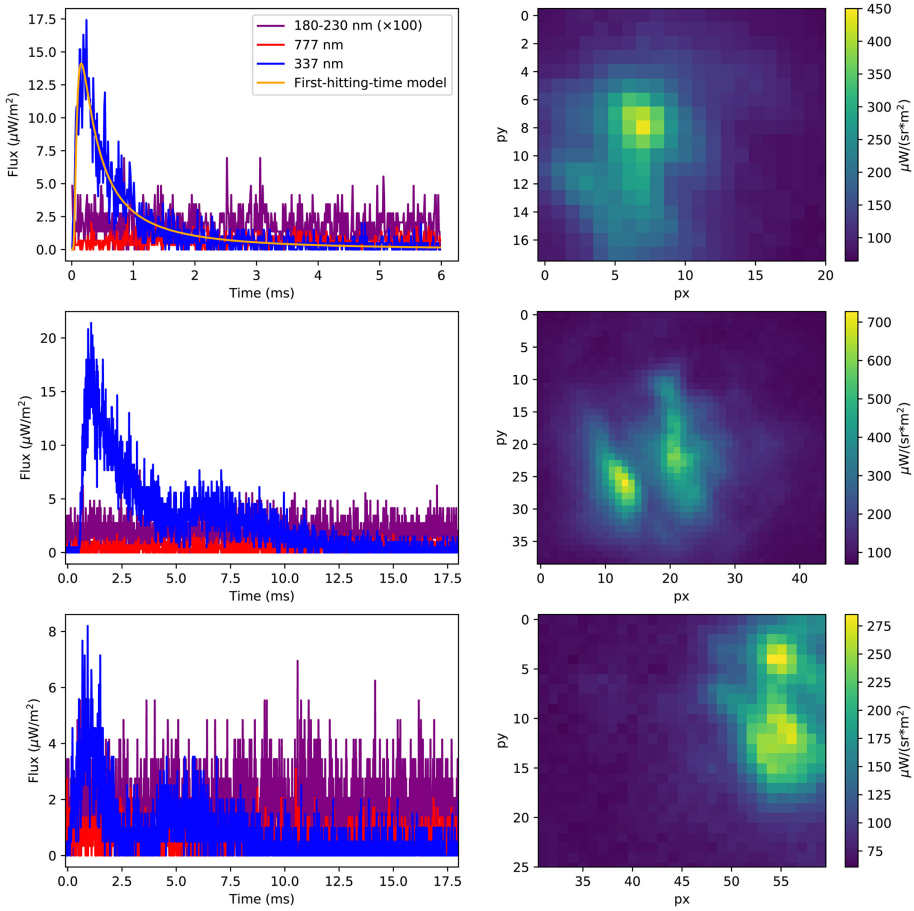

Figure 6.3. (Top panel) Photometer signal (left) and 337.0 nm image (right) recorded by MMIA at 13:09:45.0861 UTC (source) corresponding to a narrow single pulse blue event illuminating a cloud top area of 31.4 km^2. The photometric signal (blue line) is well fitted by a distribution accounting for the scattering and absorption of photons in the thundercloud (orange line). Note that the 777.4 nm signal (red line) typical of lightning is in the noise level. The 180 - 230 nm photometric signal is also represented (purple line) with a ×100 factor. (Middle and bottom panels) Photometer signals (left) and images (right) recorded by MMIA corresponding to double pulse (middle panel) and multiple pulse (bottom panel) blue flashes lasting above 14 and 8 milliseconds, respectively. Signals in the noise level are simultaneously detected in the MMIA 777.4 nm photometer and camera.

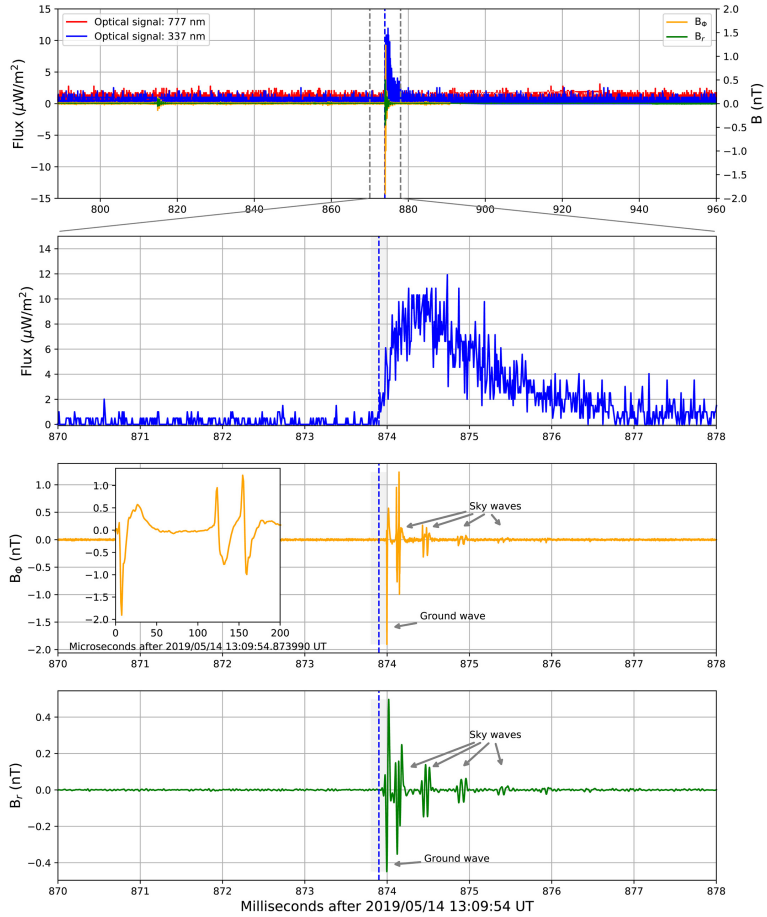

Figure 6.4. (Top panel) Comparison between the narrow single-pulse blue flash (blue line) detected by MMIA at 13:09:54.8739 UTC (source) ± 0.1 ms (shadowed region in the three bottom panels) and the VLF sferic waveforms - B_r (green line) and B_ϕ (orange line) magnetic field components - associated to the positive NBE detected at 13:09:54.87398350 UTC (source) ± 50 ns by the Melaka VLF / LF station. Note that the 777.4 nm optical signal is at the noise level. Details of the optical signal and VLF sferics of this positive NBE can be seen in the three bottom panels where it is shown the zoomed-in of the top panel region around the sferic of the positive NBE. The inset in the B_ϕ panel shows the μs time scale of the detected +NBE. The bipolar waveform of the +NBE ground wave lasts for about 25 μs.

Time (MMIA) Blue Flash UTC (Source) ± 0.1 ms	Number of Pixels / Area (km^2)	Peak Brightness ($\mu W/m^2$) / (MR)	Total Brigthness ($\mu Wms/m^2$)	Rise Time (ms)	Total Duration (ms)	L (km)
13:09:21.4903	243 / 38.9	7.76 / 65.90	7.14	0.24	2.59	2.06 - 4.13
13:09:27.1675	442 / 70.7	16.09 / 75.10	16.60	0.32	2.68	2.13 - 4.25
13:09:31.8650	488 / 78.1	8.49 / 35.90	8.55	0.27	2.80	2.33 - 4.66
13:09:34.8905	819 / 131.0	16.01 / 40.30	12.60	0.21	2.22	1.95 - 3.90
13:09:45.0861	196 / 31.4	14.44 / 15.20	8.05	0.14	1.60	1.68 - 3.37
13:09:46.7538	504 / 80.6	13.05 / 53.40	16.48	0.40	3.24	2.97 - 5.95
13:09:49.4230	149 / 23.8	21.67 / 299.00	19.94	0.24	2.59	2.35 - 4.70
13:09:49.9890	210 / 33.6	15.50 / 152.00	20.81	0.48	3.30	3.23 - 6.45
13:09:53.6693	161 / 25.8	9.20 / 118.00	7.36	0.20	2.33	2.08 - 4.17
13:09:54.8739	435 / 69.6	9.46 / 44.80	13.00	0.42	3.60	2.73 - 5.46

Table 6.1. Narrow and regular single pulse blue flashes detected by MMIA on-board ASIM. The table shows the number of pixels and area, peak and integrated photometer brightness together with the 337.0 nm photometer rise time, duration and altitude (L) below cloud top $\simeq$ 14-15 km (see Table 2) for this thunderstorm of each single pulse blue event. Note that the MMIA lightning corrected detection times at the source are found to exhibit a systematic shift of Δt = -28.7 ms ± 0.1 ms with respect to ground-based GLD360 lightning recordings at the source for the investigated thunderstorm in Indonesia. The Δt is already included in the MMIA times shown in the table. Each camera frame lasts 83 ms. Note that the sampling frequency of the photometers is 100 kHz and that the time provided by the GLD360 is assumed to be the correct time of lightning strokes, and other times are adjusted to this.

Time (GLD360) Lightning UTC (Source) ± 0.1 ms	Time (MMIA) Blue Flash UTC (Source) ± 0.1 ms	L (Optical) (km)	CTH (km)	Time (VLF) +NBE UTC (Source) ± 50 ns	H (Radio) (km)	d (Radio) (km)
	13:09:21.4903	2.06 - 4.13	14			
13:09:27.1676	13:09:27.1675	2.13 - 4.25	14	13:09:27.16753743	13	348
	13:09:31.8650	2.33 - 4.66	15			
13:09:34.8905	13:09:34.8905	1.95 - 3.90	14	13:09:34.89044770	12	345
13:09:45.0863	13:09:45.0861	1.68 - 3.36	15	13:09:45.08622757	14	351
13:09:46.7539	13:09:46.7538	2.97 - 5.95		13:09:46.75383847	11	348
13:09:49.4232	13:09:49.4230	2.35 - 4.70		13:09:49.42311687	13	354
	13:09:49.9890	3.23 - 6.45	14			
13:09:53.6694	13:09:53.6693	2.09 - 4.17	14	13:09:53.66928803	13	363
13:09:54.8740	13:09:54.8739	2.73 - 5.46	14	13:09:54.87398350	11	364

Table 6.2. Times at the source (referred to GLD360 lightning detections at the source) of seven narrow single pulse blue flashes detected by MMIA and the associated +NBEs including the source depth below the cloud top L and the altitude above sea level H determined by (*i*) fitting the photometer narrow single pulse (optical) blue flash and by (*ii*) analysing the +NBE sferic (VLF) ground and sky waves. The table also shows the specific cloud top height (CTH) in the location of the single pulse blue flash, the distance *d* of the events to the Melaka VLF/LF ground-based station derived by radio signal analysis. The times of the blue flashes are provided by the MMIA internal clock. The times of the +NBEs are determined by the Melaka VLF/LF ground-based station. Note that the MMIA lightning corrected detection times at the source are found to exhibit a systematic Δt = -28.7 ms ± 0.1 ms shift with respect to ground-based GLD360 lightning recordings at the source for the investigated thunderstorm in Indonesia. The Δt is already included in the MMIA times shown in the table. The uncertainty in H_2 is ± 1 km Li et al., 2019. CTH is the Cloud Top Height derived by the FY-4A geostationary satellite for the position of each ASIM detected single pulse blue flash. The CTH has a vertical resolution of 1 km Tan et al., 2019.

Chapter 7

Second article: "Global frequency and geographical distribution of nighttime streamer corona discharges (BLUEs) in thunderclouds"

Published in *Geophysical Research Letters*, 2021

DOI: https://doi.org/10.1029/2021GL094657

Authors

S. Soler[1],F. J. Gordillo-Vázquez[1],F. J. Pérez-Invernón[2],A. Luque[1],D. Li[1], T. Neubert[3],O. Chanrion[3],V. Reglero[4],J. Navarro-González[4],N. Østgaard[5]

Affiliations

[1] Instituto de Astrofísica de Andalucía (IAA-CSIC), Glorieta de la Astronomía s/n, 18008 Granada, Spain [2]Deutsches Zentrum für Luft- und Raumfahrt, Institut für Physik der Atmosphäre, Oberpfaffenhofen, Germany [3]National Space Institute, Technical University of Denmark (DTU Space), Kongens Lyngby, Denmark [4]Image Processing Laboratory, University of Valencia, Valencia, Spain [5]Birkeland Centre for Space Science, Department of Physics and Technology, University of Bergen, Bergen, Norway

Key points

- The first nighttime two-year climatology of streamer corona discharges (blue luminous events) in thunderclouds is presented
- Globally, the rate of blue luminous events at local midnight is $\sim$ 11 per second
- Zonal and meridional distributions of blue luminous events peak in the northern tropic and the Americas, respectively

7.1 Abstract

Blue LUminous Events (BLUEs) are transient corona discharges occurring in thunderclouds and characterized by strong 337.0 nm light flashes with absent (or weak) 777.4 nm component. We present the first nighttime climatology of BLUEs as detected by the Modular Multispectral Imaging Array (MMIA) of the Atmosphere-Space Interaction Monitor (ASIM) showing their worldwide geographical and seasonal distribution. A total (land and ocean) of $\sim$ 11 BLUEs occur around the globe every second at local midnight and the average BLUE land/sea ratio is $\sim$ 7:4. The northwest region of Colombia shows an annual nighttime peak. Globally, BLUEs are maximixed during the boreal summer-autumn, contrary to lightning which is maximed in the boreal summer. The geographical distribution of nighttime BLUEs shows three main regions in, by order of importance, the Americas, Europe/Africa and Asia/Australia.

Plain Language Summary

Blue LUminous Events are transient corona discharges occurring in thunderclouds and characterized by their distinct 337.0 nm light flashes with absent (or negligible) 777.4 nm component. We present the first two year nighttime climatology of BLUEs as detected by the Modular Multispectral Imaging Array (MMIA) of the Atmosphere-Space Interaction Monitor (ASIM) on board the International Space Station (ISS) that shows distinct worldwide geographical and seasonal distributions.

7.2 Introduction

Different observational evidence over the last 40 years suggests that cold, non-thermal streamer corona discharges are common in thunderstorms around the globe (Le Vine, 1980; Wiens et al., 2008; Bandara et al., 2019; Soler et al., 2020; Neubert et al., 2021). Fast breakdown (Rison et al., 2016; Tilles et al., 2019) suggests streamer coronas to be the cause of narrow bipolar events (NBEs). NBEs were originally detected by Le Vine (1980) in the form of strong radio frequency (RF) sources from in-cloud electrical activity. Such sources were characterized by short-duration (10 - 30 μs) bipolar sferic waveforms recorded in the very low frequency (VLF)/low frequency (LF) (10 - 400 kHz) range (Smith et al., 1999). NBEs can also appear accompanied by strong very high frequency (VHF) (30 - 300 MHz) radiation bursts.

In terms of light emissions, both impulsive and continuous streamer corona discharges in air are distinctly characterized by spectra strongly dominated by near-ultraviolet blue emissions (300 - 450 nm) corresponding to the Second Positive System (SPS) of molecular nitrogen (N_2) (Gallimberti, Hepworth, and Klewe, 1974; Grum and Costa, 1976; Ebert

et al., 2010) with its strongest transition in 337.0 nm (Gordillo-Vázquez, Luque, and Simek, 2012b; Hoder et al., 2016; Malagón-Romero and Luque, 2019; Hoder et al., 2020). Available laboratory measurements also show that red and near-infrared optical features from the First Positive System (FPS) of N_2 and the spectral contribution from oxygen atoms is negligibly small (0.5 % - 4 %) compared to N_2 SPS in both leader and leaderless streamer coronas (Gallimberti, Hepworth, and Klewe, 1974; Grum and Costa, 1976; Ebert et al., 2010). Finally, leader coronas spectra exhibit larger (double) intensity of N_2^+ First Negative System (FNS) at 391.4 nm than leaderless corona discharges (Gallimberti, Hepworth, and Klewe, 1974).

Transient (from a few to hundreds of milliseconds) bluish optical emissions from thunderstorm cloud tops were originally identified from aircraft by Wescott et al. (1995) and Wescott et al. (1996). They distinguished two types, fast upward moving jets named blue jets reaching terminal heights of 45 km - 50 km (Wescott et al., 1995), and blue starters that protrude upward from the cloud top to a maximum of $\sim$ 25 km and that were not coincident with negative or positive cloud to ground (CG) lightning strokes (Wescott et al., 1996). Multispectral video recordings show evidence that a small fraction of bluish optical emissions from both blue jets and starters are due to N_2^+ FNS (Wescott et al., 2001).

The term BLUEs can then be safely applied to in-cloud and to (partially) emerged transient electrical discharges that emit pulses of light mostly blue, that is, it could include a small fraction of red and infrared optical emissions (600-900 nm). This definition includes blue jets and starters, but also positive and negative NBEs, which are the VLF/LF radio manifestation of in-cloud streamer coronas (Rison et al., 2016; Liu et al., 2018; Tilles et al., 2019; Liu et al., 2019; Cooray et al., 2020; Soler et al., 2020; Li et al., 2021).

Optical detection of BLUEs has been increasingly efficient since the beginning of the XXI century. During the Severe Thunderstorm Electrification and Precipitation Study (STEPS) ground-based campaign in 2000 (Lyons et al., 2003), brief (33−136 ms) upward–propagating discharges called *gnomes* were filmed slightly ($\sim$ 1 km) rising out of the convective dome of a supercell storm in the Great Plains of the United States. In 2011, also from the ground, Edens (2011) reported a real color image with associated in-cloud VHF sources of a small blue starter that occurred on 4 August 2010 over an active thunderstorm in west central New Mexico. The event exhibited three diffuse streamer regions attached to leader-like channels, which appeared more white in the color image than the blue streamers emerging from the cloud top at $\sim$ 15 km and reaching a terminal altitude of $\sim$ 17 km (Edens, 2011).

Optical BLUE detections from space have been reported from the limb-pointing Imager of Sprites/Upper Atmospheric Lightning (ISUAL) onboard FORMOSAT-2 (Kuo et al., 2005; Chou et al., 2011; Kuo, Su, and Hsu, 2015; Chou et al., 2018; Liu et al., 2018). Chou et al. (2018) reported dim red emissions (623-754 nm) at the lower edge of some ISUAL detected BLUEs. A variety of BLUEs including kilometer-scale blue discharges at the cloud top layer at $\sim$ 18 km altitude, blue starters and a pulsating blue jet propagating into the stratosphere were color photographed from the International Space Station (ISS) (Chanrion et al., 2016). BLUEs have also been recently observed by the nadir-pointing MMIA onboard ASIM in the ISS since April 2018 (Soler et al., 2020; Neubert et al., 2021; Li et al., 2021).

By compositing 2 years of BLUEs data recorded by the MMIA instrument of ASIM onboard the ISS (Neubert et al., 2019) we present the first worldwide nighttime climatology of BLUEs in thunderclouds. We discuss key aspects such as average annual and seasonal distribution, regional differences, land/ocean variability, zonal/meridional distributions, and the global rate of BLUEs in local time.

7.3 Observations and Data

Observations of BLUEs were done with the MMIA high sampling rate (100 kHz) photometers in the near UV (337 nm/4 nm), tuned to the strongest line of the N_2 SPS, and in the near infrared band (777.4 nm/5 nm) for recording the atomic oxygen triplet line of lightning strokes. MMIA also incorporates a high-speed photometer in the UV (180 - 230 nm) recording part of the N_2 Lyman-Birge-Hopfield (LBH) band, and a pair of 337 nm/4 nm and 777.4 nm/5 nm filtered cameras (at 12 fps) with $\sim$ 400 m/pixel spatial resolution (Chanrion et al., 2019). An important boundary condition of this study is that MMIA observes only during nighttime.

BLUEs exhibit strong features in the 337 nm/4 nm photometer with negligible (barely above the noise level 0.4 μW/m^2) signal in the 777.4 nm/5 nm photometer, which is also continuously monitored. Once a true positive BLUE detection is confirmed, the cameras are checked for possible associated images. The climatology now presented was built with two years of worldwide MMIA level 1 (calibrated) data covering the period from 1 September 2018 to 31 August 2020.

Due to the inclination ($\sim 52^\circ$) of the ISS orbit, locations near the equator are observed less frequently than those in higher latitudes. When calculating the average global rate of BLUEs from MMIA data, the number and location of BLUE flashes observed by MMIA were computed using the observation time of MMIA (see text in Figure 7.6 in the supplementary material (SM)). The surface of the Earth was divided into $2^\circ \times 2^\circ$ grid

cells for the annual (and seasonal) geographical distributions and into 1°×1° grid cells for the annual cycle of global BLUE rate in terms of zonal and meridional distributions.

Figure 7.1 shows the appearance of three representative cases of BLUEs investigated in this global study. The top, middle and bottom panels display the temporal shape, duration and intensity of the 337.0 nm and 777.4 nm photometer light curves (left column), and the associated images in the 337.0 nm (central colum) and 777.4 nm (right column) filtered cameras. The impulsive behaviour of the 337.0 nm is clear in the three cases with peak values (and durations), from top to bottom, of ~ 15 μW/m^2 (~ 2 ms), ~ 110 μW/m^2 (~ 4 ms) and ~ 150 μW/m^2 (~ 0.3 ms). The 777.4 nm component is negligible in BLUEs displayed in the top and bottom panels, which according to their 337.0 nm light curve shape corresponds to the optical manifestation of positive (top) and negative NBEs (bottom). The event in the middle panel could be a Blue Starter exbihiting a weak (but measurable) 777.4 nm camera signal due to an upward moving leader.

7.4 Methodology

As presented in the introduction, based on what it is known about optical emisions of leaders and streamer coronas (Soler et al., 2020; Neubert et al., 2021; Li et al., 2021), and of MMIA photometer sensitivity and noise levels (Chanrion et al., 2019), an algorithm for identification of BLUEs was designed. The algorithm analyzed all the 337 nm/4 nm (blue) and 777.4 nm/5 nm (red) photometer events recorded by MMIA in the period of study. A photometer event is composed of a number N of frames (usually between 3 and 8) with a duration of ~ 83 milliseconds each. The algorithm relies on seven sequential steps that analyze the concatenated frames of an event.

1) Consider only frames of photometer events with "phot1trigger=1" (trigger of 337.0 nm photometer) regardless of other MMIA photometer triggers (details of triggering modes and MMIA-MXGS cross-triggering can be found in Chanrion et al. (2019)). 2) Given a photometer event, calculate the blue and red median values in each frame. Compute the blue and red thresholds by adding 3σ to, respectively, the means of the blue and red values below the corresponding medians. 3) If threshold values are below 1 μW/m^2, as they are commonly found, they are replaced by 1 μW/m^2 (about two or three times the noise level of the red and blue photometers). 4) Create groups defined by five or more consecutive blue counts (10 μs each) above the blue threshold. Groups separated by more than 10 milliseconds are considered different single BLUE events. 5) Given groups of blue counts, find the maximum (or peak) in each group and keep only the groups with no red sequence (above the red threshold) 15 and 5 milliseconds before and after the blue peak, respectively. 6) Disregard very weak BLUEs by requesting that the maximum blue signal is at least 3 times the blue threshold. 7) Given groups of blue

counts with red signal, keep only those events for which: (i) the red peak is above 2.5 μW/m^2 and the blue maximum is at least 10 times the red peak or, (ii) the red peak is below or equal 2.5 μW/m^2 and the blue maximum is at least 2 times the red peak. Note that 2.5 μW/m^2 was chosen as the red border value because the red signal can start to be noisy below it.

In general and in order to minimize the number of false positives, the algorithm also removes all photometer events with or without Modular X and Gamma-ray Sensor (MXGS) trigger but no MMIA trigger, both outside and over the South Atlantic Anomaly (SAA) where MMIA also operates. Note that steps 5 and mostly 7 of the algorithm already filter out a lot of false positive BLUE events in the SAA where energetic particles can trigger the photometers and usually appear in the blue and red photometers as sharp and randomly distributed events.

7.5 Results

Worldwide BLUE geographical distributions are shown in Figure 7.2, Figure 7.3 and Figure 7.4 for annual and seasonal averages, respectively. Because of the relatively short period analyzed (two years), the BLUE density maps are not fully smooth because of sampling limitations. We detected a total of about 53015 nighttime BLUEs within the ASIM-MMIA FOV. During nighttime only, ISS-LIS detected about 1.04M lightning flashes. Since ISS-LIS FOV is 2.56 times larger than MMIA FOV, we have that, during nighttime, ISS-LIS / MMIA = 1.04M /(0.053M $\times$ 2.56) = 7.7.

7.5.1 Global Annual and Zonal/Meridional Distributions

The worldwide annual average (Figure 7.2(a)) exhibit high activity BLUE spots in northern Colombia/Lake Maracaibo region (Venezuela), Peru/Bolivia border, northwestern Brazil, central Africa, northeastern Himalaya, Bangladesh and northeastern Malaysia. BLUE flash rate densities peak over northern Colombia (Santa Marta region) with values of $\sim$ 30 BLUEs km^{-2} year^{-1} (provided night and day have the same global flash rate), rather than in central Africa (with 18 BLUEs km^{-2} year^{-1}) as occur with lightning flashes (Christian et al., 2003; Blakeslee et al., 2020).

The clear bimodal peak in the zonal distribution of nighttime lightning flashes detected by the Lightning Imager Sensor (LIS) onboard the ISS (gray line in Figure 7.2(c)) is not exhibited in the zonal distribution of BLUEs, which presents an uneven three-peak equatorial structure with the highest peak in the northern tropic (blue line in Figure 7.2(c)). The meridional distribution of BLUEs (blue line in Figure 7.2(b)) clearly shows three active chimneys in the Americas, Europe/Africa and Asia/Australia. There is a fourth

chimney slightly visible around 150°W-15°S near Tahiti in Figure 7.2(a) and Figure 7.3(c) during MAM (see also Figure S11). While the nighttime lightning meridional distribution presents the largest (and sharp) peak in Eurore/Africa as shown in Figure 7.2(b) (gray line), the net contribution of BLUEs from the Americas is larger than those in the other two regions (see blue line in Figure 7.2(b).

The comparison between the annual average zonal distributions of BLUEs and nighttime lightning shows that the contribution of the tropical region between 20°S to 20°N latitude is almost a factor 3 to 4 that of the subtropics for BLUEs, while it is a factor ~ 2 for lightning, which indicates a faster (than nighttime lightning flash rate) decrease of the BLUE rate towards higher latitudes. This suggests that deeper storms give a lot more BLUEs and NBEs (Suszcynsky and Heavner, 2003; Liu, Zipser, and Nesbitt, 2007). We have used the convective available potential energy (CAPE), a reasonable good proxy of deep convection (Williams et al., 1992; Ukkonen and Mäkelä, 2019), to quantify the possible linear relationship between BLUEs and deep convection (see Figure 7.17).

7.5.2 Global Seasonal, Zonal/Meridional Distributions and Local Time Variability

The seasonal nighttime average distribution of BLUEs shown in Figure 7.3 indicates that the global BLUE electrical activity peaks during the boreal autumn (8.2 (SON), 5.9 (DJF), 6.2 (MAM) and 6.7 (JJA) BLUEs s^{-1}) while lightning peak in the boreal summer (see Figures 18 and 21). The boreal summer and spring seasons also display important worldwide BLUE activity. The months of December-February have little BLUE activity in the Northern Hemisphere that, instead, concentrates in southern America, austral Africa, Indonesia and northern Australia. The central and northern Great Plains, the Tornado alley of the United States and the Mediterranean Europe exhibit their greatest nighttime BLUE activity in the boreal fall. The Lake Maracaibo region exhibits high BLUE activity all year long except during December-February. Most BLUEs in the Indian subcontinent and the Bay of Bengal occur during the monsoon season from early June to the beginning of October. BLUEs in the pre-monsoon period (MAM) are also distinguishable in the Bay of Bengal (see Figure 7.3(c)). The nature of convection is very different in the pre-monsoon and break period, and the real monsoon season shown in Figure 7.3(d) Williams et al., 1992. See Figure S12 and further comments in the SM.

The very weak BLUE activity along the United States/Canada border (a pyroconvection region) extending to eastern and western regions in the 45°N-52°N latitude band, from the boreal autumn to spring, could be related to the United States/Canada fire season (April-October) when plenty of pyrocumulus and pyrocumulonimbus are formed (Fromm et al., 2010). However, the fact that there is no BLUE activity in the boreal summer months in that region suggests that BLUEs in that region could be connected

instead with boreal winter lightning (Montanyà et al., 2016), which are negligible in the US/Canada border during the boreal summer. Similarly, bushfire season in Australia (with significant pyroconvection activity) normally starts in July/August and extends up to March (Dowdy and Pepler, 2018) partially overlapping with the austral winter lightning season (June-August). On the other hand, the unusually intense 2019/2020 bushfire season peaked in austral summer (December 2019 / January 2020) (Schwartz et al., 2020; Liu et al., 2021b) with some (but very weak) overlapping BLUE activity to the south of Australia, which might indicate a possible BLUE connection with Australian bushfires (plus a possible austral autumn-winter lightning component).

Figure 7.4 presents the seasonal meridional (left column) and zonal (right column) nighttime distributions of the 2-year BLUE climatology (blue line) and ISS-LIS nighttime lightning (gray line). According to the meridional representation, the largest BLUE (and nighttime lightning) chimney is in the Americas during the boreal autumn and summer, but the largest BLUE chimney shifts to Asia / Australia and Europe / Africa in the boreal winter and spring, respectively. This behaviour slightly differs from that of the boreal winter and spring nighttime lightning meridional distributions, which present their largest chimney in the Europe / Africa (mostly Africa) region. The fact that the Northern hemisphere has 68% of the Earth's land by area shapes the BLUE and nighttime lightning seasonal zonal distributions. BLUEs and nighttime lightning only dominate in Southern Hemisphere during the austral summer.

As shown in Figure 7.5, on average, BLUEs peak at $\sim$ 11 flashes s^{-1} in the local midnight (00.00 local solar time), and show a decreasing global rate as local daytime approaches (and there is less MMIA observation time) characterized by a sharper slope than nighttime lightning flash rate (see Figure 7.14) for the same period. BLUEs exhibit a local midnight land/sea ratio of $\sim$ 7:4 (for $\sim$ 3:1 for lightning).

7.6 Discussion and conclusions

The ASIM-MMIA nighttime climatology of BLUEs presented in this paper is the first of its kind and complements the global frequency and 24 h lightning distribution (within $\pm$ 70° latitude) first available since 2003 (Christian et al., 2003). This was generated with data from the Optical Transient Detector (OTD), a prototype of LIS, in operation from May 1995 to March 2000. LIS was later onboard the Tropical Rainfall Measuring Mission (TRMM) also providing full day global lightning data within $\pm$ 38° latitude from early 1998 to April 2015 when TRMM was deorbited (Cecil, Buechler, and Blakeslee, 2014). More recently, since 1 March 2017, LIS is onboard the ISS providing high latitude (up to $\pm$ 52°) all-day (24 h) lightning data (Blakeslee, 2019; Blakeslee et al., 2020).

Research results through the last 40 years indicate that, in addition to lightning, kilometer scale corona electrical discharges formed by hundreds of millions of streamers (Liu et al., 2019; Cooray et al., 2020) are common in thunderclouds around the globe but their genesis (Le Vine, 1980; Smith et al., 1999; Rison et al., 2016; Tilles et al., 2019; Soler et al., 2020; Neubert et al., 2021), dynamics (Jacobson and Heavner, 2005; Wiens et al., 2008; Jacobson et al., 2013; Bandara et al., 2019; Bandara et al., 2021) and probable atmospheric chemistry impact (Shlanta and Moore, 1972; Zahn et al., 2002; Simek, 2002; Minschwaner et al., 2008; Bozem et al., 2014; Pérez-Invernón et al., 2019; Gordillo-Vázquez and Pérez-Invernón, 2021) remain to be well understood.

While the hot and thermal lightning plasma mostly excites atomic species like oxygen atoms released from thermal dissociation of O_2 leading to 777.4 nm optical emissions typical of lightning, streamer corona discharges are cold non-thermal plasmas where only heavy particles are cold and electrons are very hot. Thus corona discharges are able to activate molecular species like N_2, O_2 and H_2O by non-equilibrium electron-impact collisions (Gordillo-Vázquez et al., 2018). This underlies their different efficiencies in producing key chemical species. For instance, lightning is a key direct source of tropospheric nitride oxide (NO) that, when oxidized, produces NO_2 leading to the known lightning NO_x (LNO_x) with significant impact on tropospheric chemistry (Schumann and Huntrieser, 2007; Finney et al., 2016; Gordillo-Vázquez et al., 2019). In contrast, laboratory produced streamer coronas generate only small amounts of NO but considerable greenhouse gases such as ozone (O_3) and nitrous oxide (N_2O) (Donohoe, Shair, and Wulf, 1977; Brandvold, Martinez, and Hipsh, 1996), which is an ozone depleting gas and the third strongest greenhouse gas after carbon dioxide and methane. N_2O has the largest ($\sim$ 300 times that of CO_2 for a 100-year timescale) global warming potential of these gases (Myhre, Shindell, and Pongratz, 2014). Perturbations to concentrations of greenhouse gases affect the radiation balance more the higher the altitude of the sources. In this respect ASIM can facilitate their detection since it is more sensitive to discharges higher in the clouds.

The present results suggest that streamer corona discharges in thunderclouds are relatively common as observed by ASIM-MMIA. Thus, thundercloud streamer corona discharges, which can occur continuously in the vicinity of ordinary lightning strokes, but also in isolation, may be a critical upper troposphere source of greenhouse gases such as N_2O and O_3, and of oxidant gases like OH and HO_2, in convectively active areas that deserves further detailed studies.

Our global and seasonal nighttime thundercloud streamer corona distributions, zonal and meridional averages, and nighttime variability provide the first worldwide view of coronas occurring in thunderstorms. These results can set the path for future studies that should deepen our knowledge on key themes such as types of corona discharges in

thunderclouds, morphology (and dynamics) of optical (and radio) emissions from the heads and long-lasting glows of streamers in thundercloud coronas (Luque et al., 2016; Pérez-Invernón et al., 2020), role of meteorological conditions (Liu et al., 2021) in favoring their initiation/deactivation (Huang, Cummer, and Pu, 2021) and, finally but no less important, to explore the impact of non-equilibrium (electron driven) chemical reactions triggered by hundreds of millions of streamers in kilometer long cloud coronas (Gordillo-Vázquez and Pérez-Invernón, 2021; Brune et al., 2021) on the atmospheric chemistry of the upper troposphere and lower stratosphere.

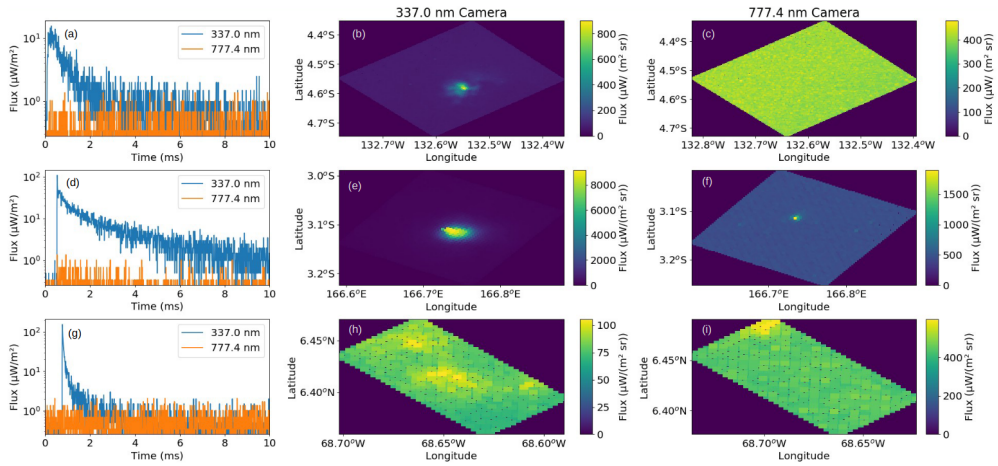

Figure 7.1. Three representative types of BLUEs investigated in this global study. The top, middle and bottom panels display the temporal shape, duration and intensity of the 337.0 nm and 777.4 nm photometer light curves (a, d, g), and the associated BLUE images in the 337.0 nm (b, e, h) and 777.4 nm (c, f, i) cameras (with 400 m pixel resolution). The impulsive behaviour of the 337.0 nm is clearly seen in the three cases while noise level signals are simultaneously detected in the 777.4 nm photometer and camera of common BLUEs (a, b, c and g, h, i panels). The (d, e, f) panels present the case of a possible Blue Starter, which include measurable 777.4 nm signals due to its leader and a 337.0 nm camera image that is saturated. The 337.0 nm light (photometer) curve of the Blue Starter hardly lasts beyond 4 ms, while the duration of the 777.4 nm light curve is about 2 ms. The three BLUEs shown occurred (from top to bottom) on 14 April 2019 at 04:49:41 UTC, 26 Feb 2019 15:10:41 UTC and 23 July 2019 at 08:15:36 in Lon, Lat (131.25°W, 4.99°S) middle of Pacific ocean, (164.60°E, 3.11°S) east of Solomon Islands, and (67.58°W, 6.01°N) north of Puerto Ayacucho in Colombia very close to the border with Venezuela, respectively.

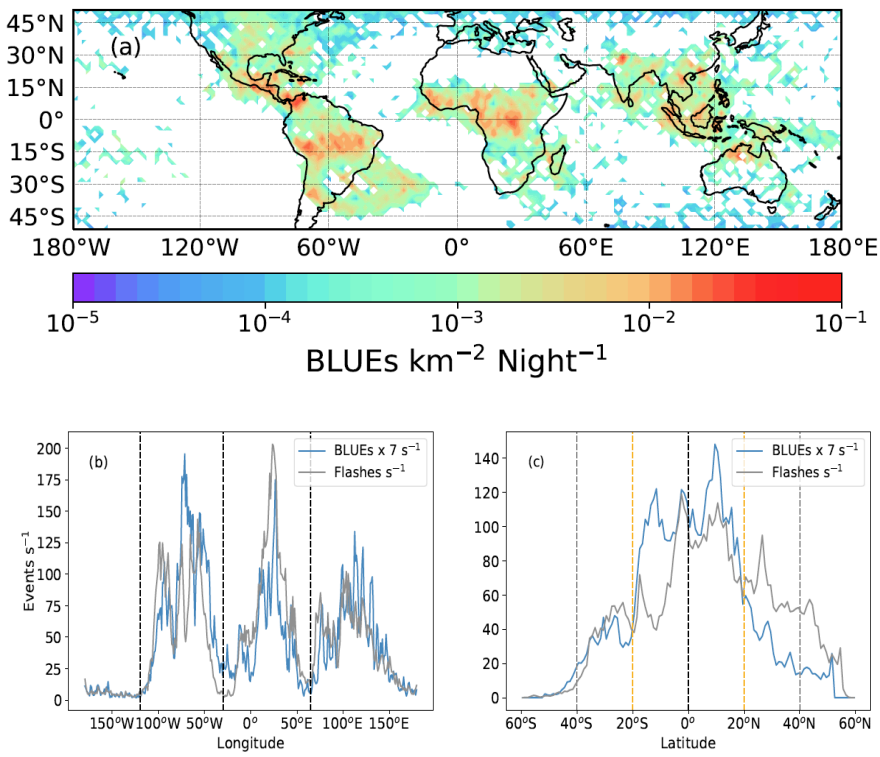

Figure 7.2. Panel (a): Two-year average (September 2018 through August 2020) nighttime climatology of global BLUE electrical activity in thunderclouds. The map is generated using 2° × 2° grid cells where the sharp pixels of the image are smoothed by drawing level lines using the python function called *contourf*. Decimal logarithm is used in the colorbar scale so that 0.08 (roughly the maximum in the map) corresponds to ∼ 30 BLUEs km^{-2} year^{-1} provided night and day have the same global flash rate. Panels (b, c): Annual cycle (for the period investigated) of ASIM-MMIA nighttime global BLUE flash rate (blue line) and ISS-LIS global nighttime flash rate (gray line) represented in meridional (b) and zonal (c) distributions. Three BLUE and nighttime lightning chimneys are clearly distinguishable in the Americas (120°W-25°W), Africa/Europe (25°W-60°E) and Asia/Australia (60°E-180°E) in the meridional distributions. There is a fourth chimney slightly visible around 150°W-15°S near Tahiti. Tropical (20°S-20°N), subtropical (40°S-20°S, 20°N-40°N) and midlatitude (60°S-40°S, 40°N-60°N) regions are indicated in the zonal distributions with dashed orange and gray vertical lines, respectively. The (b) and (c) panels were generated using 1° × 1° grid cells. A non smooth two-year average nighttime climatology map of BLUEs is shown in Figure 7.15 of the SM. Note that the global BLUE rates are scaled up 7 times for best comparison with global nighttime lightning flash rates.

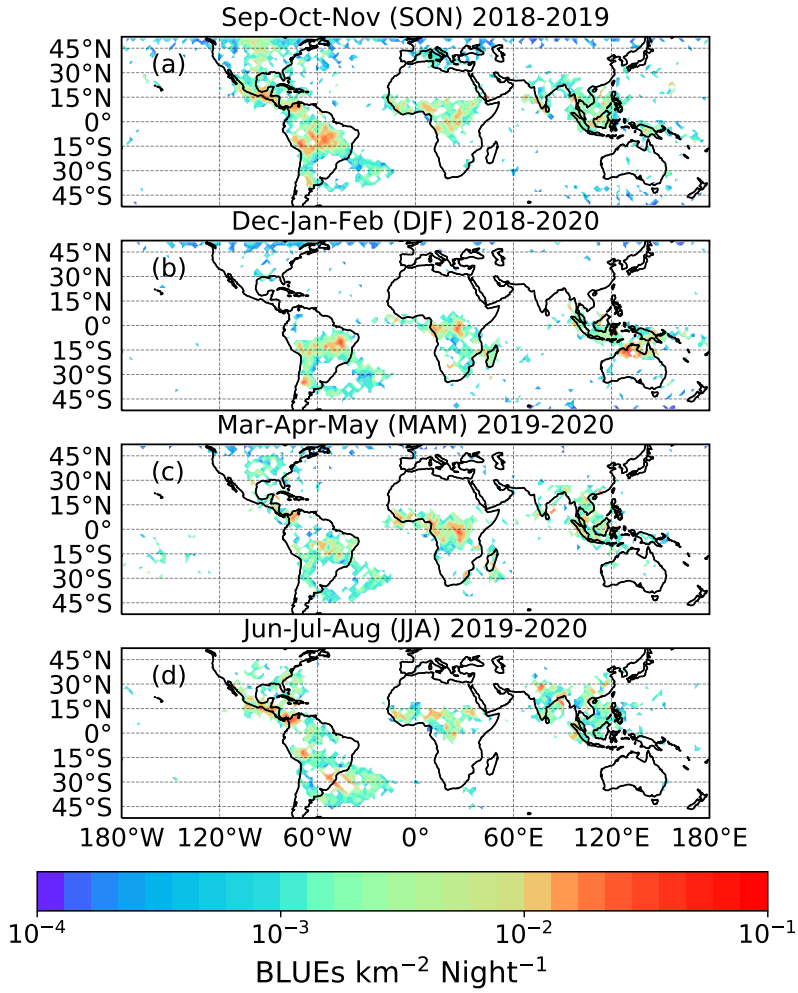

Figure 7.3. Nighttime seasonal distribution of BLUE electrical activity in thunderclouds. The global nighttime seasonal BLUE rates are: 8.2 (SON), 5.9 (DJF), 6.2 (MAM) and 6.7 (JJA) BLUEs s^{-1}. Note that these global nighttime seasonal BLUE rates are biased (underestimated) due to the nighttime only ASIM-MMIA observation time mode (see Figure 7.5) that shortens as ISS moves since it is not a geostationary platform. Thus, the most representative nighttime BLUE rate would be that at 0 h local time (see Figure 7.5). These maps are generated using 2° × 2° grid cells where the sharp pixels of the image are smoothed by drawing level lines using the python function called *contourf*. Note that decimal logarithm is used in the colorbar. Non smooth seasonal maps are shown in Figure 7.16 of the SM.

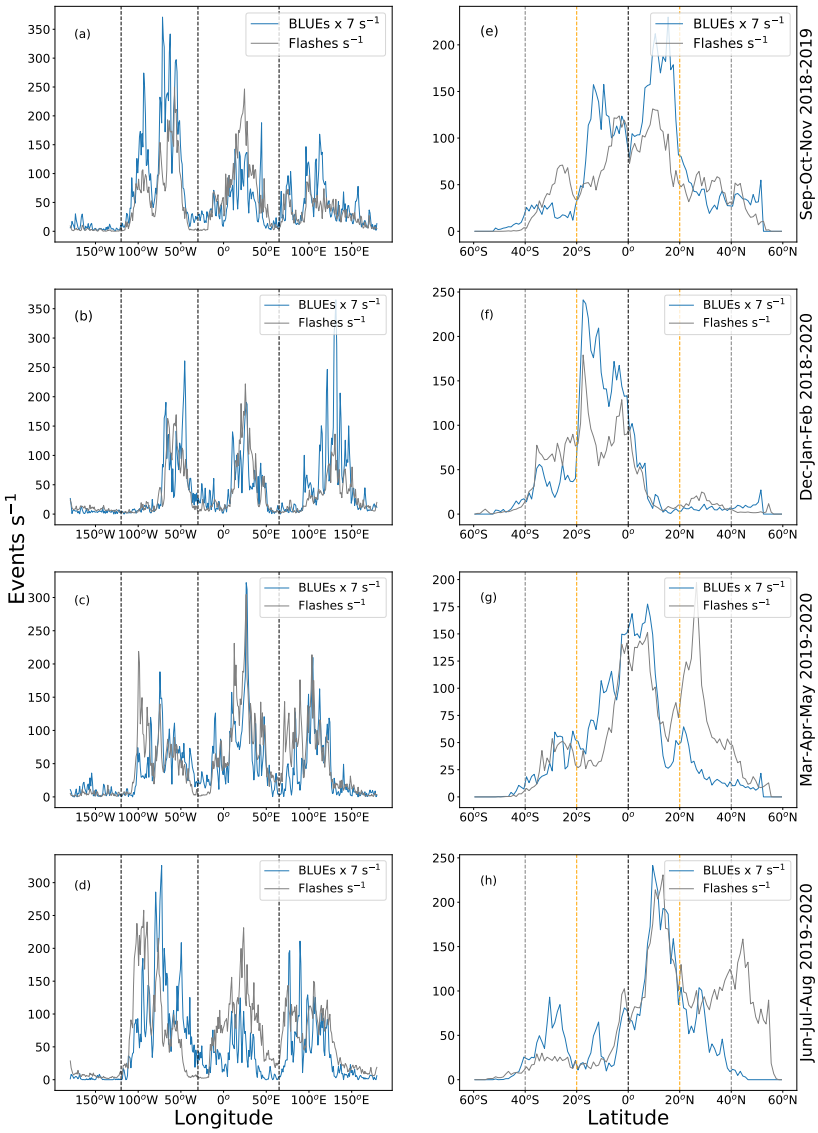

Figure 7.4. Seasonal meridional (left) and zonal (right) nighttime distributions of 2-year (1 September 2018 to 31 August 2020) BLUE climatology and ISS-LIS nighttime lightning in the same period. Grid cells and vertical lines as in Figure 7.2. Note that, for comparison, seasonal meridional/zonal 24 h (day and night) distribution of the two-year ISS-LIS lightning climatology is shown in Figure 7.13 of the SM. Note that the global seasonal BLUE rates are scaled up 7 times for best comparison with global nighttime lightning flash rates.

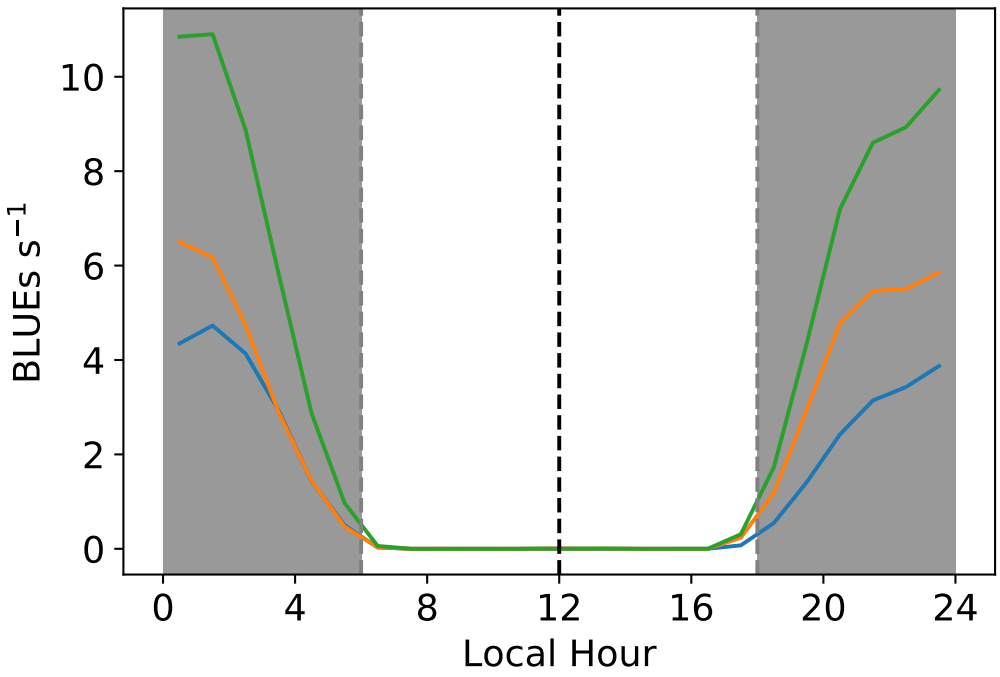

Figure 7.5. Diurnal (24 h) variability of global total (green line), land (orange line) and ocean (blue line) BLUE flash rate as a function of the local solar hour. The net zero rate during local daytime is caused by the fact that ASIM-MMIA can only observe during local nighttime. Local nighttime periods appear shadowed in the figure. Note that, for comparison, Figure 7.14 in the SM shows the diurnal (day and night) cycle of ISS-LIS total, land and ocean lightning flash rates for the two-year period investigated.

Acknowledgements

ASIM is a mission of ESA's SciSpace programme for scientific utilization of the ISS and non-ISS space exploration platforms and space environment analogues. ASIM and the ASIM Science Data Centre are funded by ESA and by national grants of Denmark, Norway and Spain. This work was supported by the Spanish Ministry of Science and Innovation under project PID2019-109269RB-C43 and the FEDER program. SS acknowledges a PhD research contract through the project PID2019-109269RB-C43. FJPI acknowledges the sponsorship provided by the Federal Ministry for Education and Research of Germany through the Alexander von Humboldt Foundation. AL and DL were supported by the European Research Council (ERC) under European Union H2020 programme/ERC grant agreement 681257. SS, FJGV, AL and DL acknowledge financial support from the State Agency for Research of the Spanish MCIU through the "Center of Excellence Severo Ochoa" award for the Instituto de Astrofísica de Andalucía (SEV-2017-0709).

Data availability statement

ASIM level 1 data are proprietary and cannot be publicly released at this stage. Interested parties should direct their request to the ASIM Facility Science Team (FST). ASIM data request can be submitted through: `https://asdc.space.dtu.dk` by sending a message to the electronic address asdc@space.dtu.dk. ISS-LIS data in `https://ghrc.nsstc.nasa.gov/lightning/data/data_lis_iss.html` are freely accessed from the NASA Global Hydrology Resource Center.

7.7 Appendix

1. Text
2. Figures 15 to 26

7.7.1 Introduction

We include in this supplementary material a number of complementary figures to those presented in the main text of the paper. Special care has been taken to compare nighttime global average and seasonal climatologies of ISS-LIS lightning and ASIM-MMIA BLUEs in the same period so that a deeper comparison can be carried out by readers. Some non-smooth figures are also included so that readers can judge data as they are shown without applying smoothing procedures aimed at producing good-viewing figures without sacrifying key scientific details. Finally, we also include some comments and quantifications on the relationship between BLUEs and deep convection.

7.7.2 Text

Figure 7.6 displays the time that locations on the Earth are within the FOV of the MMIA instrument onboard the International Space Station (ISS) as it orbits around the globe at an altitude of $\sim$ 400 km. The MMIA field of view (FOV) considered is of 400 km $\times$ 400 km with a spatial resolution of 0.4 km/pixel. To generate the ISS-Lightning Imager Sensor (LIS) climatology we have also created and used a figure (not shown) analogous to Figure 7.6 but using a LIS FOV of 640 km $\times$ 640 km with a spatial resolution of 5 km/pixel, which is within the LIS pixel resolution ($\sim$ 4 km at nadir an $\sim$ 6 km at off−nadir boundaries (Blakeslee et al., 2020)). The map shown in Figure 7.6 for MMIA (and the analogous one for ISS-LIS) was generated using a time resolution of 1 minute.

With the ISS at an approximately stable altitude of $\sim$ 400 km, the ISS passes over the same place on Earth every 3 days. Figure 7.6 for ISS-MMIA (and the analogous one for ISS-LIS) represents 3 cycles of 3 days which is a sufficiently good representation of the observation time in a given grid cell. The BLUE or lightning flash rates were calculated by, respectively, dividing the number of BLUE or lightning flashes detected in a grid cell by the observation time for that cell. Therefore, the BLUE or lightning rates for the entire globe were computed as the sum of all grid cell BLUE or lightning flash rates (Christian et al., 2003). Note that, as a first reasonable approximation, we have assumed a detection efficiency (DE) of 100 % for MMIA (since it operates during nighttime only), and also for nighttime and full day (24 h) ISS-LIS.

We have a total of 53015 BLUE events in the Field of View (FOV) of the MMIA 337 nm photometer and 2.04 million (2.04 M) in the ISS-LIS FOV. If about 53000 BLUEs are recorded only during nighttime we could expect approximately 106000 BLUEs during the full day (24 h). Since MMIA FOV is 2.56 times smaller than ISS-LIS FOV, the ratio ISS-LIS / MMIA = 2.04M / (0.106M $\times$ 2.56) = 7.56. Consider also that we can have small variations due to the projection of the FOV in diferent latitudes.

Finally, only during nighttime, ISS-LIS detects about 1.04M lightning, which is slightly higher than during daytime. Thus, during nighttime we have that ISS-LIS / MMIA = 1.04M / (0.053M $\times$ 2.56) = 7.7.

Figure 7.7 illustrates steps 2 and 3 of the algorithm designed and implemented for searching BLUEs with MMIA 100 kHz photometers.

In order to enrich the discussion and compare with the 2-year (1 September 2018 to 31 August 2020) nighttime climatology of BLUEs we include annual nighttime (Figure 7.8-top), 24 h (Figure 7.8-bottom), and seasonal nighttime distributions (Figure 7.9) of the ISS-LIS lightning climatology considering an average 5 km/pixel (and an assumed

average DE of 100 %) resulting in a 2-year average nighttime global-scale flash rate of $\sim$ 48 (nighttime only) and 46.8 (24 h) flashes s^{-1}, respectively. For this we have used the recently released nonquality-controlled (NQC) version 1 science lightning ISS-LIS data (Blakeslee, 2019). The version 1 NQC data are appropriate for science and applications and have been validaded as described in Blakeslee et al. (2020).

Figure 7.10 shows meridional (with longitude) and zonal (with latitude) nighttime and 24 h (night and day) distributions of the 2-year period from 1 September 2018 to 31 August 2020 of the ISS-LIS lightning climatology. Figure 7.11 presents seasonal meridional and zonal nighttime distributions of 2-year ISS-LIS lightning climatology. Note that the nighttime period always refers to local hours between 18:00 h (included) and 06:00 (not included) when ASIM-MMIA perform observations.

Full day (24 h) ISS-LIS seasonal lightning climatology for the 2-year period investigated here (1 September 2018 to 31 August 2020) is shown in Figure 7.12 while Figure 7.13 displays the corresponding full day ISS-LIS seasonal meridional and zonal lightning flash rate distributions for the same 2-year period.

Figure 7.14 shows the diurnal (24 h) cycle of ISS-LIS (in local solar time and UTC) global total, land and ocean lightning flash rates for the 2-year period of interest here that overlaps with ASIM-MMIA nighttime observations.

Figure 7.15 and Figure 7.16 display the non smooth 2-year average (1 September 2018 to 31 August 2020) nighttime climatology of global BLUE electrical activity in thunderclouds and their seasonal distribution, respectively. These plots are included so that the reader can have the opportunity to compare with smoothed figures shown in Figure 7.1 and Figure 7.2 of the main paper.

Finally, we include Figure 7.17 to illustrate and quantify the possible linear relationship between BLUEs and deep convection. We have chosen the convective available potential energy (CAPE) as a proxy of deep convection as initially indicated by Williams et al. (1992) and recently revisited by Ukkonen and Mäkelä (2019). We have used ERA-5 monthly average values of CAPE to generate seasonal zonal (with latitude) and meridional (with longitude) distributions within the period of time of our study (1 Sept 2018 to 31 Aug 2020). The seasonal CAPE maps show that, in general, there are stronger CAPEs in regions with more BLUEs. However, CAPE can be very high in the ocean where it is not that common to find many BLUEs.

The seasonal CAPE-BLUEs per second relationships are quantified using the Pearson linear correlation coefficient (R) (varying between -1 and +1, with +1 being perfect

linear correlation, 0 null linear correlation, and -1 perfect linear anti-correlation). The correlations are better for the zonal distributions ($0.77 < R < 0.89$, with DJF and MAM being the best) than for the meridional distributions ($0.42 < R < 0.64$, with DJF and JJA being the best).

Figure 7.17 shows some different convection features between the pre-monsoon (MAM) and break period, and the real monsoon season (from early June to early October) (Williams et al., 1992). In order to distinguish between pre-monsoon and monsoon we can assume as a first approximation that the pre-monsoon covers MAM, followed by a break before the real monsoon season in JJA-SO (from early June to early October). If we look at the Bay of Bengal region (7°N - 22°N, 75°E - 95°E) in Figure 7.17 we can distinguish slight but distinct features when we compare meridional/zonal MAM with meridional/zonal JJA in the Bay of Bengal region (7°N - 22°N, 75°E - 95°E). For instance, we can notice (i) larger meridional and zonal CAPE during JJA (real monsoon) than during MAM (pre-monsoon), and (ii) steeper zonal decrease (between 7°N and 22°N) of BLUEs per second in MAM than in JJA.

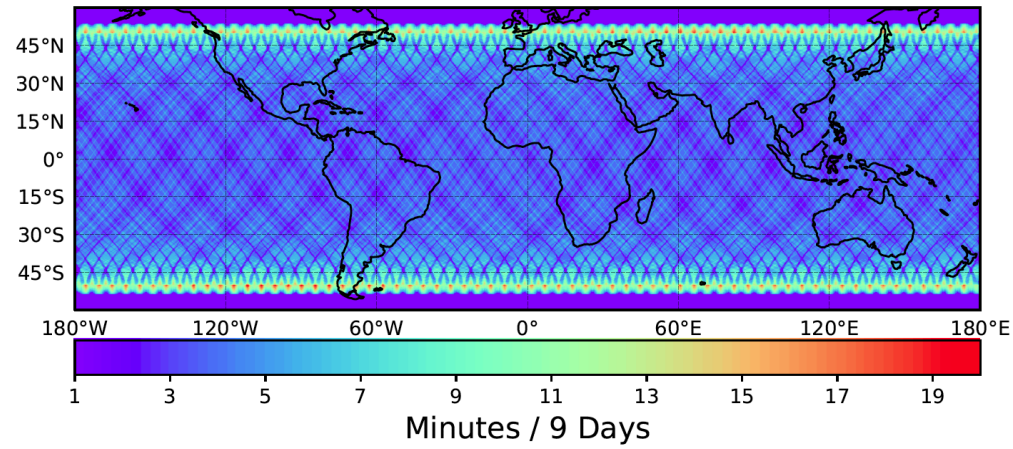

Figure 7.6. Time that locations on the Earth are within the FOV of the MMIA instrument onboard the International Space Station (ISS) as it orbits around the globe. Because of the ISS inclination, more time is spent in high latitudes than in mid and tropical latitudes. For example, the colorbar indicates that every 9 days the ISS spends $\sim$ 18 minutes in latitudes $> 50°$ N/S, while it stays between $\sim$ 1 and $\sim$ 5 minutes in the $0°$ - $40°$ N/S, and between $\sim$ 7 and $\sim$ 15 minutes in the $40°$ - $50°$ N/S region. The map is generated using grid cells of $0.1° \times 0.1°$ and a MMIA FOV of 400 km $\times$ 400 km. An analogous figure for ISS-LIS with a FOV of 640 km $\times$ 640 km (spatial resolution of 5 km /pixel) was generated and used to compute the ISS-LIS climatology during the period of study (1 Septembre 2018 to 31 August 2020). The time resolution used to generate this figure was 1 minute.

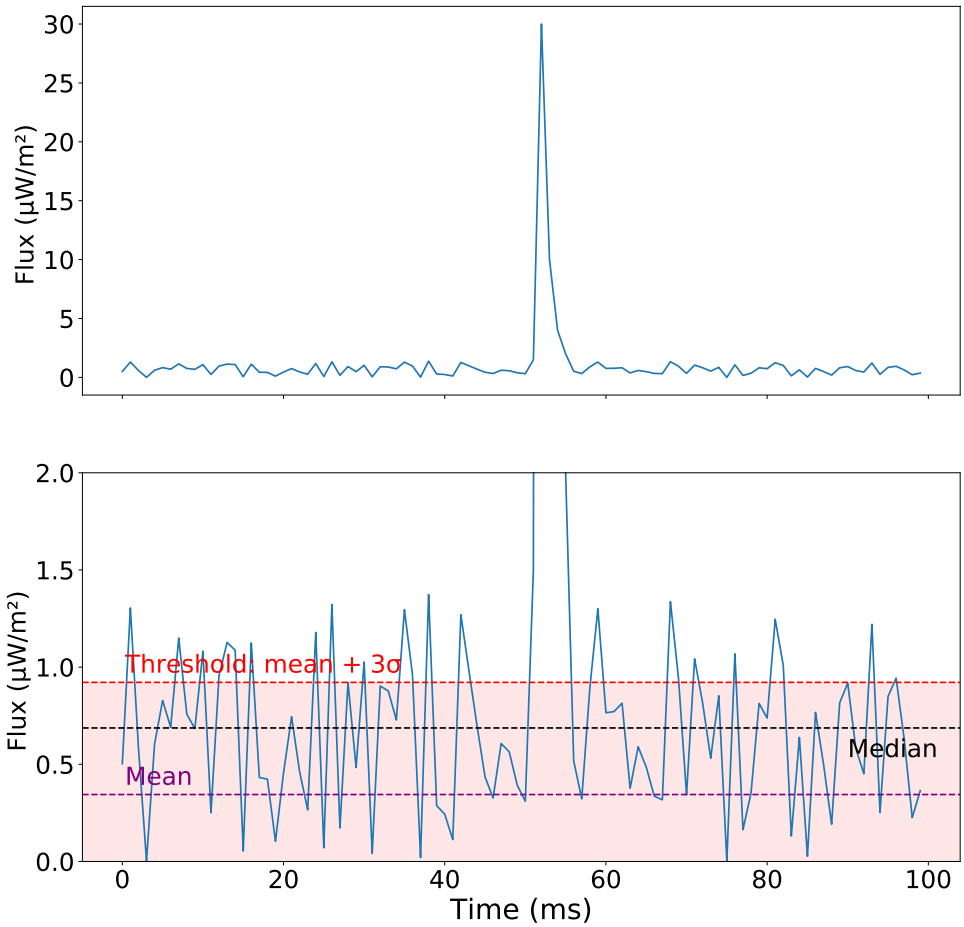

Figure 7.7. Graphical illustration of steps 2 and 3 of the algorithm used to search for BLUEs with 100 kHz MMIA photometers. The bottom panel represents a zoom in of the signal shown in the upper panel. The mean is calculated for the values below the median. Note that the data displayed (blue line) do not correspond to any particular real 337.0 nm event as they are only used for illustration purposes. Step 2 is sequentially illustrated in the top and bottom panels. Step 3 only consists in the replacement of the lower than 1 μW/m^2 threshold value by 1 μW/m^2.

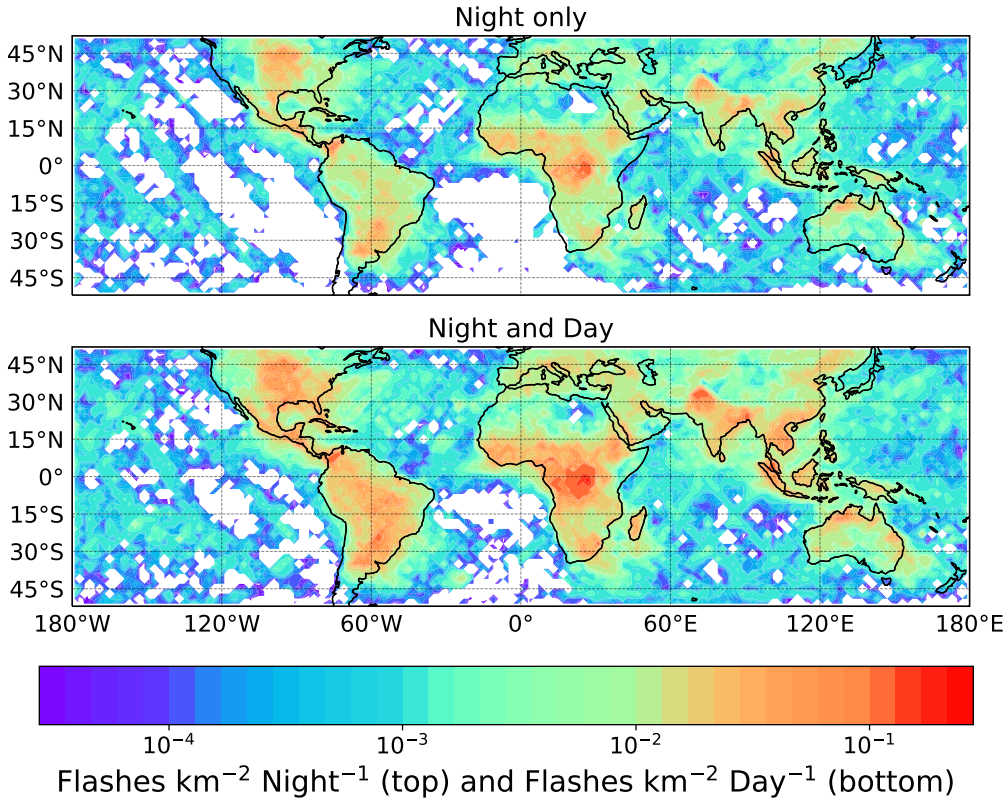

Figure 7.8. Annual nighttime (top panel) and 24 h (night and day, bottom panel) lightning flash distributions from the ISS-Lightning Imager Sensor (LIS) climatology for the 2-year period from 1 September 2018 to 31 August 2020 with an average spatial resolution of 5 km/pixel and an assumed average detection efficiency (DE) of 100 %. Nighttime and daytime periods refer to local hours between 18:00 h (included) and 06:00 h (not included), and between 06:00 h (included) and 18:00 h (not included), respectively. The selected ISS-LIS nighttime period exactly matches ASIM-MMIA observation time of BLUEs. The obtained ISS-LIS annual global flash rates at nighttime, daytime and 24 h (night and day) are 48.0, 45.6 and 46.0 flashes s^{-1}, respectively, in good agreement with the numbers obtained in Blakeslee et al. (2020) for their three-year period. These maps have been generated using grid cells of 1° × 1°. Note that the colorbar scale is in decimal logarithm and covers two year of data.

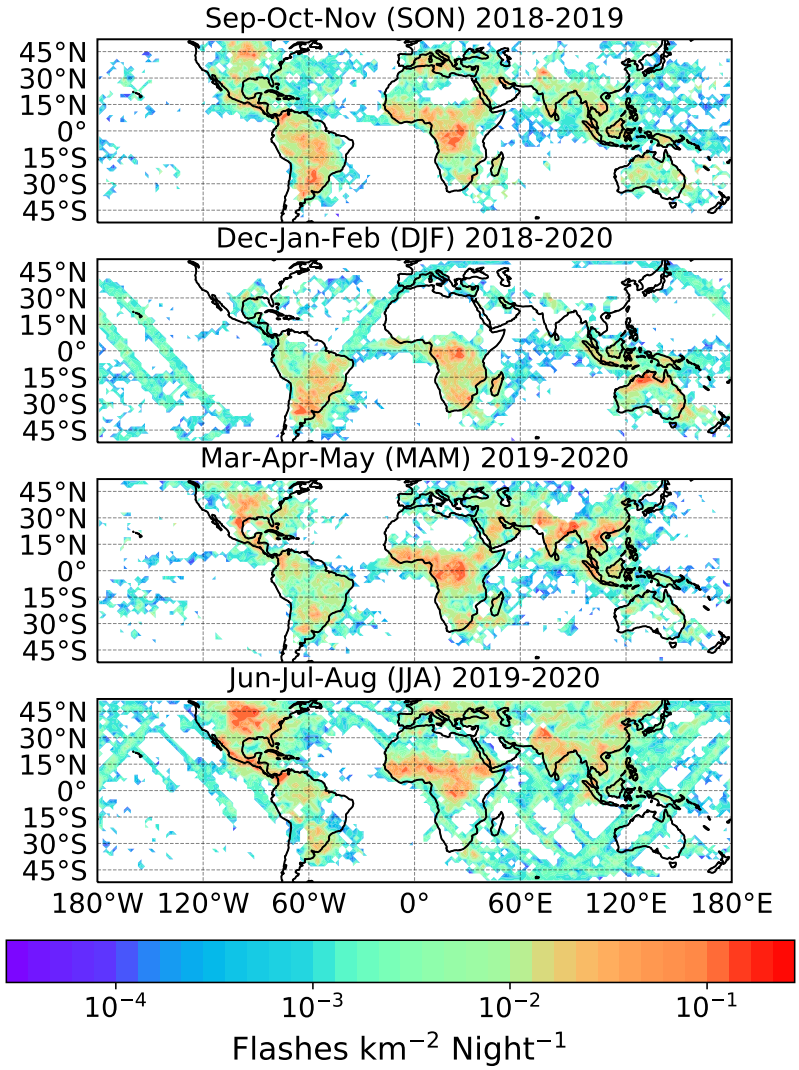

Figure 7.9. Seasonal nighttime lightning flash distributions from the ISS-Lightning Imager Sensor (LIS) climatology for the 2-year period from 1 September 2018 to 31 August 2020 with an average spatial resolution of 5 km/pixel and an assumed average detection efficiency (DE) of 100 %. The obtained ISS-LIS seasonal nighttime only lightning global flash rates are: 45.9 (SON), 33.7 (DJF), 50.4 (MAM) and 61.9 (JJA) flashes s^{-1}, respectively. Grid cells as in Figure 7.8.

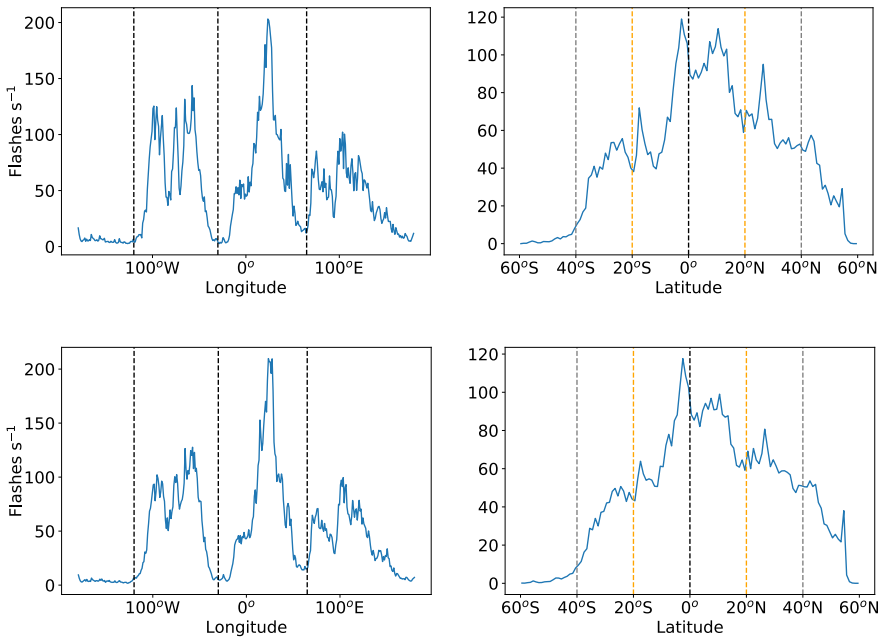

Figure 7.10. Meridional (left panels) and zonal (right panels) nighttime (top panels) and 24 h (night and day, bottom panels) distributions for the 2-year period from 1 September 2018 to 31 August 2020 ISS-LIS lightning climatology. The dashed vertical lines in the meridional distributions indicate different continental regions such as the Americas (120°W-30°W), Europe / Africa (30°W-60°E), and Asia / Australia (60°E-180°E). The dashed orange and black vertical lines in the zonal distributions indicate tropical (20°S-20°N), subtropical (40°S-20°S and 20°N-40°N), and mid-latitude (60°S-40°S and 40°N-60°N) regions. Grid cells as in Figure 7.8.

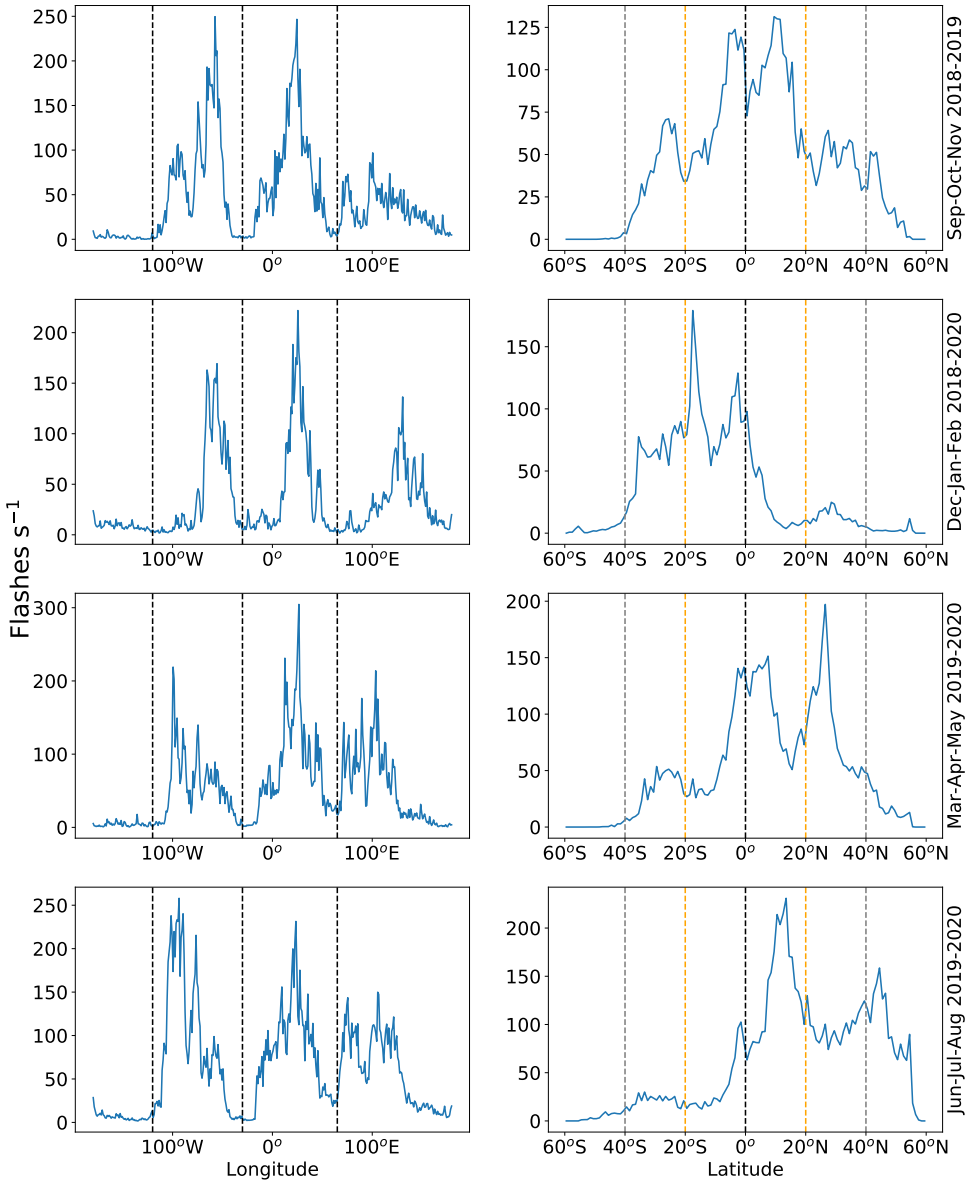

Figure 7.11. Seasonal meridional (left column) and zonal (right column) nighttime distributions of 2-year ISS-LIS lightning climatology for the period 1 September 2018 to 31 August 2020. Grid cells and vertical lines as in Figure 7.10.

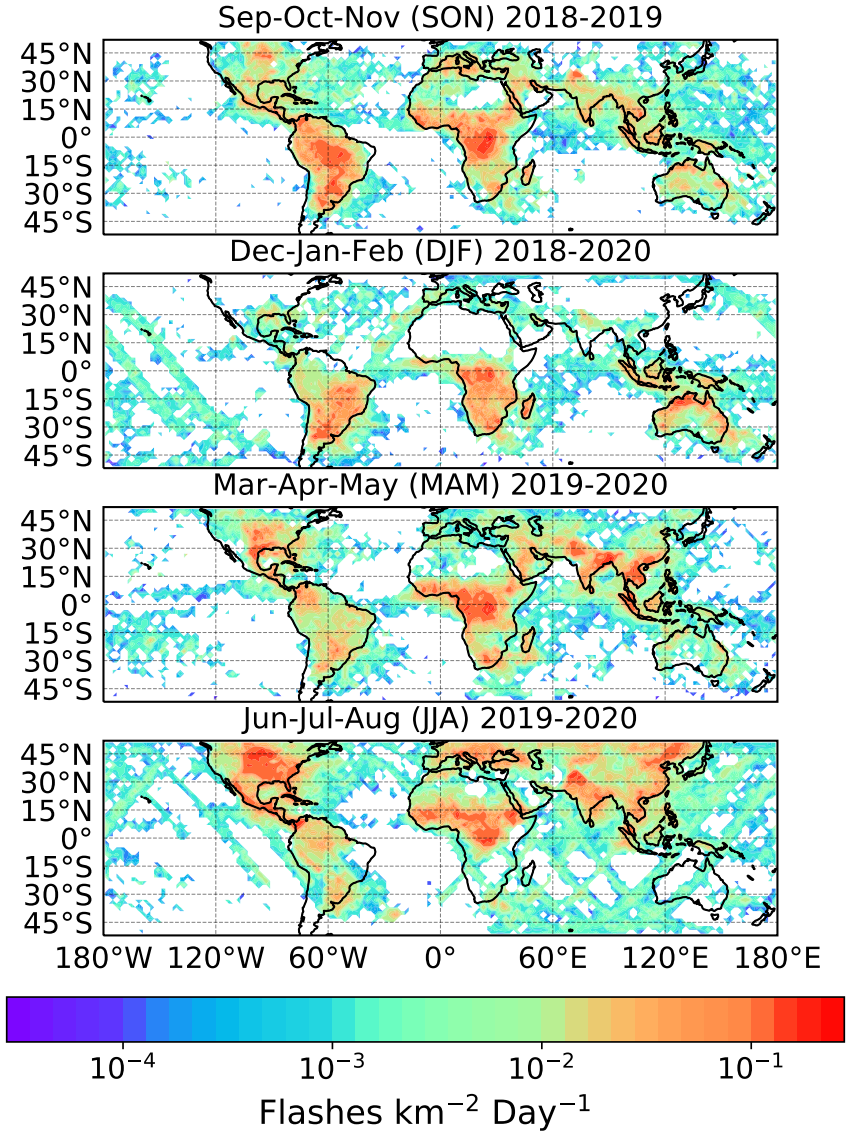

Figure 7.12. Full day (night and day) ISS-LIS seasonal lightning climatology for the 2-year period 1 September 2018 to 31 August 2020 investigated here. The obtained ISS-LIS seasonal 24 h lightning global flash rates are: 47.5 (SON), 32.0 (DJF), 47.0 (MAM) and 60.8 (JJA) flashes s^{-1}, respectively. Grid cells as in Figure 7.8.

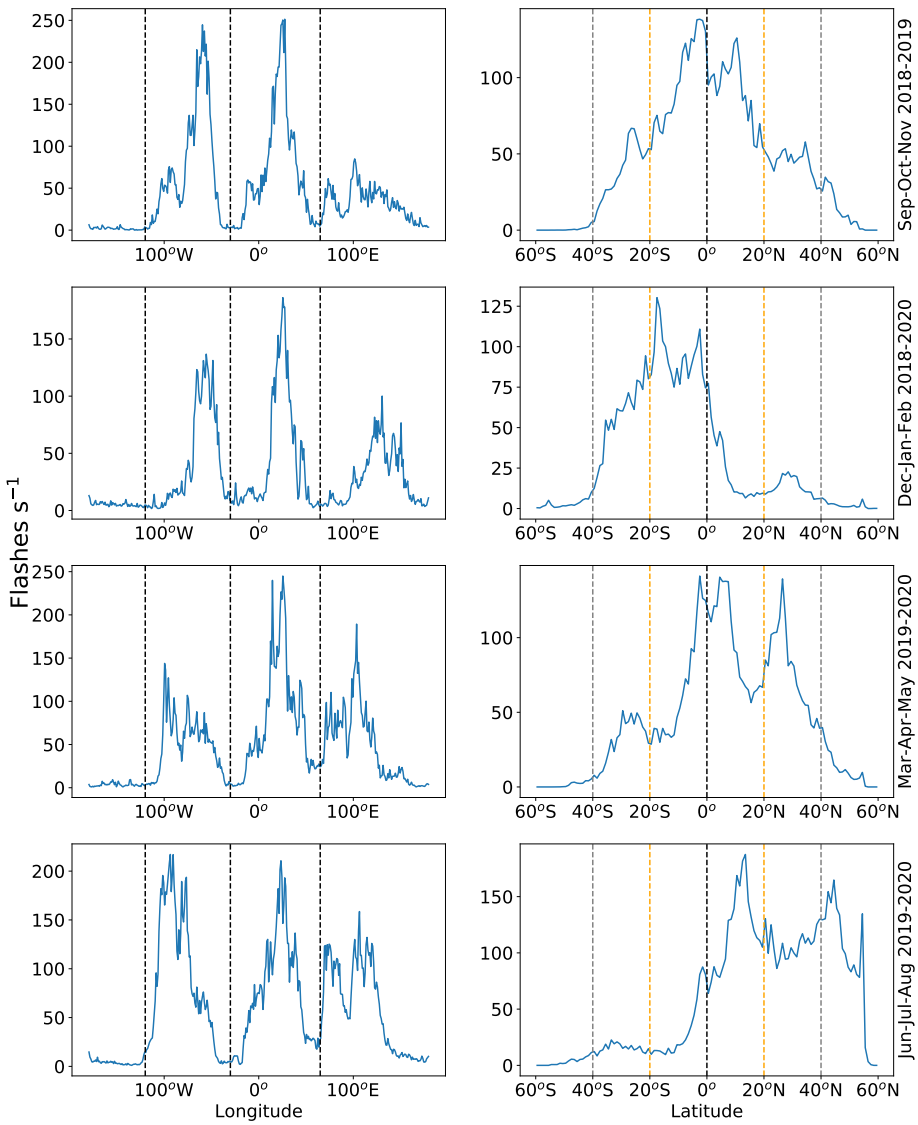

Figure 7.13. Full day (night and day) ISS-LIS seasonal meridional (left column) and zonal (right column) lightning flash rate distributions for the 2-year period 1 September 2018 to 31 August 2020. Grid cells and vertical lines as in Figure 7.10.

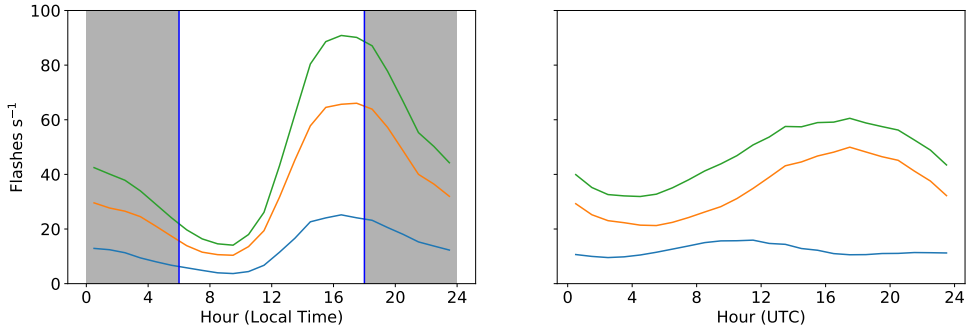

Figure 7.14. Diurnal (day and night) cycle of ISS-LIS global total (green line), land (orange line) and ocean (blue line) lightning flash rates for the two-year period from 1 September 2018 to 31 August 2020 overlapping with ASIM-MMIA observations. Left and right panels display diurnal variability with local solar time and UTC time, respectively. The local daytime period between the two solid blue lines in the left panel corresponds to the same hours as in Figure 7.4 (main paper) when ASIM-MMIA can not operate. Note that local nighttime periods appear shadowed in the left figure and that data points are placed in the middle between two hours so that, for instance, the point at 0.5 h represents the number of flashes s^{-1} between 0 h and 1 h.

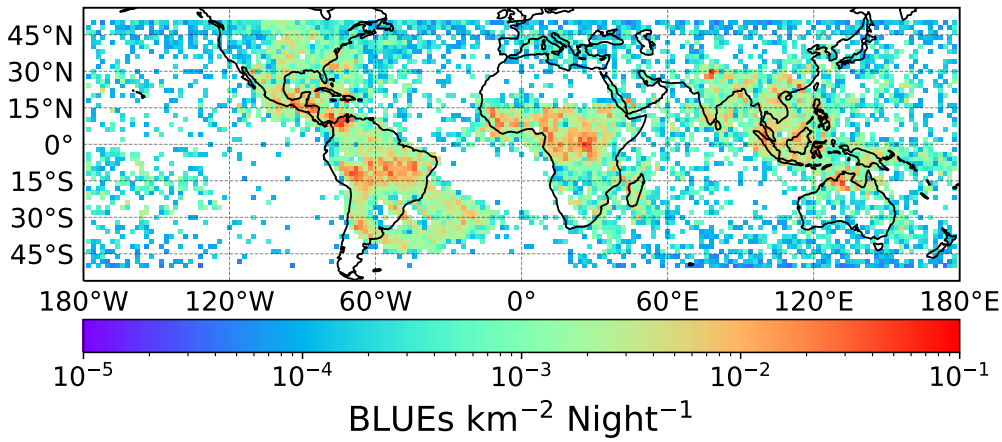

Figure 7.15. Non smooth two-year average (September 2018 through August 2020) nighttime climatology of global BLUE electrical activity in thunderclouds from ASIM-MMIA onboard the ISS. The non smooth map is generated using $2° \times 2°$ grid cells. Note that the scale in the colorbar is the same as that in Figure 7.1 (top) of the main paper.

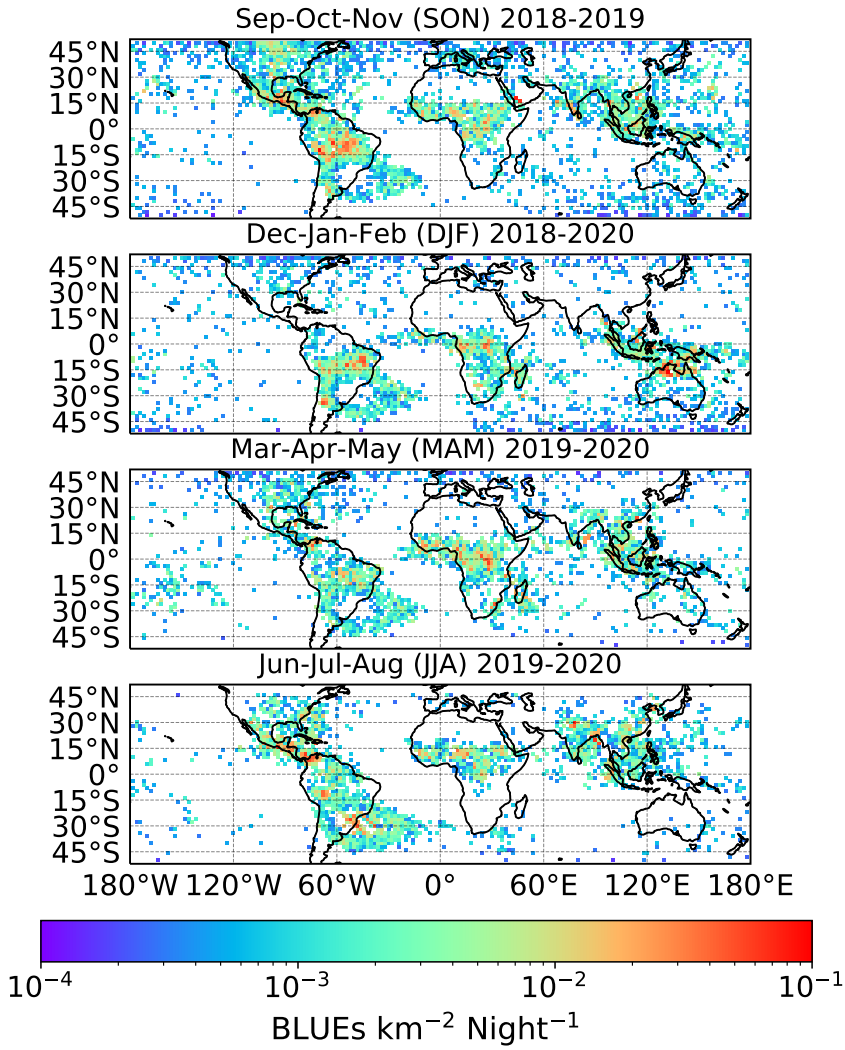

Figure 7.16. Non smooth nighttime seasonal distribution of BLUE electrical activity in thunderclouds. September to November (top panel), December to February (second panel from top), March to May (third panel from top), June to August (bottom panel). These non smooth maps are generated using $2^\circ \times 2^\circ$ grid cells. Note that the scale in the colorbar is the same as that in Figure 7.2 of the main paper.

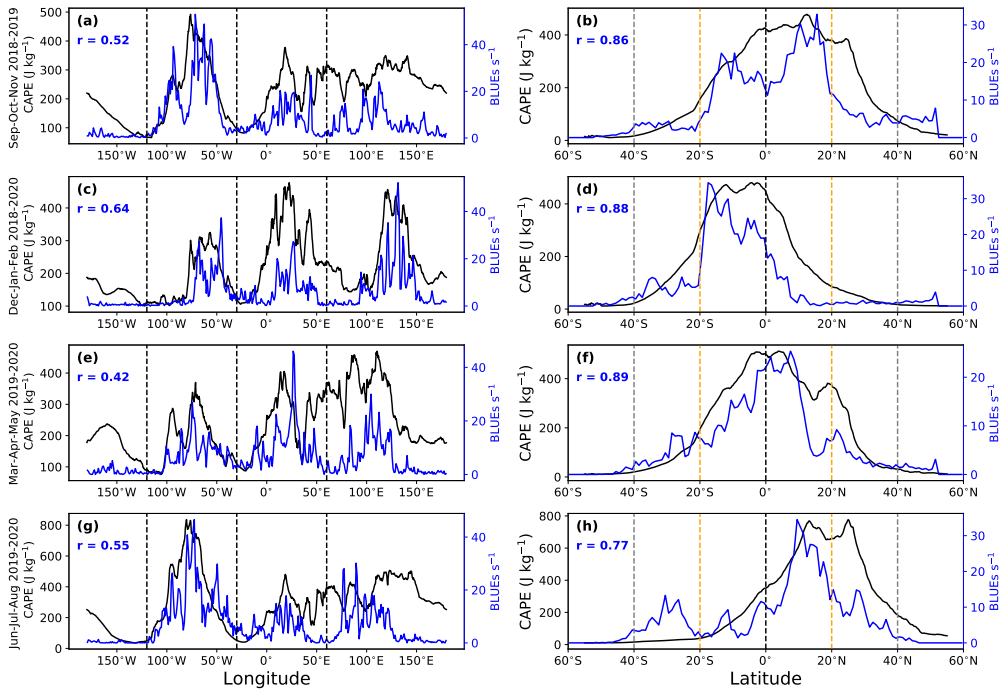

Figure 7.17. Seasonal meridional (left) and zonal (right) nighttime distributions of 2-year (1 September 2018 to 31 August 2020) BLUE climatology (blue line) and monthly average values of CAPE (black line) in the same period. Vertical lines as in Figure 7.2 of the main paper. The Pearson linear correlation coefficient (R) is shown in the inset of each panel.

Chapter 8

Third article: "Global distribution of key features of streamer corona discharges in thunderclouds"

Published in *Journal of Geophysical Research - Atmospheres*, 2022

DOI: https://doi.org/10.1029/2022JD037535

Authors

S. Soler[1],F. J. Gordillo-Vázquez[1],F. J. Pérez-Invernón[1],A. Luque[1],D. Li[1], T. Neubert[2],O. Chanrion[2],V. Reglero[3],J. Navarro-González[3],N. Østgaard[4]

Affiliations

[1] Instituto de Astrofísica de Andalucía (IAA-CSIC), Glorieta de la Astronomía s/n, 18008 Granada, Spain [2]National Space Institute, Technical University of Denmark (DTU Space), Kongens Lyngby, Denmark [3]Image Processing Laboratory, University of Valencia, Valencia, Spain [4]Birkeland Centre for Space Science, Department of Physics and Technology, University of Bergen, Bergen, Norway

Key points

- BLUEs are found between $\sim$ 1 km and $\sim$ 4 km below cloud tops in the tropics and $\leq$ 1 km in mid and higher latitudes
- Two distinct populations of BLUEs with peak power density < 25 μWm^{-2} (common) and ≥ 25 μWm^{-2} (rare) are observed
- Fast rise time (< 0.05 ms) BLUEs occur very superficially (< 1 km) near cloud tops with high power density ≥ 100 μWm^{-2}

8.1 Abstract

We present nighttime worldwide distributions of key features of Blue LUminous Events (BLUEs) detected by the Modular Multispectral Imaging Array (MMIA) of the Atmosphere-Space Interaction Monitor (ASIM). Around 10 % of all detected BLUEs exhibit an impulsive single pulse shape. The rest of BLUEs are unclear (impulsive or not) single, multiple or with ambiguous pulse shapes. BLUEs exhibit two distinct populations with peak power density < 25 μW m^{-2} (common) and ≥ 25 μW m^{-2} (rare) with different rise times and durations. The altitude (and depth below cloud tops) zonal distribution of impulsive single pulse BLUEs indicate that they are commonly present between cloud tops and a depth of $\leq$ 4 km in the tropics and $\leq$ 1 km in mid and higher latitudes. Impulsive single pulse BLUEs in the tropics are the longest (up to $\sim$ 4 km height) and have the largest number of streamers (up to $\sim 3{\times}10^9$). Additionally, the analysis of BLUEs has turned out to be particularly complex due to the abundance of radiation belt particles (at high latitudes and in the South Atlantic Anomaly (SAA)) and cosmic rays all over the planet. True BLUEs can not be fully distinguished from radiation belt particles and cosmic rays unless other ground-based measurements associated with the optically detected BLUEs are available. Thus, the search algorithm of BLUEs presented in Soler et al. (2021) is now completed with a new additional step that, if used, can considerably smooth the SAA shadow but can also underestimate the number of BLUEs worldwide.

Plain Language Summary

The presence of corona electrical discharges in thunderclouds has been suspected for a long time. These thunderstorm coronas can be observed as Blue LUminous Events (BLUEs) formed by a large number of streamers characterized by their distinct 337.0 nm light flashes with absent (or negligible) 777.4 nm component (typical of lightning leaders). The Modular Multispectral Imaging Array (MMIA) of the Atmosphere-Space Interaction Monitor (ASIM) has successfully allowed us to map and characterize BLUEs. The results presented here include a global analysis of key properties of BLUEs such as their characteristic rise times and duration, their depth with respect to cloud tops, vertical length and number of streamers. This study also includes two different global annual average climatologies of BLUEs depending on considerations about the rise time and total duration of BLUEs worldwide.

8.2 Introduction

Radio, optical and some indirect chemical recordings since the early 1980s suggest that cold, non-thermal streamer corona discharges are common in thunderstorms worldwide

(Le Vine, 1980; Wiens et al., 2008; Bozem et al., 2014; Liu et al., 2018; Bandara et al., 2019; Soler et al., 2020; Neubert et al., 2021; Li et al., 2021). Fast breakdown (Rison et al., 2016; Tilles et al., 2019) seems to underlie streamer coronas that cause the so-called Narrow Bipolar Events (NBEs) originally detected by Le Vine (1980) in the form of strong Very High Frequency (VHF) sources from in-cloud discharges.

Typical light spectra of streamer corona discharges in air are strongly dominated by near-ultraviolet blue emissions (300 - 450 nm) corresponding to the Second Positive System (SPS) of molecular nitrogen (N_2) (Gallimberti, Hepworth, and Klewe, 1974; Grum and Costa, 1976; Ebert et al., 2010) with the strongest transition at 337.0 nm (Gordillo-Vázquez, Luque, and Simek, 2012b; Hoder et al., 2016; Malagón-Romero and Luque, 2019) and generally undetectable oxygen atom 777.4 nm emissions typical of lightning. Optical signals from lightning stroke flashes are characterized by including both 337.0 nm emissions and, especially, strong 777.4 nm optical emissions (Christian, Blakeslee, and Goodman, 1989; Christian et al., 2003; Blakeslee et al., 2020; Montanyà et al., 2021). However, BLUEs exhibit strong optical emissions in the 337.0 nm and negligible (at the noise level) 777.4 nm emissions (Soler et al., 2020). Corona streamers can appear alone as leaderless corona discharges and / or in combination with hot leaders of lightning, blue jets (Wescott et al., 1995) and blue starters (Wescott et al., 1996; Edens, 2011).

The term Blue LUminous Events (BLUEs) has been recently applied to in-cloud and to partially emerged transient electrical discharges that emit pulses of light mostly blue, that is, they could include a small fraction of red (from the first positive system of N_2) and infrared optical emissions (777.4 nm from atomic oxygen). This definition includes blue jets and starters, but also positive and negative NBEs, which are the VLF/LF radio manifestation of in-cloud leaderless streamer coronas (Kuo, Su, and Hsu, 2015; Rison et al., 2016; Liu et al., 2018; Tilles et al., 2019; Liu et al., 2019; Cooray et al., 2020; Soler et al., 2020; Neubert et al., 2021; Li et al., 2021). Apart from distinct optical emissions directly associated with corona streamers, the dissimilarity between BLUEs and lightning discharges is also manifested by the fact that BLUEs can occur individually with no associated lightning discharges or they can be the initial event of lightning discharges (Soler et al., 2020; Soler et al., 2021; López et al., 2022; Li et al., 2022).

BLUEs optical detections from space have been reported from the limb-pointing Imager of Sprites/Upper Atmospheric Lightning (ISUAL) onboard FORMOSAT-2 (Kuo et al., 2005; Chou et al., 2011; Kuo, Su, and Hsu, 2015; Chou et al., 2018; Liu et al., 2018). A variety of BLUEs including kilometer-scale blue discharges at the cloud top layer at ~ 18 km altitude, blue starters and a pulsating blue jet propagating into the stratosphere were color photographed from the International Space Station (ISS) (Chanrion et al., 2016).

BLUEs have also been recently observed by the nadir-pointing MMIA onboard ASIM in the ISS since April 2018 (Soler et al., 2020; Neubert et al., 2021; Li et al., 2021; Husbjerg et al., 2022). However, it is a known issue that powerful NBEs are highly likely to be misclassified or simply missed by lightning locating systems (Zhu et al., 2022). For 1022 NBEs reported by Leal, Rakov, and Rocha (2019), the misclassification rates were 78 % and 56 % for the National Lightning Detection Network (NLDN−GLD360) and the Earth Network Total Lighting Network (ENTLN), respectively. They also found that the percentage of misclassified NBEs becomes even higher for higher intensity events. Connected to this, Chanrion et al. (2016) saw BLUEs from the ISS without any GLD360 detections. Thus, ground based detection of BLUEs by lightning networks remains a challenge.

A number of recent thunderstorm case-based works have detailed studied properties of BLUEs associated with positive NBEs (Soler et al., 2020), negative NBEs (Neubert et al., 2021; Li et al., 2021; Liu et al., 2021) and multiple pulse BLUEs (Li et al., 2022) using MMIA data of thunderclouds in several locations of the world. Additionally, a recent study presented the first worldwide nighttime climatology of BLUEs in thunderclouds derived from 2 years of BLUEs data recorded by MMIA in ASIM (Soler et al., 2021).

Here we focus on analyzing key properties of worldwide nighttime BLUEs detected by MMIA between 1 April 2019 and 31 March 2021 (note that ASIM can only observe during the night). Our study also discusses BLUEs depending on considerations about the rise time and total duration of BLUEs in the planet. We investigate intrinsic properties of BLUE events including temporal features like pulse shape (single, multiple or irregular), rise times and total duration times. We analyze the 337.0 nm Peak Power Density (PPD) and total brightness, and the depth below thundercloud tops where BLUEs occur as a function of the latitude and longitude. Finally, we also present worldwide zonal and meridional distributions for the vertical lengths and approximate number of streamers of single pulse BLUEs.

8.3 Observations and Data

Observations of BLUEs were carried out with the MMIA high sampling rate (100 k samples/s) photometers in the near UV (337 nm/4 nm), tuned to the strongest line of the N_2 SPS, and in the near infrared band (777.4 nm/5 nm) for recording the atomic oxygen triplet line of lightning. MMIA also incorporates a high-speed photometer in the UV (180 - 230 nm), capable of recording part of the N_2 Lyman-Birge-Hopfield (LBH) band, and a pair of 337 nm/4 nm and 777.4 nm/5 nm filtered cameras (at 12 fps) with $\sim$ 400 m/pixel spatial resolution (Chanrion et al., 2019).

BLUEs exhibit strong features in the 337 nm/4 nm photometer with negligible (or very minor) signal in the 777.4 nm/5 nm photometer, which is continuously monitored (Soler et al., 2020). Once a true positive BLUE detection is confirmed, the cameras are checked for possible associated images.

The two worldwide annual average distributions of nighttime BLUEs presented and discussed here (see Figure 8.1 and Figure 8.2) were obtained with global ASIM-MMIA level 1 (calibrated) data in a period of two years (1 April 2019 - 31 March 2021) shifted seven months ahead (see section 4 for details) with respect to the earlier two-year period explored in Soler et al. (2021). The BLUEs shown in Figure 8.1 and Figure 8.2 can have any temporal shape, that is, no distinction has been made here among BLUEs with a single (impulsive or not) pulse, multiple pulses or any other irregular pulse shape. The first global average distribution (GD-1) of BLUEs presented was derived using the algorithm described in Soler et al. (2021).

In order to explore the possible influence of Radiation Belt Particles (RBP) and Cosmic Rays (CR) on our dataset, the second global average distribution (GD-2) of nighttime BLUEs discussed here includes the condition that 337.0 nm events are removed in the entire planet when their rise times (τ_{rise}) are $\leq$ 40 μs and their total duration (τ_{total}) times are $\leq$ 150 μs (see Figure 8.2). This is a new (optional) step in the Soler et al. (2021) algorithm that by default allows events with any duration above 50 μs. In spite of this, there are still some hundreds of BLUEs with duration below 50 μs (see GD-2 in the right column of Figure 8.10 and Figure 8.11). This is fully compatible with point 4 of our BLUE search algorithm that reads "create groups defined by five or more consecutive blue counts (10 microseconds each) above the 337.0 nm photometer threshold" (Soler et al., 2021), and with the criterion on how the total duration of an event is calculated (from the fitted signal) getting the position in time of the blue peak and then go backward and forward until the signal drops below 10 % of the maximum.

When our algorithm searches for a BLUE event it needs to find at least 5 counts above the threshold, so apparently we can assume that all events should last at least 50 μs. However, when we apply this criteria to very sharp BLUEs with a high Peak Power Density we can see that, in some cases, the total time can be less than 50 μs (as mentioned above).

It is worth mentioning here that ultrahigh energy ($> 10^{19}$ eV) CRs are being monitored from the ISS by the nadir-facing Multiwavelength Imaging New Instrument for the Extreme Universe Space Observatory (Mini-EUSO) telescope in operation since October 2019 (Bacholle et al., 2021; Miyamoto et al., 2021). Mini-EUSO observes the nighttime Earth in the near ultraviolet (UV) - blue range (290 nm $-$ 430 nm), with a spatial resolution of about 6.3 km (FOV of 300 km $\times$ 300 km) and a temporal resolution of 2.5 μs.

According to Mini-EUSO observations, ultrahigh energy CRs cross one or a few pixels of the photocathode detector releasing a high-intensity light curve that can last a maximum of ≤ 150 μs with a sharp increase (≤ 40 μs) (see Figure 5 in Miyamoto et al. (2021)).

The global distributions of nighttime BLUEs in Figure 8.1 and Figure 8.2 include $\sim$ 46,000 events and 26,500 events, respectively. One can note that it is then quite possible that not all the $\sim$ 20,000 events removed in GD-2 with respect to GD-1 are RBPs and CRs. The presence of the South Atlantic Anomaly (SAA) can be distinguished within a rectangle with borders in latitudes 5°S and 45°S, and longitudes 0° and 100°W in Figure 8.1 for GD-1. Note that the SAA's shadow is mostly removed in Figure 8.2 for GD-2 but with the drawback of probable underestimation of the number of BLUEs worldwide in GD-2.

The seasonal nighttime average distributions of BLUEs according to GD-1 and GD-2 are further shown in Figure 8.3 and Figure 8.4, respectively. In both seasonal distributions, BLUEs are more common in the boreal summer closely followed by the boreal autumn. The main visual difference between Figure 8.1 and Figure 8.3, and the distributions of BLUEs in Soler et al. (2021) is the disappearance of events occurring in high latitudes during the annual average and during the SON, DJF and MAM.

8.4 Methodology

The key features of the BLUEs were obtained by applying different types of fits (depending on whether the light source is considered point-like (see Figure 8.13 of the supplementary material) or extended (see Figure 8.14 of the supplementary material)) to the impulsive 337.0 nm light curves among the $\sim$ 46,000 and $\sim$ 26,500 BLUEs registered worldwide according to the global annual average distributions shown in Figure 8.1 and Figure 8.2. However, as commented below, the two types of fits considered here are valid provided that the 337.0 nm light curve of the BLUEs exhibit a relatively clear (single pulse) impulsive shape, which occurs in only $\sim$ 12 % and $\sim$ 10 % of the $\sim$ 46,000 and $\sim$ 26,500 BLUEs detected by MMIA in the investigated period (1 April 2019 - 31 March 2021) and distributed according GD-1 and GD-2, respectively. Clear impulsive single pulse BLUEs are considered when the fittings have $R^2 > 0.75$, being R^2 the so-called coefficient of determination (used as a metric of fit goodness), which can change between negative values and 1 (perfect fit). A number of correlations have been established between the above mentioned characteristics of BLUEs.

By assuming a point-like source for the light source deep in the cloud, the first hitting time (FHT) fit (Soler et al., 2020) provides a first approximation to the single pulse BLUE

depth with respect to cloud tops within thunderstorms, 337.0 nm peak power density (and total brightness), rise and total times (Soler et al., 2020; Luque et al., 2020).

The tail of the light curve from an extended source (see Figure 8.14 of the supplementary material) that spans altitudes close to the cloud top to a maximum distance L_0 inside the cloud can also be fitted to obtain the best-fit cutoff (characteristic photon diffusion) time $\tau_D = L_0^2/4\mathrm{D}$, and the total number of source photons (N) (Li et al., 2021), with D being a diffusion coefficient (Soler et al., 2020). For short times after the optical emission and assuming that the mean absorption time (τ_A) of the photons inside the cloud is much larger than τ_D, the fit discussed in Li et al. (2021) predicts a $\sim (\tau_D t)^{-1/2}$ dependence for the photon flux exiting the cloud top. From N and τ_D one can obtain the number of streamers in the BLUE as well as its maximum length L_0 (Li et al., 2021) (for more details, see the supplementary material).

We have assumed that extended sources are located in the perfect nadir (no angle with vertical). However, this might not always be the case and such an assumption could underestimate the total optical energy of all the 337.0 nm photons emitted by a BLUE.

Finally, we found that $\sim$ 2700 events (with $R^2 > 0.75$) in GD-1 and $\sim$ 262 events (with $R^2 > 0.75$) in GD-2 can be fit by both the point-like and the extended-source models (see Table 3). Likely these are cases where the optical source is both small and close to the cloud top.

Table 3 shows the total number of BLUE events in GD-1 and GD-2 discriminating according to their type (point-like or extended). Note that for the point-like sources the total time is derived from the first hitting time (FHT) model fitting, while for the extended sources the total time is obtained from the raw data (since the fitting used for the extended sources does not include the rise).

8.5 Results and discussion

In order to provide some perspective to the reader, Figure 8.5 and Figure 8.6 show four maps that display, in four intervals of peak power density (PPD), the geographical distribution (per $2^\circ \times 2^\circ$ grid cell) of the $\sim$ 46,000 and $\sim$ 26,500 BLUEs detected by ASIM-MMIA corresponding to the GD-1 and GD-2 annual average distributions. Panels (a), (b), (c) and (d) of Figure 8.5 and Figure 8.6 show BLUEs with PPD < 25 μW m^{-2}, between ≥ 25 μW m^{-2} and 50 μW m^{-2}, between ≥ 50 μW m^{-2} and 100 μW m^{-2} and ≥ 100 μW m^{-2}, respectively.

In regard to the $\sim$ 53,000 BLUEs earlier reported in Soler et al. (2021), there are 3183 with PPD $\geq$ 100 μW m^{-2}. Of these 3183, 2992 events, that is, $\sim$ 94 % (mostly in latitudes above 35°N and below 35°S) concentrate between 1 September 2018 and 31 March 2019 during the first seven months of the 2-year period evaluated in Soler et al. (2021), while in the following 17 months there are only $\sim$ 6 % of the 3183 BLUEs worldwide with PPD $>$ 100 μW m^{-2}. Interestingly, we only found 282 BLUEs with PPD $>$ 100 μW m^{-2} when searching (with exactly the same algorithm as in Soler et al. (2021)) in the two-year period 1 April 2019 - 31 March 2021.

It is important to note that on March 2019 there was an update of the ASIM-MMIA cosmic ray rejection algorithm software (ON only over the SAA before March 2019, ON everywhere after March 2019) that could have influenced the above findings.

The trend described above for the PPD $\geq$ 100 μW m^{-2} range is also identified (using exactly the same algorithm as in Soler et al. (2021)) in the other three lower PPD ranges between 1 September 2018 and 31 March 2019. However, the difference in the number of BLUEs (relative importance) of each PDD range with respect to succesive periods of seven months (1 September 2019 - 31 March 2020, and 1 September 2020 - 31 March 2021) is $\sim$ 6 %.

Consequently, in our study we decided to move forward seven months the period of time chosen to carry out the analysis of characteristics of BLUEs presented here.

8.5.1 Distribution of BLUEs according to altitude and peak power density

The worldwide distribution of BLUE altitudes in terms of the latitude is displayed in Figure 8.7 (a, c) for GD-1 and (b, d) for GD-2. All panels in Figure 8.7 and Figure 8.8 except panels (c, d) of Figure 8.7 display 5374 (GD-1) BLUE events ($\sim$ 12 % of $\sim$ 46,000) and 2242 (GD-2) BLUE events ($\sim$ 10 % of $\sim$ 26,500) with good quality fitting ($R^2 > 0.75$), that is, those that are closest to impulsive single pulse point-like sources. However, panels (c, d) of Figure 8.7 show most of the $\sim$ 46,000 BLUEs of GD-1 (panel (c)) and $\sim$ 26,500 BLUEs of GD-2 (panel (d)) detected by ASIM-MMIA that are fittable independently of the fitting quality, that is, for any value of R^2. Thus, Figure 8.7 (c, d) shows the altitude distribution of BLUE events which 337.0 nm light curves might not be fully explained by single pulse point-like sources.

The approximate altitude distributions of BLUEs (see Figure 8.7 (a)-(d)) are derived by assuming that the global cloud top height distribution can be approximated by the annual mean variation of the tropopause heights with the latitude (Offroy et al., 2015; Heumesser et al., 2021). BLUEs can, however, occur associated with deep convection

scenarios and are often detected in overshooting cloud tops extending across the local tropopause (Liu et al., 2018), which would break down the above mentioned assumption and can introduce an altitude uncertainty of $\sim$ 1-3 km (Liu et al., 2018).

In order to compare and / or validate the geographical (Figure 8.2) and altitude (Figure 8.7 (b, d)) distributions of BLUEs obtained in this paper for GD-2 we compared them (see Figure 8.29 and Figure 8.30 of the supplementary material) with several case-based studies of BLUEs already published (provided the events occurred within the dates of our climatology). Figure 8.29 shows local maps with numbers 1, 2, 3, and 4 on them indicating the centroid of the set of BLUEs investigated in the case-based studies reported in: (1) Li et al. (2021) and Liu et al. (2021a) over Southern China, (2) López et al. (2022) over Colombia, (3) Soler et al. (2020) over Indonesia and (4) the study by Li et al. (2022) about multiple pulse BLUEs over nearby Malaysia. The numbers 1 through 4 in Figure 8.30 are placed in the mean altitude and in the centroid (in terms of latitude and longitude) of the reported BLUE events in the mentioned local studies. Number with a $'$ indicates the mean height obtained by radio (VLF / LF) for the same set of BLUE events. The red dashes lines (above and below the solid red line) indicate the $\pm$ 3 km uncertainty associated with our approximation to globally compute the tropopause in each latitude. It can be seen that strong thunderstorms with overshooting tops penetrating into the lower stratosphere (cases 1 and 4) can create some discrepancies between the heights obtained by optical (applied globally in our analysis) and radio but, in any case, within the uncertainty of the method chosen to represent the tropopause at a global scale.

The red line in panels (a)-(d) in Figure 8.7 marks the annual mean variation of the tropopause heights with latitude. Two zonal layers of BLUEs (see greenish zones) can be distinguished: a top layer of shallow BLUEs ($\leq$ 0.5 km depth), and a deeper (2.5 km - 5 km depth) layer of BLUEs mostly located among tropical latitudes (10°S to 20°N).

Figure 8.7 (e, f) and Figure 8.8 show detailed GD-1 (left column) and GD-2 (right column) latitudinal and longitudinal distributions of impulsive single pulse BLUEs with respect their different depths below thundercloud tops around the globe and peak power densities. A thin and shallow layer of BLUEs at depth $\leq$ 1 km below cloud tops is visible across all latitudes (see Figure 8.7 (e, f)). This usually corresponds to the location of negative NBEs (Wu et al., 2014; Li et al., 2021). A second thicker and deeper layer between $\sim$ 1.25 km and $\sim$ 3.25 km below thundercloud tops is also distinguishable within the tropics and part of the subtropical regions (Figure 8.7 (e, f)). The longitudinal distributions of depths clearly exhibits three BLUE chimneys (see Figure 8.8 (c, d)) with the Americas chimney in GD-1 (see Figure 8.8 (c)) more populated due to the South America contribution. A fourth dim chimney is also visible in the Pacific ocean. This

changes in GD-2 where the most populated chimney is Asia/Australia (see Figure 8.8 (d)) and with the Pacific chimney remaining.

Figure 8.7 (e, f) and Figure 8.8 show detailed GD-1 (left column) and GD-2 (right column) latitudinal and longitudinal distributions of impulsive single pulse BLUEs with their peak power density (μW/m^2). Large ($\geq$ 50 μW/m^2) peak power BLUE events appear scattered across all latitudes and longitudes. Most single pulse BLUEs exhibit peak power densities $<$ 25 μW/m^2 (as shown in Figure 8.5 and Figure 8.6 for BLUES with all sorts of pulse shapes).

BLUEs with peak power densities below 25 μW/m^2 are common within the tropics, within the Indian subcontinent and near the ocean of the Asia/Australia BLUE chimney. The three BLUE chimneys appear in the meridional distribution of BLUEs shown in panels (c) through (f) of Figure 8.8.

8.5.2 Global distribution of BLUEs according to rise and total times

Figure 8.9 presents zonal (a)-(d) and meridional (e)-(h) distributions of the rise and total duration times of impulsive single pulse BLUEs of GD-1 (left column) and GD-2 (right column)), respectively. Note that the rise and total times are calculated as the elapsed times since the raw (or fitted) signal is above 10 % of the maximum until it reaches the maximum (rise time), and until it passes the maximum and decreases again to 10 % of the maximum (total time). For point-like sources the rise and total time are derived from the first hitting time (FHT) model fitting, while for extended sources the total time is obtained from the raw data. The presence of the SAA can be clearly seen between 5°S and 20°S in panels (a, c) of Figure 8.9 for GD-1, and between 0° and 100°W in panels (e, g) of Figure 8.9 for GD-1.

Single pulse BLUEs with fast ($\leq$ 30 μs) rise times and short ($\leq$ 0.5 ms) total times occur across all latitudes and longitudes. Zonal distributions show that the single pulse BLUEs concentrated within the tropics exhibit rise and total times ranging from 50 μs to 0.5 ms, and from 0.8 ms to $\sim$ 4 ms, respectively. Complementarily, meridional distributions displayed in Figure 8.9 (e)-(h) show that single pulse BLUEs in the three main chimneys exhibit roughly the same rise and total duration times with the Europe/Africa chimney being the one with slightly faster and shorter rise times and durations.

The left / right columns of Figure 8.10 for GD-1 / GD-2 show the connection between the peak power density (μW m^{-2}) and total brightness (μW ms m^{-2}) of impulsive single pulse BLUEs and their rise and total duration times. Both magnitudes (peak power density and maximum brightness) exhibit two clear populations. The most numerous

population includes single pulse BLUEs with fast ($\leq$ 50 μs) rise times and short ($\leq$ 0.5 ms) durations reaching peak powers and total brightnesses of up to 200 μW m^{-2} and 30-40 μW ms m^{-2}, respectively. The second group of single pulse BLUEs reaches longer rise times (up to $\sim$ 0.8 ms) and total times (up to $\sim$ 4 ms) associated with lower peak powers ($\leq$ 50 μW m^{-2}) and total brightnesses ($\sim$ 25 μW ms m^{-2}). The two groups of BLUEs with fast ($\leq$ 50 μs) and slow ($>$ 50 μs and up to $\sim$ 0.8 ms - 1.0 ms) rise times are consistent with those mentioned in Husbjerg et al. (2022).

8.5.3 Correlations between BLUE's depth and their rise and total times

The left / right columns of Figure 8.11 for GD-1 / GD-2 represent how light scattering affects key features (rise time and total time) of the 337.0 nm light curves of BLUEs. In order to appropriately visualize the relationships between rise and total times we have plotted the total and rise times as a function of the depth below cloud top (panels (a, c) for GD-1 and (b, d) for GD-2), and the total time vs rise time for GD-1 (panel (e)) and for GD-2 (panel (f)).

In general, the closer the BLUE source to the cloud top, the faster rise times and shorter duration times due to the weak scattering (as reported in Li et al. (2021)). On the contrary, when BLUE sources are deeply buried in storm clouds (like the ones in Soler et al. (2020)), scattering by cloud droplets and ice crystals blurs their image as observed from above and produced 337.0 nm light curves characterized by relatively long rise times (0.2 ms $-$ 0.5 ms) and total duration times ($>$ 1.5 ms). Therefore, shallow ($\leq$ 1 km depth) single pulse BLUEs exhibit fast rise times below $\sim$ 50 μs and total duration times below $\sim$ 0.5 ms. Deeper single pulse BLUES occurring between $\sim$ 1 km and $\sim$ 4 km below cloud tops are characterized by rise and total times that increase up to about 0.8 ms (for 4 km) and 5 ms (for $\sim$ 3 km), respectively. The bottom branch of Figure 8.11 (a, c) for GD-1 also shows some few BLUEs that, even occurring deeper (1-8 km below cloud tops) in thunderclouds, still exhibit fast rise times of $\leq$ 60 μs and short durations ($\leq$ 200 μs). This result is not physically possible and should be disregarded. These few unphysical events in Figure 8.11 (a, c) for GD-1 disappear almost completely in Figure 8.11 (b, d) for GD-2.

Figure 8.11 (e) for GD-1 and Figure 8.11 (f) for GD-2 show the connection between the total time duration of single pulse BLUEs and their rise time. For fast ($\leq$ 40 μs) rise times, the total duration ranges from $\sim$ 100 μs to $\sim$ 300 μs. However, as the rise time increases beyond $\sim$ 40 μs, panels (e, f) of Figure 8.11 show a main branch in the top associated with single pulse BLUEs with relatively long (0.4 ms to 5 ms) total durations.

It is also interesting to note that, as shown in panels (a) for GD-1 and (b) for GD-2 of Figure 8.10, fast ($\leq$ 40 μs) rise time BLUEs come with a 337.0 peak power density that can reach values of up to $\sim$ 200 μW m^{-2}. When rise times are beyond 50 μs the BLUEs' peak power density stays below $\sim$ 50 μW m^{-2} and exhibits a decreasing trend as rise time increases from $\sim$ 0.1 ms to $\sim$ 1 ms.

8.5.4 Global zonal/meridional distributions of BLUEs' streamers and lengths

Figure 8.12 presents the zonal and meridional distributions of the lengths (L_0) and number of streamers (k) for GD-1 (left column) and GD-2 (right column) of single pulse BLUEs, respectively. The lengths of most single pulse BLUEs roughtly vary between $\sim$ 100 m and $\sim$ 1500 m in GD-1 (see panels (a) and (c) in Figure 8.12). However, the group of tropical BLUEs with lengths between 2 km and up to $\sim$ 5 km dominate in GD-2 (see panels (b) and (d) in Figure 8.12).

According to our analysis, the number of streamers in single pulse BLUEs ranges between 10^8 and 10^9 in agreement with previous results (Liu et al., 2019; Cooray et al., 2020; Li et al., 2021). BLUEs with most streamers concentrate between 20°S and 20°N (see panels (e) for GD-1 and (f) for GD-2 of Figure 8.12) with the tropical band including some BLUEs with up to $\sim$ 2-3$\times10^9$ streamers. The meridional distribution of BLUEs' streamers (see panels (g) for GD-1 and (h) for GD-2 of Figure 8.12) exhibit a three chimney structure with the Asia/Australia chimney including some BLUEs with up to $\sim$ 2-3$\times10^9$ streamers.

8.6 Conclusions

We have found in this study that approximately $\sim$ 10 % to $\sim$ 12 % of all BLUEs detected globally are impulsive single pulse ones. However, there can still be ambiguous (mostly not impulsive) single pulse events with $R^2 < 0.75$. A systematic analysis has been undertaken to determine the geographical (zonal and meridional) distribution of key properties of BLUEs including impulsive single pulse ones. In particular, our analysis focussed on quantifying their altitudes and depths below thundercloud tops, characteristic rise and total duration times, peak power density, total brightness, vertical extension and number of streamers.

Our study concludes that the over detection (concentrated between 1 September 2018 and 31 March 2019) of BLUEs shown in Soler et al. (2021) in the high latitudes of the northern and southern hemispheres was caused by a combined effect of (i) an update in the ASIM-MMIA cosmic rejection algorithm software (ON only over the SAA before

March 2019, ON everywhere after March 2019), (ii) cosmic rays and the particle flux from the inner radiation belts detectable in the SAA and in the high latitudes of the northern and southern hemispheres.

As a consequence of this, two new worldwide annual average (and seasonal) distributions of nighttime BLUEs were generated and presented here using global ASIM-MMIA level 1 (calibrated) data in a different two-year period (1 April 2019 - 31 March 2021) shifted seven months ahead with respect to the earlier two-year period explored in Soler et al. (2021). While the first global average distribution (GD-1) of BLUEs is derived using exactly the same algorithm described in Soler et al. (2021), the second distribution (GD-2) removes events in all planet (including the SAA) with rise time (τ_{rise}) $\leq$ 40 μs and total duration (τ_{total}) $\leq$ 150 μs. This remarkably removes the SAA shadow in GD-1 but can also underestimate the number of BLUEs in South America and, consequently, the total number of BLUEs that could range between the $\sim$ 26,500 obtained for GD-2 and the $\sim$ 46,000 counted for GD-1.

Two distinct populations of BLUEs with peak power density $<$ 25 μWm^{-2} (common) and $\geq$ 25 μWm^{-2} (rare) are observed. While BLUEs with small to moderate ($<$ 25 μWm^{-2}) peak power can occur over land and the maritime regions, BLUEs with large ($>$ 50 μW/m^2) peak power occur scattered across all latitudes and longitudes mainly over land.

BLUEs are globally found between the cloud tops and $\sim$ 4 km below cloud tops in the tropics and $\leq$ 1 km in mid and higher latitudes. Fast rise time ($<$ 0.05 ms) BLUEs with short ($<$ 0.5-0.6 ms) total times occur (across all latitudes and longitudes) very superficially ($<$ 1 km) near cloud tops with high power density $\geq$ 100 μWm^{-2}. BLUEs with peak powers below 50 μWm^{-2} have longer ($>$ 50 μs) rise times and longer ($>$ 0.5 ms) durations.

Zonal distributions show that BLUEs concentrated within the tropics exhibit rise and total times ranging from 50 μs up to 0.5 ms, and from 0.8 ms up to $\sim$ 4 ms, respectively. Complementarily, meridional distributions show that BLUEs in the three chimneys exhibit roughly the same rise and total duration times with the Europe/Africa chimney being the one with slightly faster rise times and shorter durations.

The vertical length of BLUEs as well as their number of streamers are two interesting features of in-cloud corona discharges that have also been characterizated and geographically analysed in this work. The vertical extension of most impulsive single pulse BLUEs changes between $\sim$ 100 m and $\sim$ 1500 m with a group of longer (up to $\sim$ 4-5 km) BLUEs located within the tropics in the three main BLUE chimneys especially visible in GD-2.

The obtained climatology for the features of BLUEs opens the door to investigate the relationship between characteristics of BLUEs and meteorological parameters. The observed variability in some features of BLUEs, such as their depth, number of streamers, the rise time and the total duration of their optical pulses, indicates that they can be influenced by some meteorological parameters like the convective available potential energy (CAPE)(see Figure 7.17 in the supplementary material of Soler et al. (2021), and Husbjerg et al. (2022)). These findings suggest that monitoring the occurrence and the features of BLUEs could serve as an indicator to characterize severe weather (deep convection episodes) (Liu et al., 2018; Soler et al., 2021; Husbjerg et al., 2022). In particular, Husbjerg et al. (2022) show difference in convection levels for lightning producing storms and BLUE producing storms.

Recent airborne observations (Brune et al., 2021) and laboratory experimental results (Jenkins, Brune, and Miller, 2021) indicate that considerable amounts of oxidant species (OH, HO_2) could be directly produced by visible and subvisible (corona) electrical discharges in thunderstorm anvils and not only be the indirect result of atmospheric chemical processes after the injection of lightning NO_x (Schumann and Huntrieser, 2007; Finney et al., 2016; Gordillo-Vázquez et al., 2019). The production of OH and HO_2 recently reported by Jenkins, Brune, and Miller (2021) could also be due to air plasma streamers in corona discharges occurring in thunderstorm anvils (Zahn et al., 2002; Minschwaner et al., 2008; Bozem et al., 2014; Pérez-Invernón et al., 2019; Gordillo-Vázquez and Pérez-Invernón, 2021) since thundercloud coronas (Soler et al., 2020; Li et al., 2021; Liu et al., 2021a) are now known to be more frequent (about 10 per second worldwide) (Soler et al., 2021) than previously suspected. Corona discharges in thunderclouds are especially frequent in the Tornado alley in North America (Soler et al., 2021) where airborne observations by Brune et al. (2021) have recently reported significant regional transient enhancements of OH and HO_2 concentrations during thundercloud electrical activity.

In summary, the geographical (and seasonal) distributions of BLUEs and all their characteristics presented here (including the knowledge of the altitude distribution of impulsive single pulse BLUEs and their number of streamers) can be critical parameters to explore how corona discharges in thunderclouds could contribute to the global chemical budget of important oxidant species like OH and HO_2, and key greenhouse gases such as ozone (O_3) and nitrous oxide (N_2O) in the climate sensitive region of the upper troposphere and lower stratosphere region.

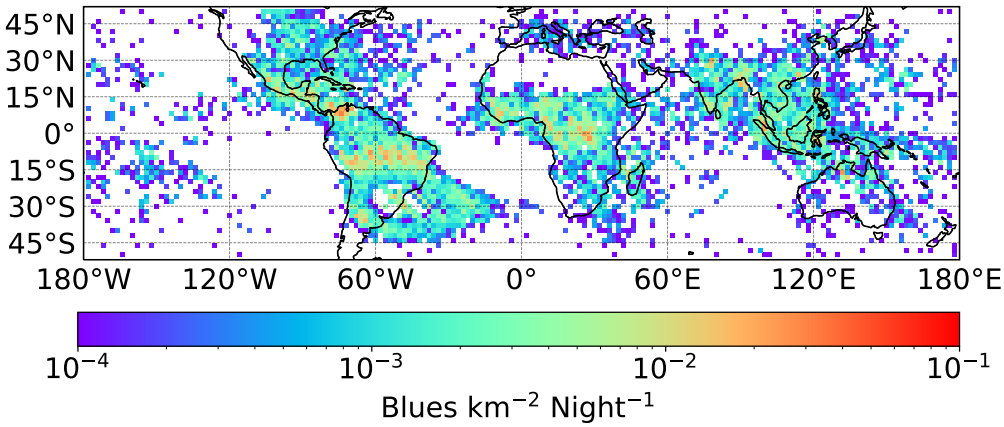

Figure 8.1. Two-year average (1 April 2019 through 31 March 2021) nighttime climatology of global BLUE electrical activity in thunderclouds (GD-1) showing $\sim$ 46,000 BLUEs. The map is generated using 2° $\times$ 2° grid cells. The BLUEs shown can have any temporal shape, that is, no distinction has been made here among BLUEs with a single (impulsive or not) pulse, multiple pulses or any other irregular pulse shape. The annual global rate of GD-1 BLUEs peak at 9.5 events s^{-1} in the local midnight (00.00 local solar time), and show a decreasing global rate as local daytime approaches (and there is less MMIA observation time). On average, the global annual average rate of BLUEs in GD-1 is 6.0 events s^{-1}. Note that ASIM can only observe during the night.

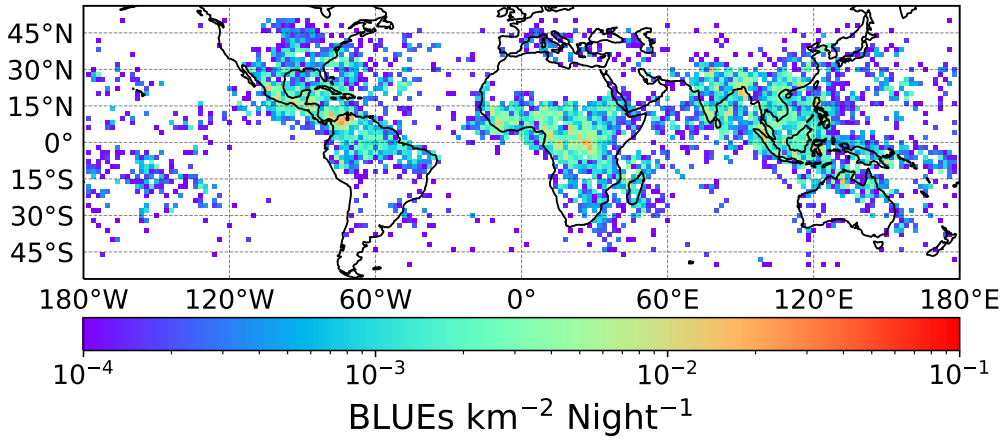

Figure 8.2. Two-year average (1 April 2019 through 31 March 2021) nighttime climatology of global BLUE electrical activity in thunderclouds (GD-2) removing events in all planet (including the SAA) with rise time (τ_{rise}) $\leq$ 40 μs and total duration (τ_{total}) $\leq$ 150 μs. The map is generated using 2° × 2° grid cells. Note that it is quite possible that not all the removed $\sim$ 20000 events with respect to GD-1 are radiation belt particles and cosmic rays. Consequently, the number of BLUEs ($\sim$ 26,500) shown in this GD-2 distribution is most probably underestimated. The BLUEs shown can have any temporal shape, that is, no distinction has been made here among BLUEs with a single (impulsive or not) pulse, multiple pulses or any other irregular pulse shape. The annual global rate of GD-2 BLUEs peak at 5.5 events s^{-1} in the local midnight (00.00 local solar time), and show a decreasing global rate as local daytime approaches (and there is less MMIA observation time). On average, the global annual average rate of BLUEs in GD-2 is 3.5 events s^{-1}. Note that ASIM can only observe during the night.

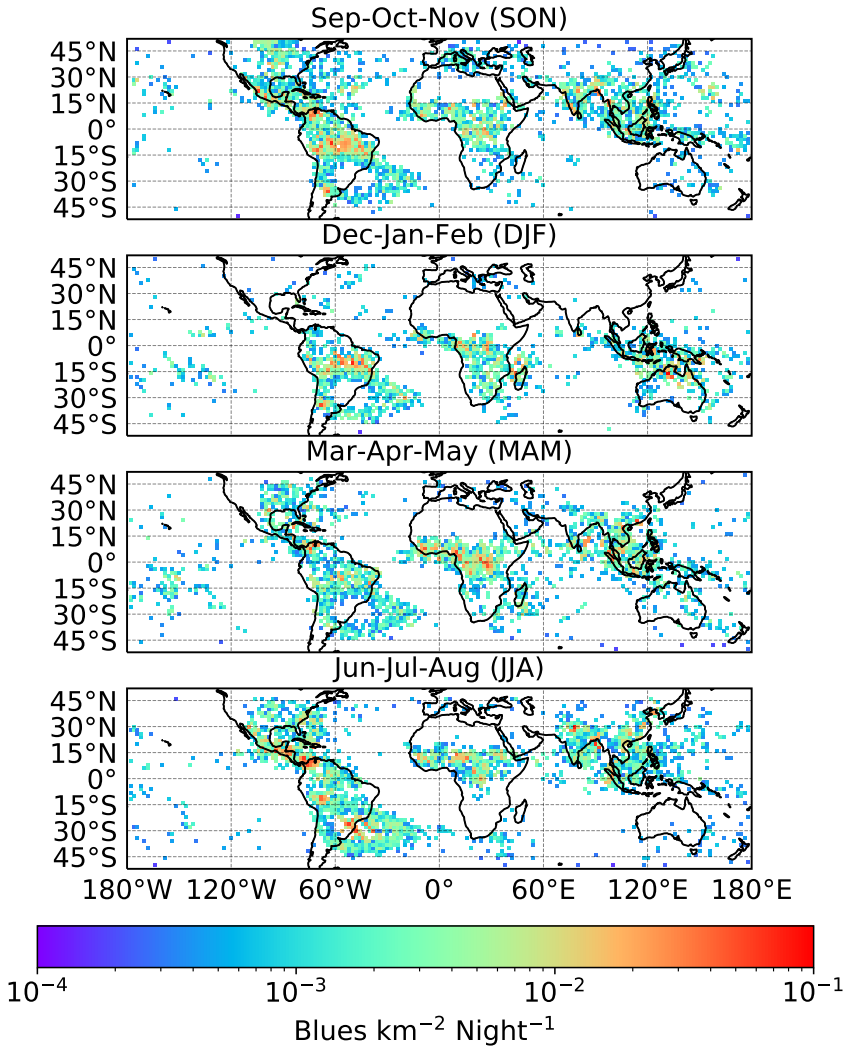

Figure 8.3. Nighttime seasonal distribution of BLUE electrical activity in thunderclouds associated to GD-1 in Figure 8.1. The global nighttime seasonal BLUE rates are: 6.7 (SON), 4.7 (DJF), 5.9 (MAM) and 6.8 (JJA) BLUEs s^{-1}. These maps are generated using 2° × 2° grid cells. The BLUEs shown can have any temporal shape, that is, no distinction has been made here among BLUEs with a single (impulsive or not) pulse, multiple pulses or any other irregular pulse shape.

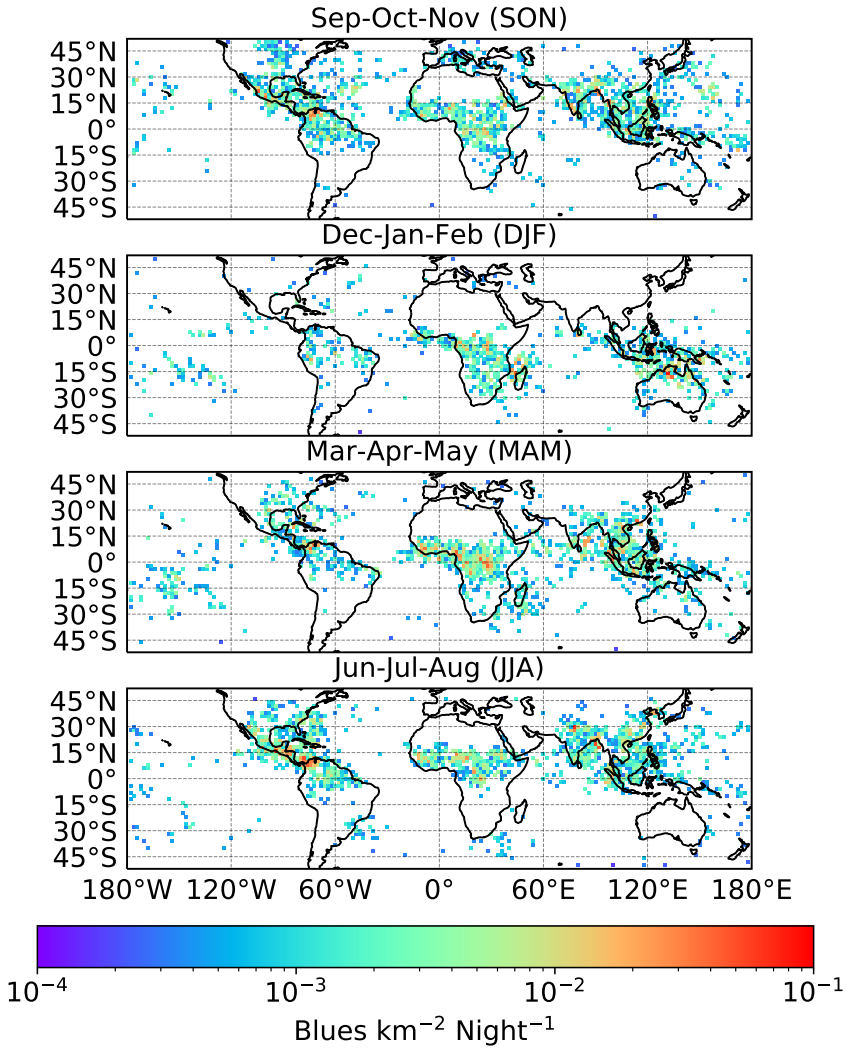

Figure 8.4. Nighttime seasonal distribution of BLUE electrical activity in thunderclouds associated to GD-2 in Figure 8.2. The global nighttime seasonal BLUE rates are: 3.7 (SON), 2.6 (DJF), 3.7 (MAM) and 4.0 (JJA) BLUEs s^{-1}. These maps are generated using 2° × 2° grid cells. The BLUEs shown can have any temporal shape, that is, no distinction has been made here among BLUEs with a single (impulsive or not) pulse, multiple pulses or any other irregular pulse shape.

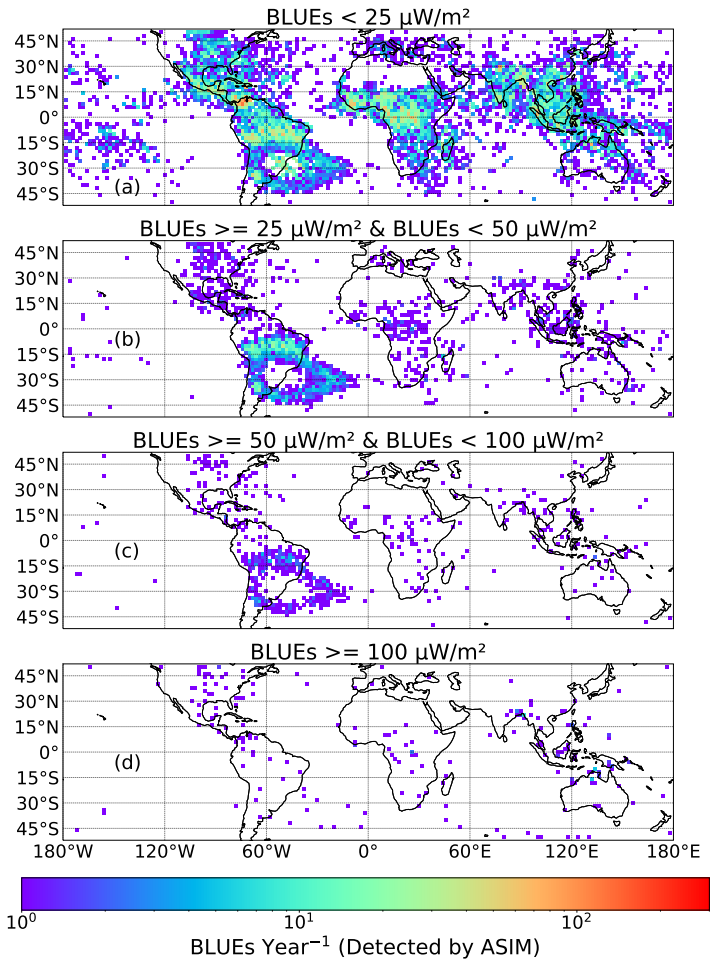

Figure 8.5. Geographical distribution (in 2°×2° grid cells) of the ∼ 46,000 nighttime GD-1 BLUEs detected by ASIM-MMIA in the two-year period from 1 April 2019 to 31 March 2021. Panels (a), (b), (c) and (d) show BLUEs of any shape with peak power density (PPD) between ≥ 3 μW m^{-2} and < 25 μW m^{-2}, between ≥ 25 μW m^{-2} and < 50 μW m^{-2}, between ≥ 50 μW m^{-2} and < 100 μW m^{-2}, and ≥ 100 μW m^{-2}, respectively. There are 39980 BLUEs in panel (a) (19990/year), 4367 in panel (b) (2183.5/year), 833 in panel (c) (416.5/year), and 282 in panel (d) (141/year). The BLUEs shown in these maps can have any temporal shape, that is, no distinction has been made here among BLUEs with a single (impulsive or not) pulse, multiple pulses or any other irregular pulse shape.

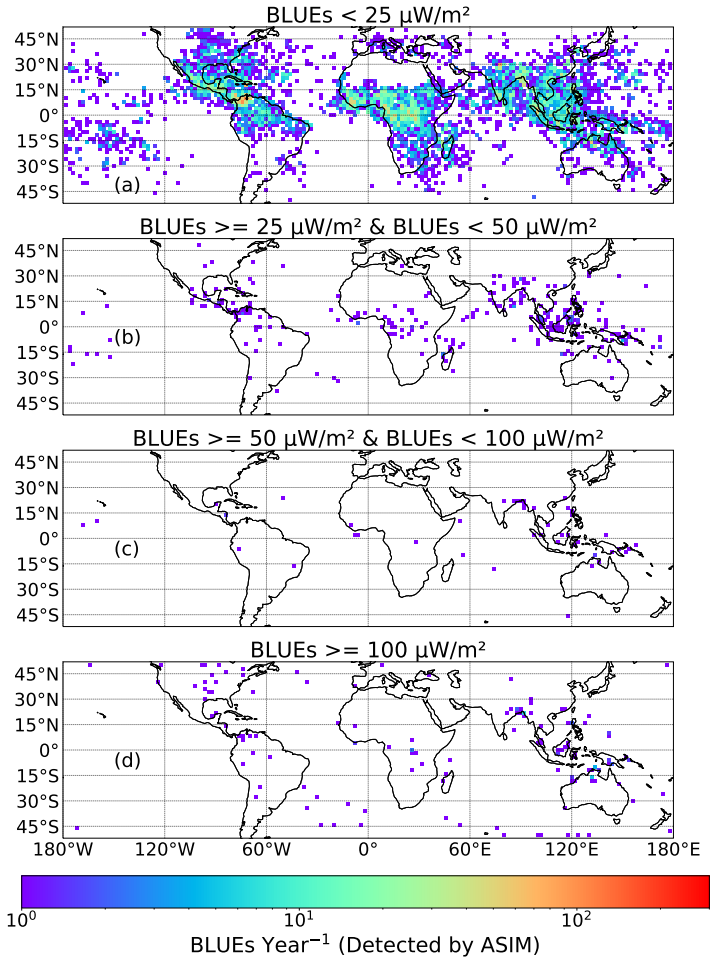

Figure 8.6. Geographical distribution (in 2°×2° grid cells) of the ∼ 26,500 nighttime GD-2 BLUEs detected by ASIM-MMIA in the two-year period from 1 April 2019 to 31 March 2021 removing events in all the planet (including the SAA) with rise time (τ_{rise}) ≤ 40 μs and total duration (τ_{total}) ≤ 150 μs. Panels (a), (b), (c) and (d) show BLUEs of any shape with peak power density (PPD) between ≥ 3 μW m^{-2} and < 25 μW m^{-2}, between ≥ 25 μW m^{-2} and < 50 μW m^{-2}, between ≥ 50 μW m^{-2} and < 100 μW m^{-2}, and ≥ 100 μW m^{-2}, respectively. There are 25720 BLUEs in panel (a) (12860/year), 380 in panel (b) (190/year), 52 in panel (c) (26/year), and 204 in panel (d) (102/year). The BLUEs shown in these maps can have any temporal shape, that is, no distinction has been made here among BLUEs with a single (impulsive or not) pulse, multiple pulses or any other irregular pulse shape.

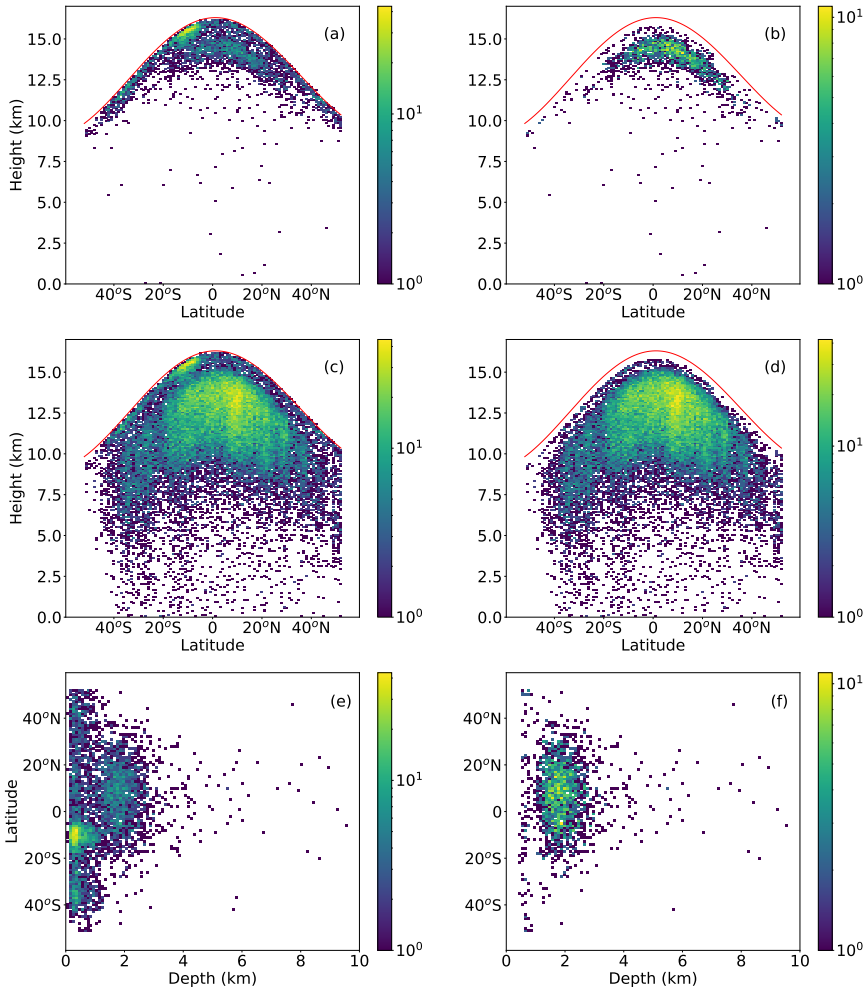

Figure 8.7. Approximate altitude distributions of GD-1 (left column) and GD-2 (right column) impulsive single pulse BLUEs (with R^2>0.75) (a, b), all sort of first hitting time (FHT) fittable BLUEs in GD-1 and GD-2 with any value of R^2 (c, d). Zonal distributions of GD-1 and GD-2 impulsive single pulse BLUE depths (e, f). Note that, always, GD-1 is in the left column and GD-2 is in the right column. The colorbar indicates number of events.

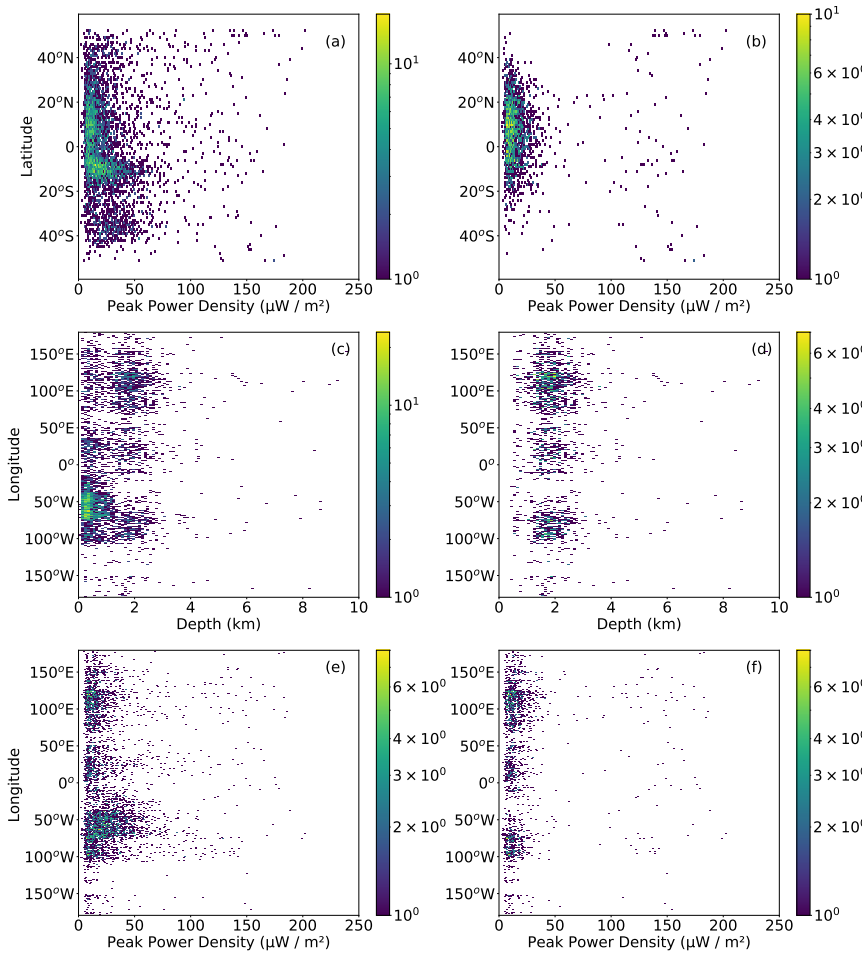

Figure 8.8. Zonal distributions of GD-1 and GD-2 impulsive single pulse BLUE peak power density (a, b). Meridional distributions of impulsive single pulse BLUE depths (c, d) and peak power density (e, f). Note that, always, GD-1 is in the left column and GD-2 is in the right column. The colorbar indicates number of events.

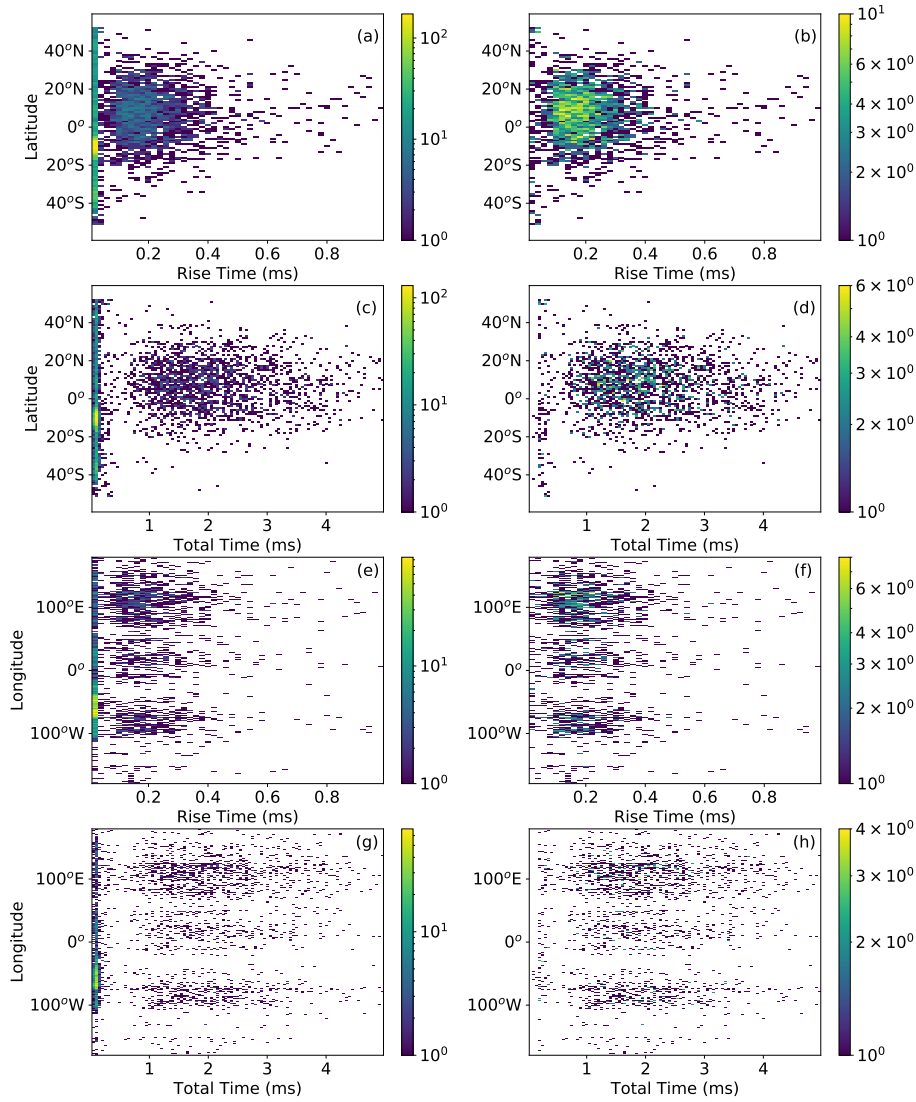

Figure 8.9. Zonal (a)-(d) and meridional (e)-(h) distributions of rise times (a, b, e, f) and total times (duration) (c, d, g, h) of impulsive single pulse BLUEs in GD-1 (left column) and GD-2 (right column). Note that, always, GD-1 is in the left column and GD-2 is in the right column. The colorbar indicates number of events.

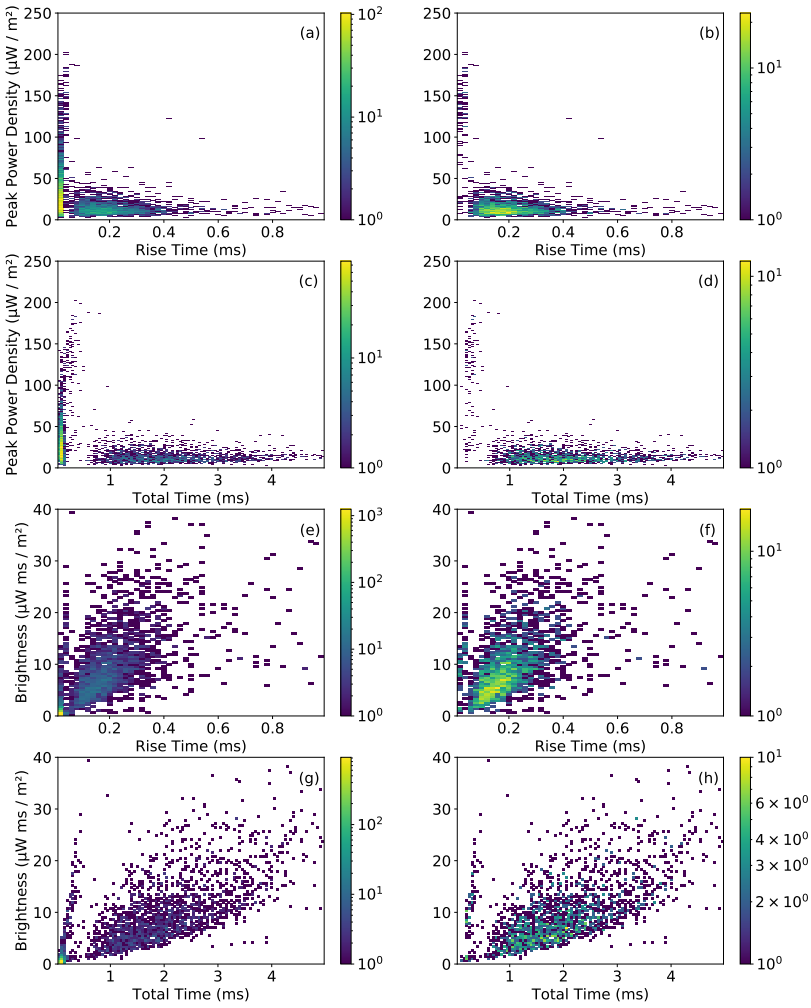

Figure 8.10. Variation of the peak power density (a)-(d) and total brightness (e)-(h) as a function of the GD-1 (left column) and GD-2 (right column) impulsive single pulse BLUE rise times (a, b, e, f) and total time (duration) (c, d, g, h). Note that the rise and total times are calculated as the elapsed times since the raw signal is above 10 % of the maximum until it reaches the maximum (rise time), and until it passes the maximum and decreases again to 10 % of the maximum (total time). Note that, always, GD-1 is in the left column and GD-2 is in the right column. The colorbar indicates number of events.

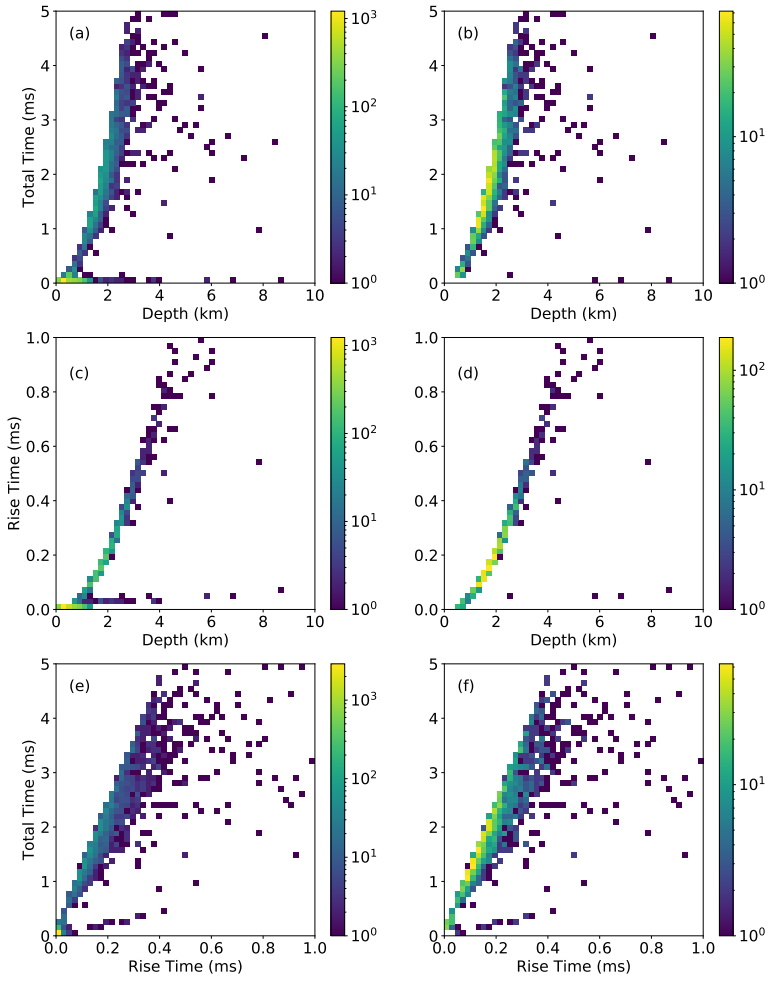

Figure 8.11. Total times (duration) and rise times of impulsive single pulse BLUEs in GD-1 (left column) and GD-2 (right column) as a function of depth (a)-(d). Panels (e) and (f) show the relationship between total times (duration) and rise times for GD-1 (left column) and GD-2 (right column). Note that panels (a, c) of GD-1 show the presence of some few unphysical events located deep (1-8 km below cloud tops) in thunderclouds characterized by simultaneously exhibiting very short total times ($\leq$ 200 μs) and rise times ($\leq$ 60 μs). This is mostly solved in panels (b, d) of GD-2. Note that, always, GD-1 is in the left column and GD-2 is in the right column. The colorbar indicates number of events.

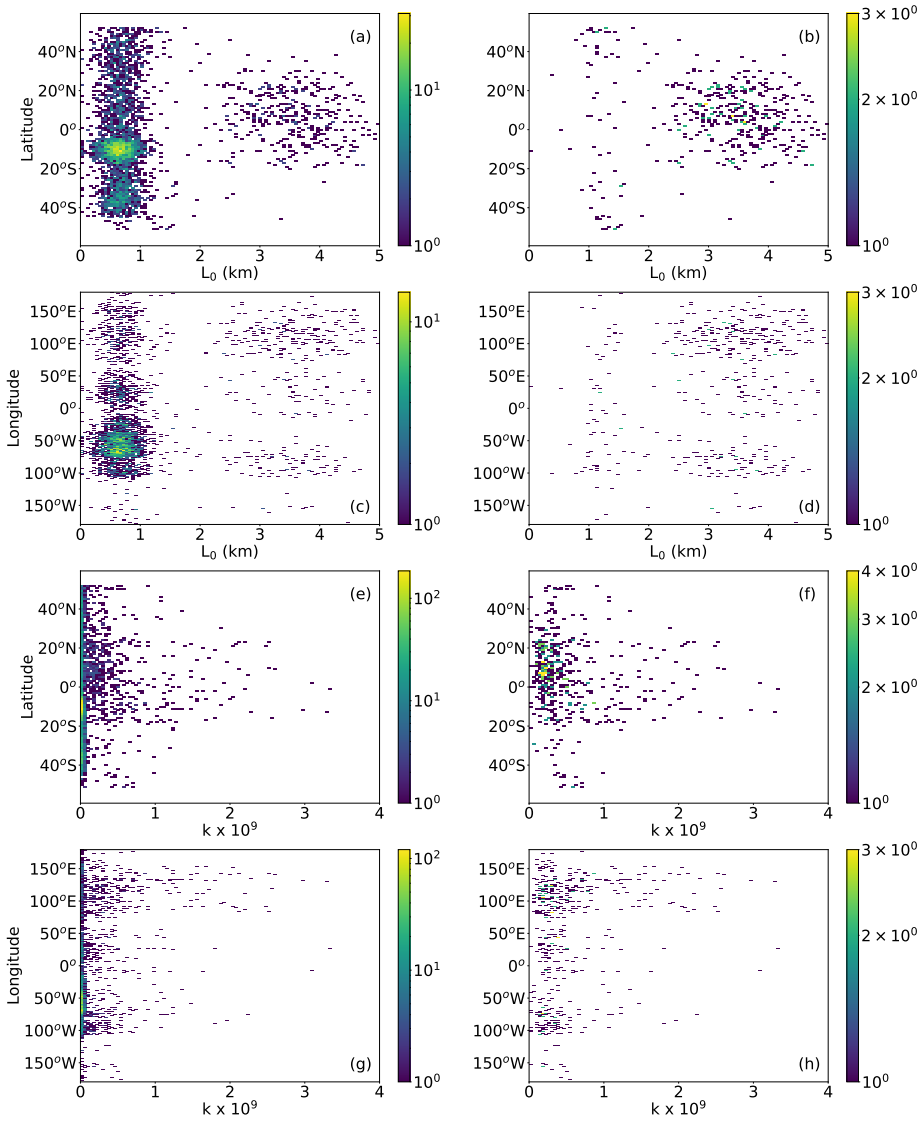

Figure 8.12. Zonal and meridional distributions of the lengths (L_0) (a)-(d) and number of streamers ($k \times 10^9$) (e)-(h) of impulsive single pulse BLUEs in GD-1 (left column) and GD-2 (right column). Note that, always, GD-1 is in the left column and GD-2 is in the right column. The colorbar indicates number of events.

	GD-1	GD-2 eliminate events worldwide with ($\tau_{rise} \leq 40$ μs and $\tau_{total} \leq 150$ μs)
TOTAL	46283	26355
Point-like source ($R^2 > 0.75$)	5374	2242
Extended source ($R^2 > 0.75$)	4258	553
Common ($R^2 > 0.75$)	2717	262

Table 8.1. Total number of BLUE events in GD-1 and GD-2 discriminating according to their type (point-like or extended). Note that for the point-like sources the total time is derived from the first hitting time (FHT) model fitting, while for the extended sources the total time is obtained from the raw data.

8.6.1 Appendix

1. Text

2. Figures 39 to 58

8.6.2 Introduction

We include in this supplementary material a number of complementary figures to those presented in the main text of the paper.

8.6.3 Text

The equations used to fit point-like and extended light sources in thunderclouds are:

For point-like sources, the flux per photon in the source is given by Soler et al. (2020):

$$f(t) = \frac{\theta(t-t_0)e^{2\sqrt{\nu\tau}}}{\tau\sqrt{\pi}} \left(\frac{\tau}{t-t_0}\right)^{3/2} e^{-\tau/(t-t_0)-\nu(t-t_0)}, with \int_{-\infty}^{\infty} f(t)dt = 1 \tag{8.1}$$

where θ is the step function, t_0 is the emission time and $\tau_D = L^2/4D$ is the characteristic time of the process. Given a photometer signal, we fit it to equation (8.1) and we obtain values for the parameters t_0, τ_D and ν. Then the depth L of the event relative to the cloud top can be estimated as $L = (4D\tau_D)^{1/2}$ with the diffusion coefficient $D = 3 \times 10^9$ m^2 s^{-1} associated to a photon mean free path of $\Lambda = 4$ m corresponding to a droplet concentration $n = 10^8$ m^{-3} and a radius of $r = 20$ μm (Soler et al., 2020). This equation does not need initial values, the fitting procedure with python can easily obtain values for t_0, τ_D and ν.

For extended sources Li et al., 2021:

$$f(t) = \frac{N}{L_0} \left(\frac{D}{t}\right)^{1/2} (1 - e^{-\tau_D/t})e^{-t/\tau_A}, \tag{8.2}$$

where N is the number of source photons, $\tau_D = L_0^2/4D$ is the characteristic time of the process, L_0 is the vertical length (from the cloud top) of the BLUEs and τ_A is the mean absorption time of the photons inside the cloud. The values of τ_A are usually much larger than τ_D so that the term $\exp^{-t/\tau_A}$ becomes ~ 1. Note that the value of the diffusion coefficient used in equation (2) and (3) (see below) is the same one used in equation (1) above.

In order to convert (2) to the flux (W m^{-2}) detected by ASIM, one needs to multiply (2) by the 337.0 nm photon energy (5.89×10^{-19} J) and by a geometrical factor that

includes the Lambertian radiation pattern $\cos(\theta)$ / πR^2 with R the distance in kilometers to ASIM and θ the angle between the observation path and the vertical. We assumed $\theta = 0°$. Note that the values of R change according to the altitude of the International Space Station in each detection.

The final form of the equation (2) that we fit is:

$$f(t) = 5.89 \times 10^{-19} \frac{N}{\pi R^2} \left(\frac{1}{4\tau_D t} \right)^{1/2} (1 - e^{-\tau/t}), \tag{8.3}$$

For the fitting of equation (3), the initial guess of parameters is $N = 10^{21}$ and $\tau_D = 10^{-3}$. From the value of τ_D we can derive the vertical length L_0 of the events.

The number of points chosen for the fitting of equations (1) and (3) is 500 (5 ms) and 400 (4 ms), respectively.

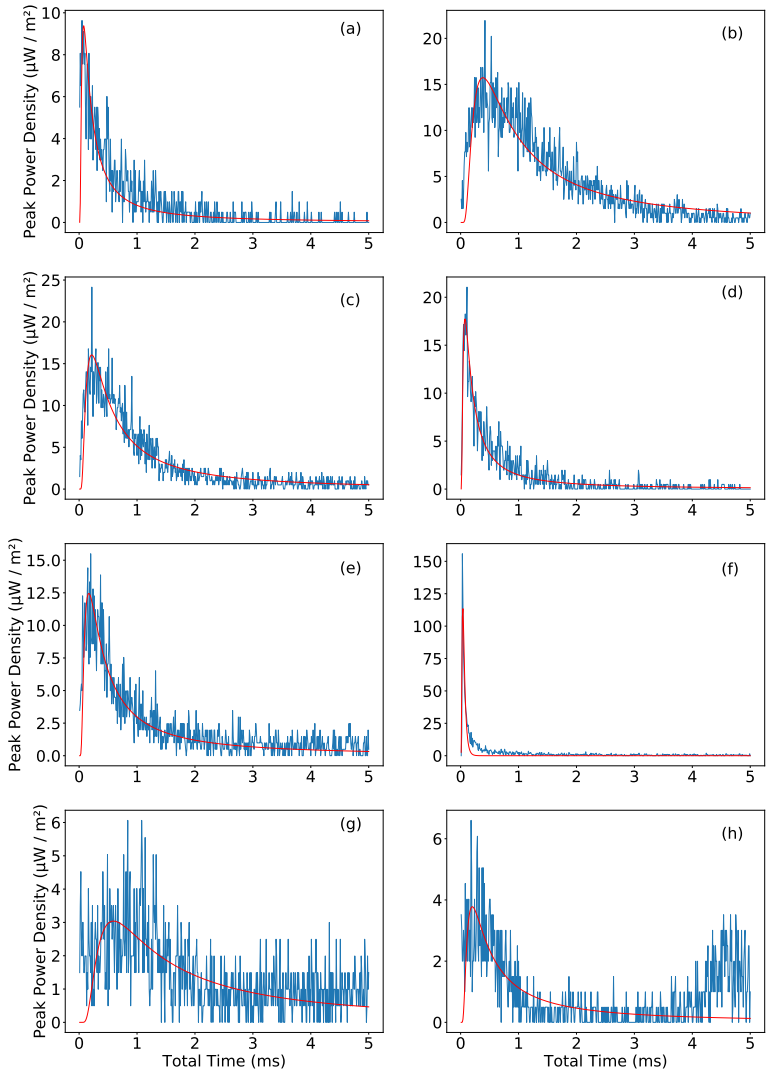

Figure 8.13. Examples of eight impulsive single pulse BLUEs fitted (red line) with the first hitting time (FHT) model resulting in a R^2 of (a) 0.75, (b) 0.80, (c) 0.85, (d) 0.90, (e) 0.79, (f) 0.86, (g) 0.24, and (h) 0.21.

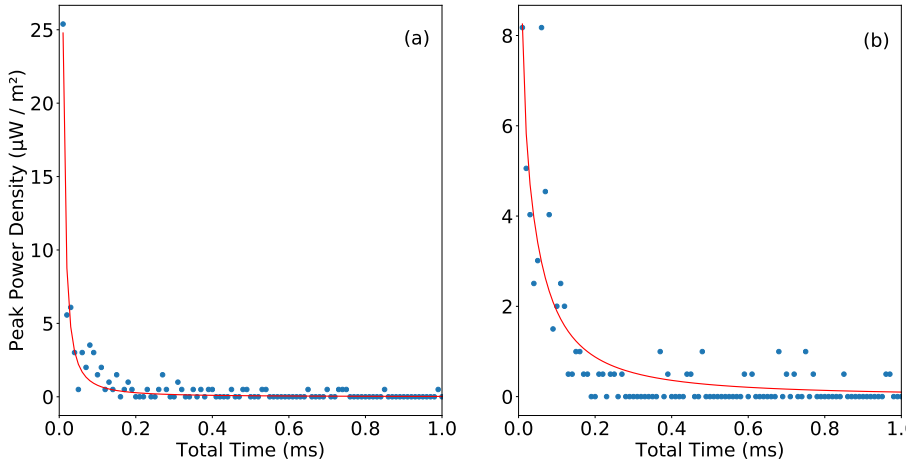

Figure 8.14. Examples of two BLUE events fitted (red line) assuming that they are extended sources reaching the cloud top. The fit results in a R^2 of (a) 0.94, and (b) 0.75.

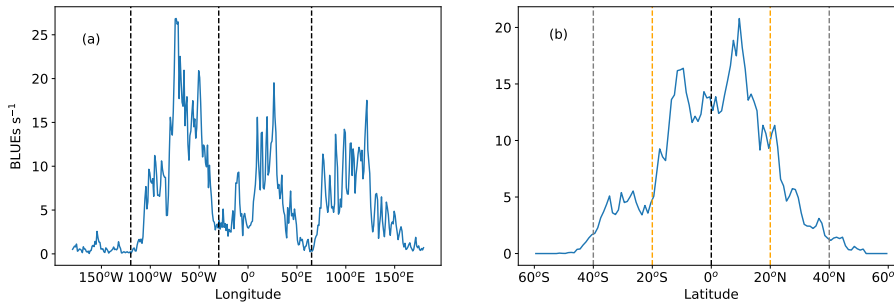

Figure 8.15. Meridional (a) and zonal (b) geographical distribibutions associated to the two-year (1 April 2019 through 31 March 2021) GD-1 nighttime climatology of BLUEs (see Figure 8.1 of main paper). These plots were generated using $1^\circ \times 1^\circ$ grid cells.

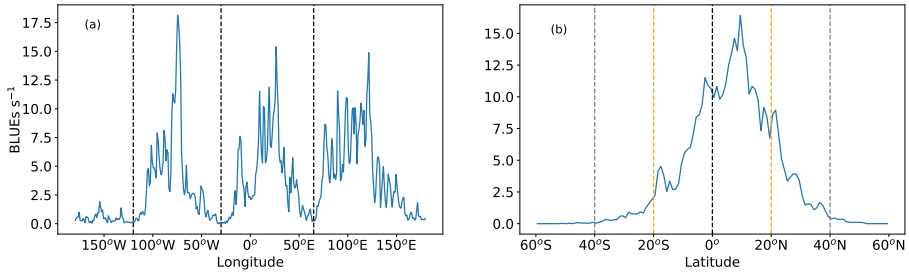

Figure 8.16. Meridional (a) and zonal (b) geographical distribibutions associated to the two-year (1 April 2019 through 31 March 2021) GD-2 nighttime climatology of BLUEs (see Figure 8.2 of main paper). These plots were generated using $1^\circ \times 1^\circ$ grid cells.

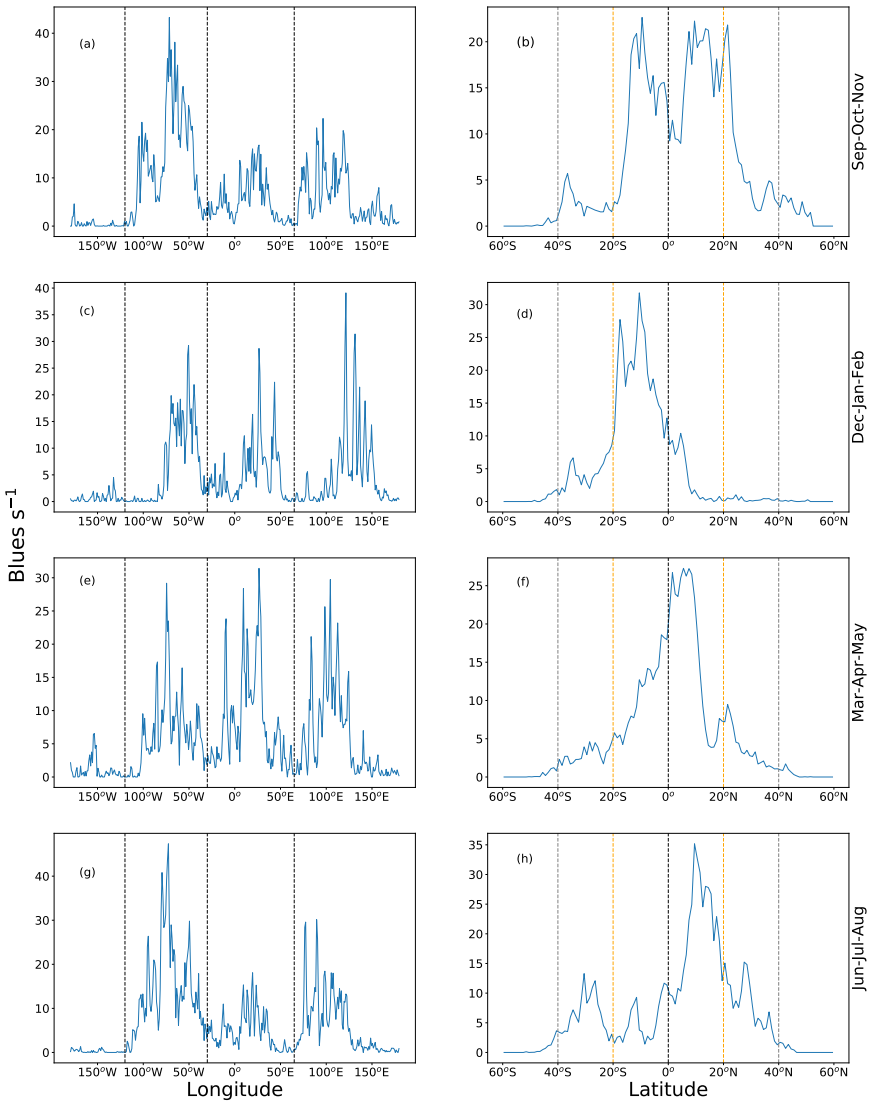

Figure 8.17. Seasonal meridional (left) and zonal (right) distributions associated to the two-year (1 April 2019 through 31 March 2021) seasonal GD-1 nighttime climatology of BLUEs (see Figure 8.3 of main paper).

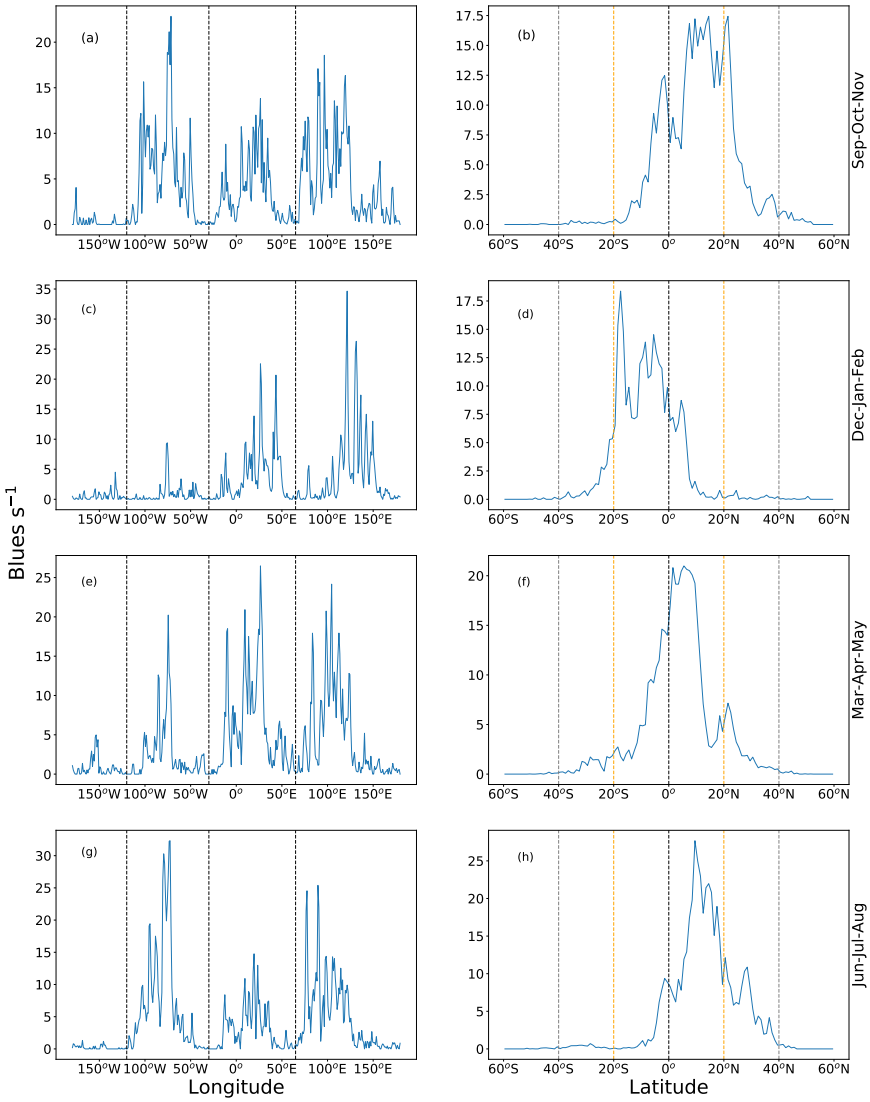

Figure 8.18. Seasonal meridional (left) and zonal (right) distributions associated to the two-year (1 April 2019 through 31 March 2021) seasonal GD-2 nighttime climatology of BLUEs (see Figure 8.4 of main paper).

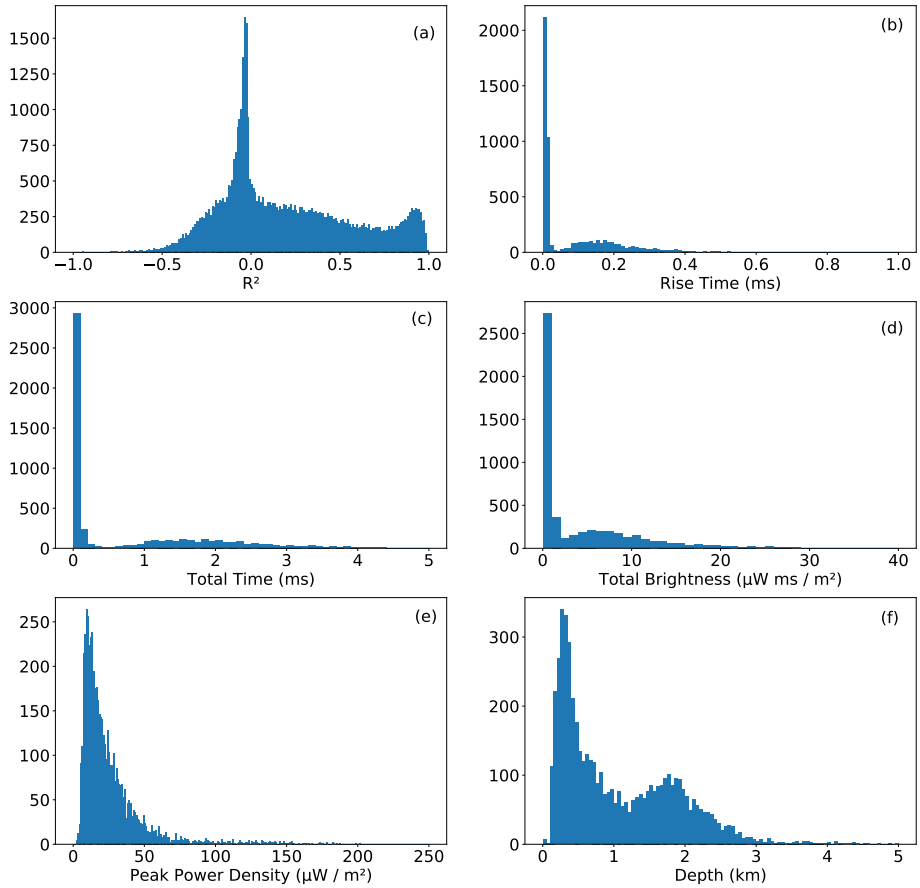

Figure 8.19. Histograms for BLUEs in GD-1 (see Figure 8.1 of main paper) recorded by ASIM-MMIA within 1 April 2019 to 31 March 2021. Events in panels (b) through (f) are fitted with the first hitting time (FHM) model (Soler et al., 2020; Luque et al., 2020) assuming point-like light sources. The different histograms show the number of BLUEs for different (a) R^2 (bin or step = 0.01), (b) Rise Time (ms) (bin = 0.01), (c) Total Time (ms) (bin = 0.1), (d) Total Brightness (μW ms m^{-2}) (bin = 1), (e) Peak Power Density (μW m^{-2}) (bin = 1), and (f) Depth (km) (bin = 0.05) below cloud tops. Note that impulsive singe pulse BLUEs are only those for which $R^2 > 0.75$ (panels (b) through (f)). Please note that the word bin is used with the meaning of step.

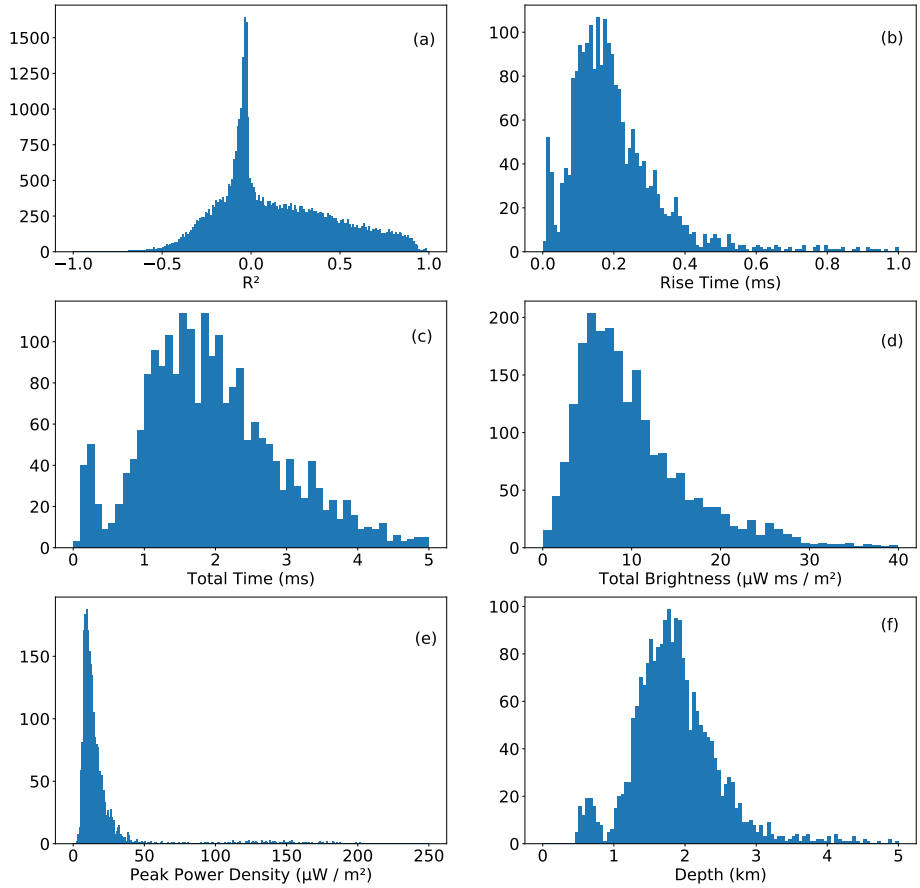

Figure 8.20. Histograms for BLUEs in GD-2 (see Figure 8.2 of main paper) recorded by ASIM-MMIA within 1 April 2019 to 31 March 2021. Events in panels (b) through (f) are fitted with the first hitting time (FHM) model (Soler et al., 2020; Luque et al., 2020) assuming point-like light sources. The different histograms show the number of BLUEs for different (a) R^2 (bin = 0.01), (b) Rise Time (ms) (bin = 0.01), (c) Total Times (ms) (bin = 0.1), (d) Total Brightness (μW ms m^{-2}) (bin = 1), (e) Peak Power Density (μW m^{-2}) (bin = 1), and (f) Depth (km) (bin = 0.05) below cloud tops. Note that impulsive singe pulse BLUEs are only those for which $R^2 > 0.75$ (panels (b) through (f)). Please note that the word bin is used with the meaning of step.

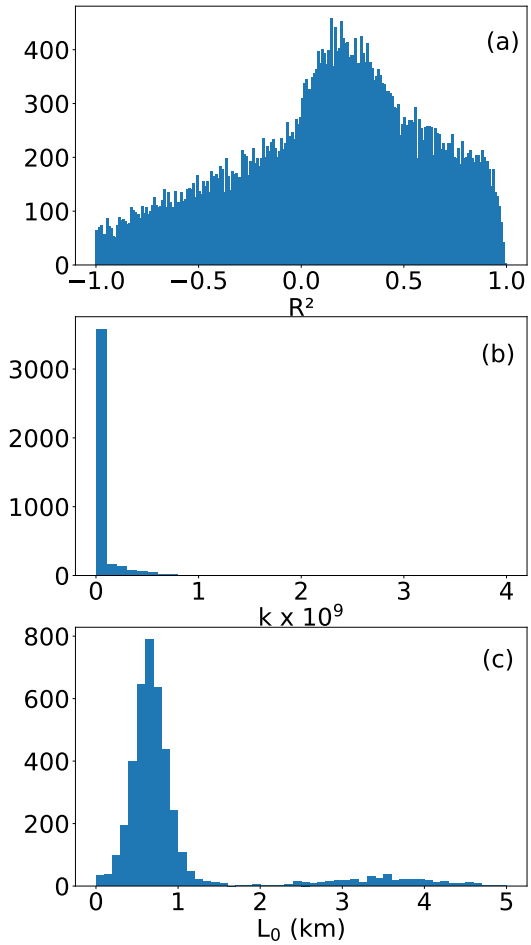

Figure 8.21. Histograms for BLUEs in GD-1 (see Figure 8.1 of main paper) recorded by ASIM-MMIA within 1 April 2019 to 31 March 2021. Events in panels (b) and (c) are fitted according to Li et al. (2021) assuming they are extended light sources that span altitudes from the cloud top to a maximum distance L_0 inside the cloud. The fit is over the time after the peak to obtain the best-fit cutoff (characteristic photon diffusion) time $\tau_D = L_0^2/4\mathrm{D}$, and the total number of source photons (N) (Li et al., 2021). The different histograms show the number of BLUEs for different (a) R^2 (bin = 0.01), (b) Number of streamers ($k\times10^9$) (bin = 0.03) for events with $R^2 > 0.75$, and (c) Vertical length (L_0) (bin = 0.1) for events with $R^2 > 0.75$. Please note that the word bin is used with the meaning of step.

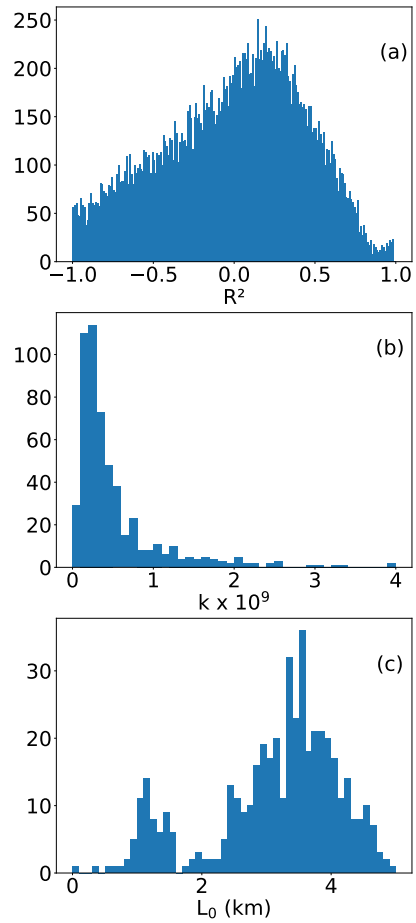

Figure 8.22. Histograms for BLUEs in GD-2 (see Figure 8.2 of main paper) recorded by ASIM-MMIA within 1 April 2019 to 31 March 2021. Events in panels (b) and (c) are fitted according to Li et al. (2021) assuming they are extended light sources that span altitudes from the cloud top to a maximum distance L_0 inside the cloud. The fit is over the time after the peak to obtain the best-fit cutoff (characteristic photon diffusion) time $\tau_D = L_0^2/4\mathrm{D}$, and the total number of source photons (N) (Li et al., 2021). The different histograms show the number of BLUEs for different (a) R^2 (bin = 0.01), (b) Number of streamers ($k\times10^9$) (bin = 0.03) for events with $R^2 > 0.75$, and (c) Vertical length (L_0) (bin = 0.1) for events with $R^2 > 0.75$. Please note that the word bin is used with the meaning of step.

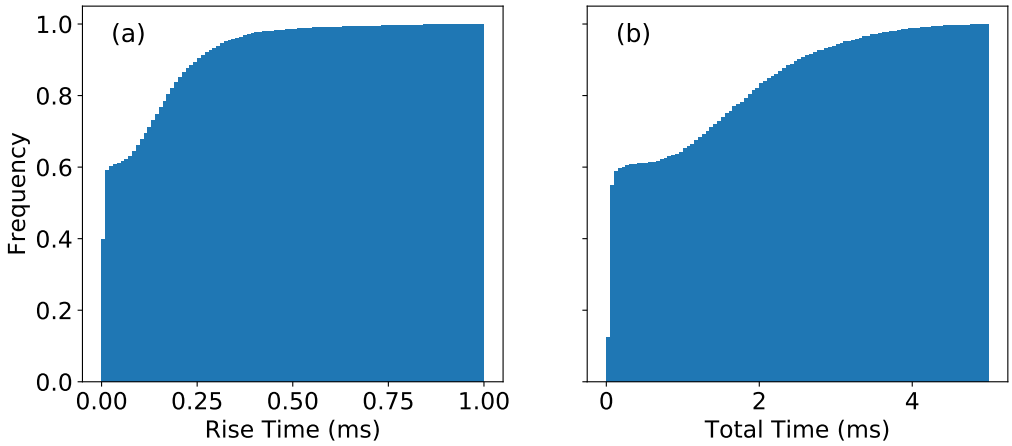

Figure 8.23. Frequency histograms showing the cumulative frequency of impulsive single pulse BLUEs (with $R^2 > 0.75$) in GD-1 (see Figure 8.1 of main paper) with different (a) Rise Times (ms) (bin = 0.01 ms) and (b) Total times (ms) (bin = 0.05 ms). These histograms indicate that, for instance, 60 % of impulsive single pulse BLUEs among all BLUEs in GD-1 have rise times and durations $\leq$ 30 μs and $\leq$ 300 μs, respectively. Note that GD-1 (in Figure 1 of main paper) represents the geographical distribution of BLUEs with all sort of temporal shapes, not only impulsive single pulse ones. Please note that the word bin is used with the meaning of step.

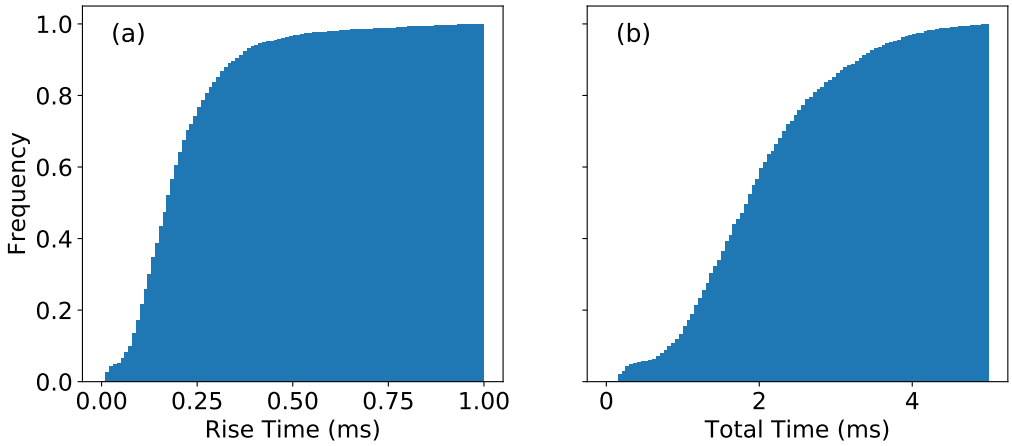

Figure 8.24. Frequency histograms showing the cumulative frequency of impulsive single pulse BLUEs (with $R^2 > 0.75$) in GD-2 (see Figure 8.2 of main paper) with different (a) Rise Times (ms) (bin = 0.01 ms) and (b) Total times (ms) (bin = 0.05 ms). These histograms indicate that, for instance, 10 % of impulsive single pulse BLUEs among all BLUEs in GD-2 have rise times and durations $\leq$ 80 μs and $\leq$ 900 μs, respectively. Note that GD-2 (in Figure 8.2 of main paper) represents the geographical distribution of BLUEs with all sort of temporal shapes, not only impulsive single pulse ones. Please note that the word bin is used with the meaning of step.

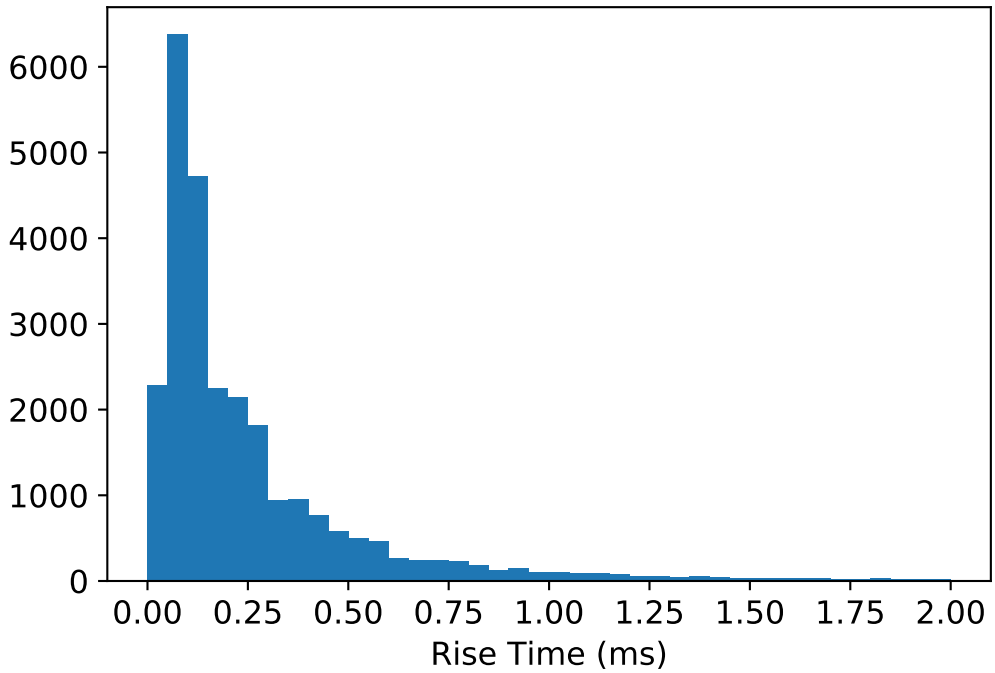

Figure 8.25. Histogram showing the number of BLUEs with all sort of temporal shapes (not only impulsive single pulse ones) geographically distributed according to GD-2 (see Figure 8.2 of main paper) with different rise times (ms) (bin = 0.05 ms). Please note that the word bin is used with the meaning of step.

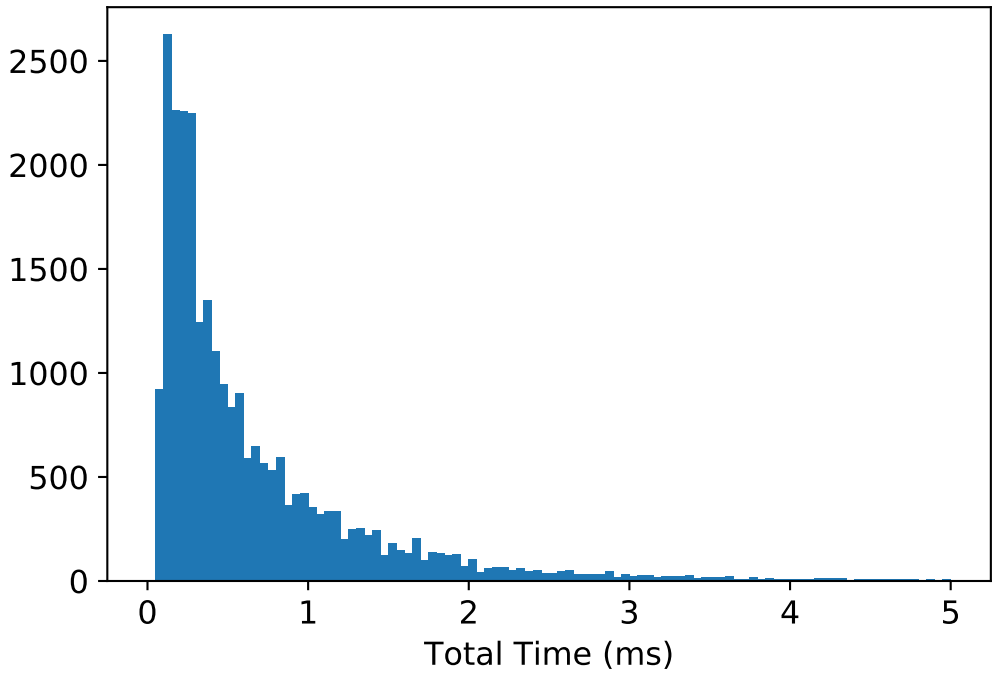

Figure 8.26. Histogram showing the number of BLUEs with all sort of temporal shapes (not only impulsive single pulse ones) geographically distributed according to GD-2 (see Figure 8.2 of main paper) with different total times (ms) (bin = 0.05 ms). Please note that the word bin is used with the meaning of step.

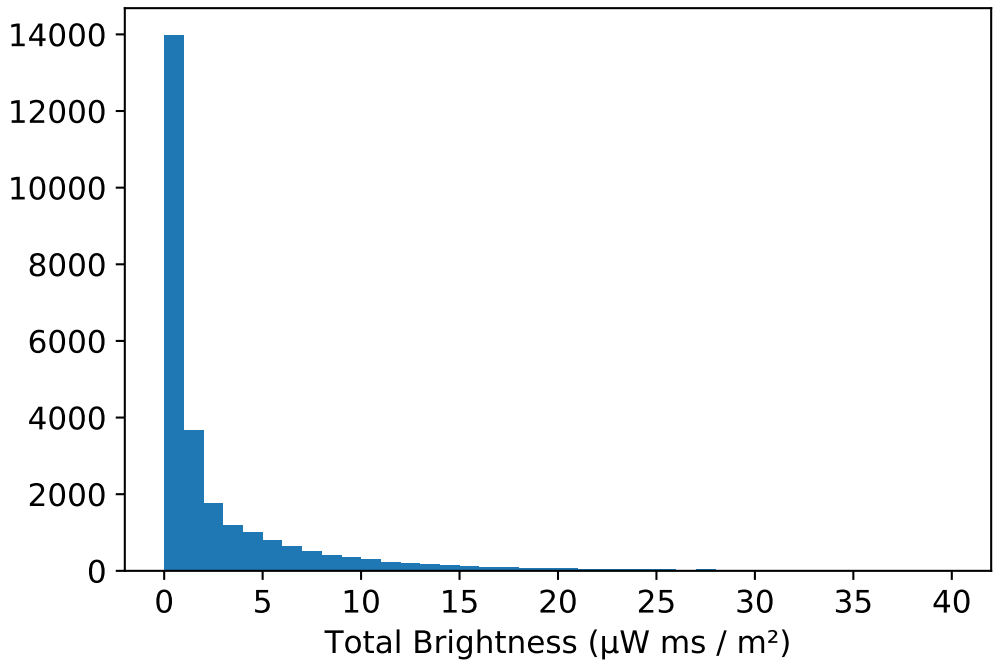

Figure 8.27. Histogram showing the number of BLUEs with all sort of temporal shapes (not only single pulse ones) geographically distributed according to GD-2 (see Figure 8.2 of main paper) with different total brightness (μW ms m^{-2}) (bin = 1 μW ms m^{-2}). Please note that the word bin is used with the meaning of step.

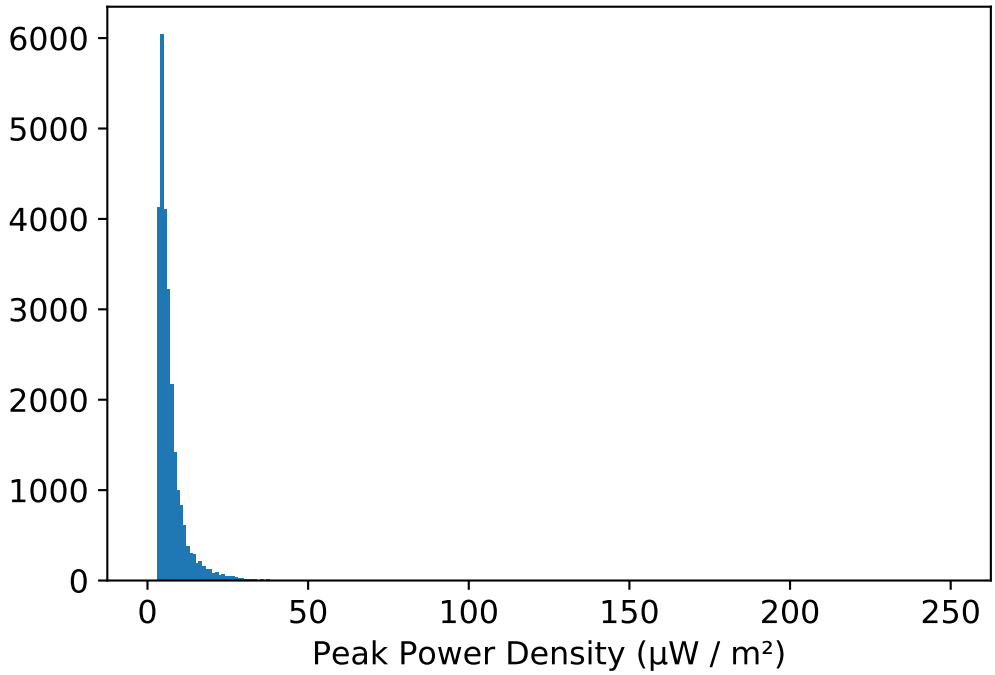

Figure 8.28. Histogram showing the number of BLUEs with all sort of temporal shapes (not only single pulse ones) geographically distributed according to GD-2 (see Figure 8.2 of main paper) with different peak power density (μW m^{-2}) (bin = 1 μW m^{-2}) and a threshold of 3 μW m^{-2}. Please note that the word bin is used with the meaning of step.

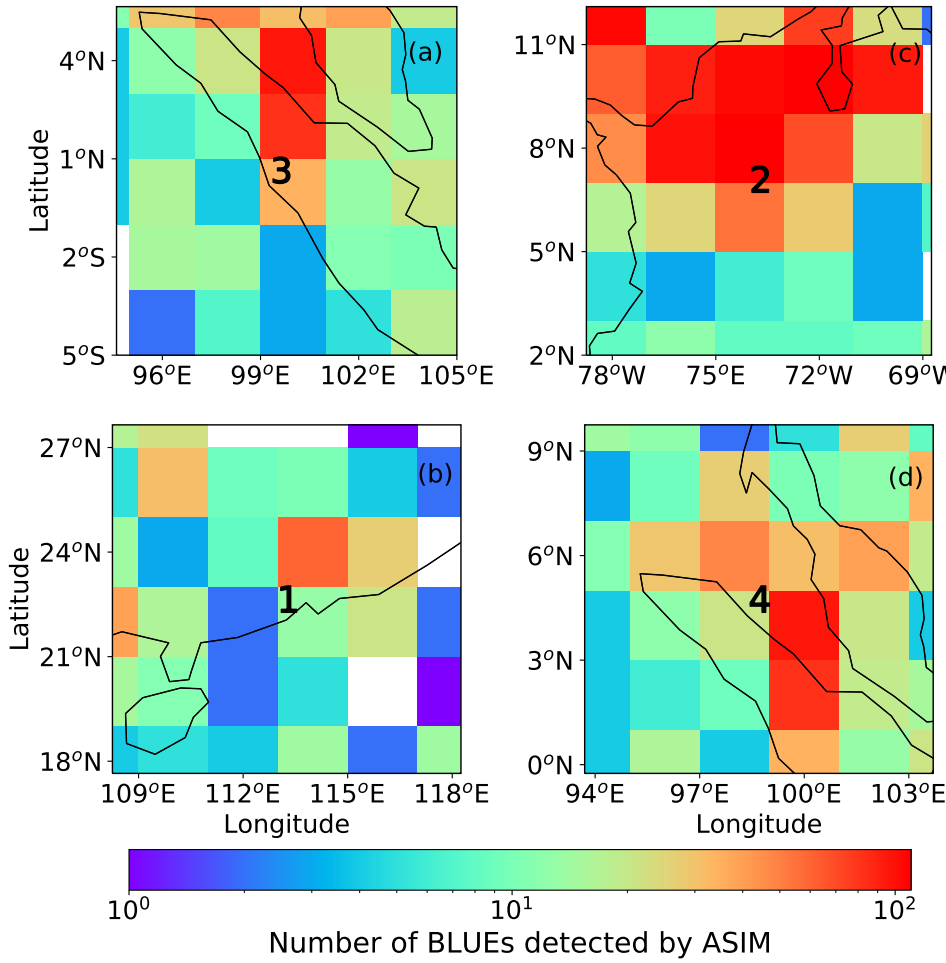

Figure 8.29. Local maps (from GD-2) with numbers on them indicating the centroid of the set of BLUEs investigated in: (1) Li et al. (2021) and Liu et al. (2021a) over Southern China, (2) López et al. (2022) over Colombia, (3) Soler et al. (2020) over Indonesia and (4) Li et al. (2022) over nearby Malaysia.

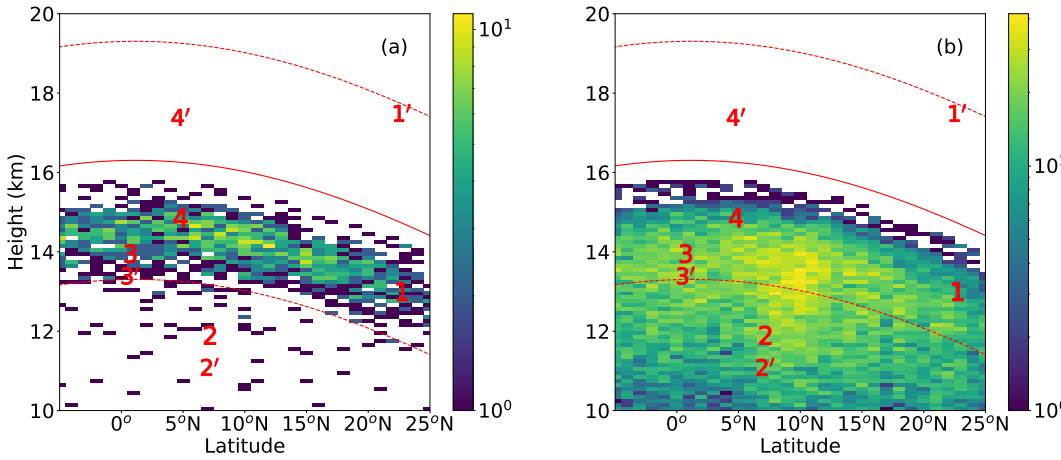

Figure 8.30. Approximate altitude distributions of GD-2 (see Figure 8.8 of main text) impulsive single BLUEs (with $R^2 > 0.75$ (a), and all sort of first hitting time (FHT) fitable BLUEs with any value of R^2 (b). The numbers in panels (a) and (b) are associated with the case-based papers mentioned in the caption of Figure 8.29 and they are placed in the mean altitude (obtained by optical means as explained in Soler et al. (2020)) of the reported events (BLUEs) in each case-based paper. Each number is placed in the centroid (in terms of latitude and longitude) of the set of BLUEs investigated in each of the above mentioned case-based papers. The numbers with prime indicate mean height obtained by radio (VLF / LF) for the same set of BLUE events of each case-based paper. The red dashes lines (above and below the solid red line) indicate the ± 3 km uncertainty associated with our approximation to globally compute the tropopause in each latitude. It can be seen that strong thunderstorms with overshooting tops penetrating into the lower stratosphere (cases 1 and 4) can create some discrepancies between the heights obtained by optical (applied globally in our analysis) and radio but, in any case, within the uncertainty of the method chosen to represent the tropopause at a global scale.

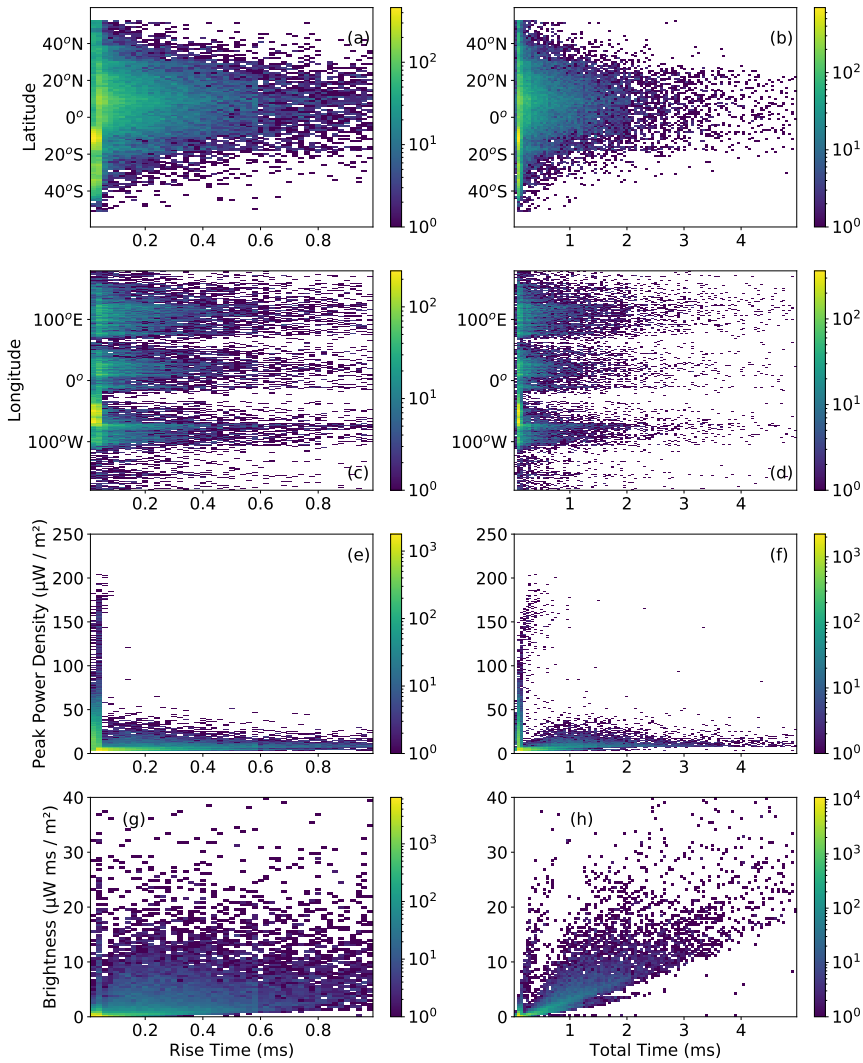

Figure 8.31. Zonal (a, b) and meridional (c, d) distributions of rise times and total times (duration) of BLUE with all sort of shapes (single pulse (impulsive or not), multiple pulse, irregular pulse) distributed according to GD-1. Variation of the peak power density and total brightness as a function of the BLUE rise times (e, g) and total time (duration) (f, h). The colorbar indicates number of events.

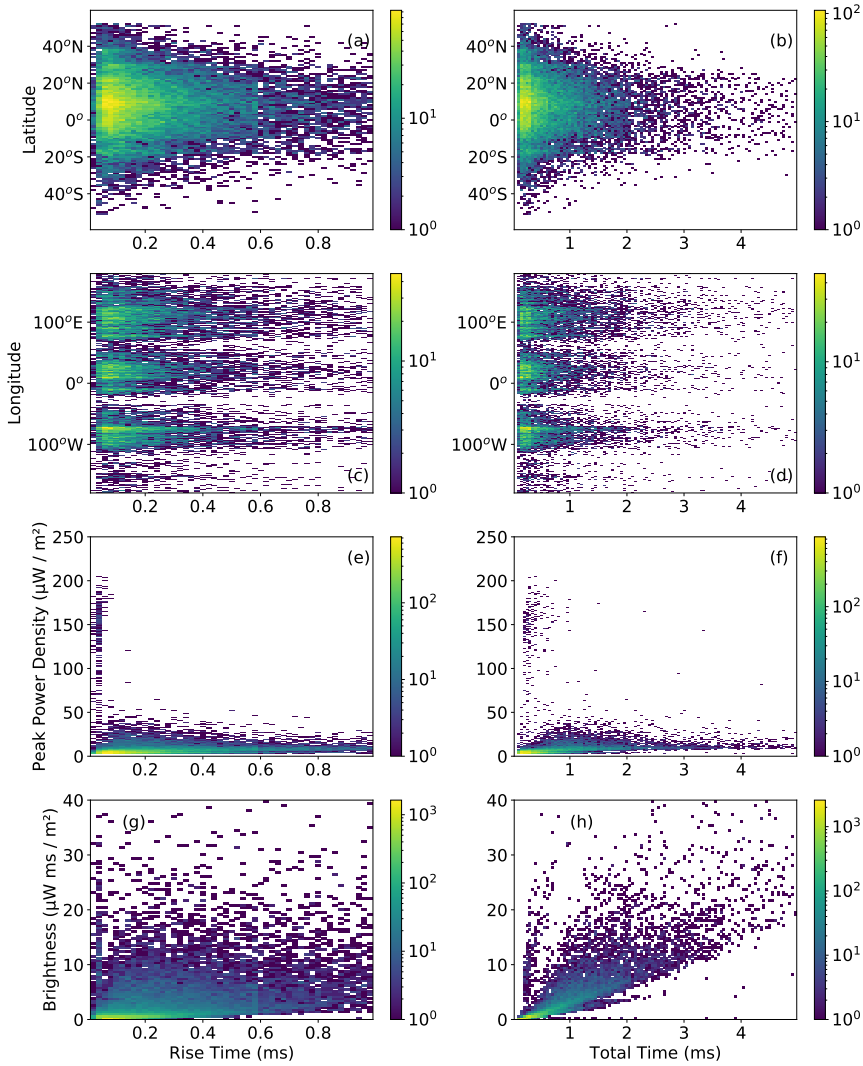

Figure 8.32. Zonal (a, b) and meridional (c, d) distributions of rise times and total times (duration) of BLUE with all sort of shapes (single pulse (impulsive or not), multiple pulse, irregular pulse) distributed according to GD-2. Variation of the peak power density and total brightness as a function of the BLUE rise times (e, g) and total time (duration) (f, h). The colorbar indicates number of events.

Bibliography

Adachi, T. et al. (2008). "Electric fields and electron energies in sprites and temporal evolutions of lightning charge moment". In: *Journal of Physics D: Applied Physics* 41.23, p. 234010. DOI: 10.1088/0022-3727/41/23/234010.

Babich, L. P. (2005). " Analysis of a new electron-runaway mechanism and record-high runaway-electron currents achieved in dense-gas discharges". In: *Physics Uspekhi* 48, p. 1015. DOI: 10.1070/PU2005v048n10ABEH002805.

Babich, L. P. et al. (2013). "Analysis of the experiment on registration of X-rays from the stepped leader of a cloud-to-ground lightning discharge". In: *Journal of Geophysical Research: Space Physics* 118, p. 2573. DOI: 10.1002/jgra.50236.

Bacholle, S et al. (2021). "Mini-EUSO mission to study Earth UV emissions on board the ISS". In: *The Astrophysical Journal Supplement Series* 253.2, p. 36. DOI: 10.3847/1538-4365/abd93d.

Bandara, S. et al. (2019). "Characterizing three types of negative narrow bipolar events in thunderstorms". In: *Atmospheric Research*. DOI: 10.1016/j.atmosres.2019.05.013.

Bandara, S. et al. (2021). "Groups of narrow bipolar events within thunderstorms". In: *Atmospheric Research* 252, p. 105450. DOI: 10.1016/j.atmosres.2021.105450.

Blaes, P. R., R. A. Marshall, and U. S. Inan (2016). "Global occurrence rate of elves and ionospheric heating due to cloud-to-ground lightning". In: *Journal of Geophysical Research: Space Physics* 121, p. 699. DOI: 10.1002/2015JA021916.

Blakeslee, R. J. (2019). "Non-Quality Controlled Lightning Imaging Sensor (LIS) on International Space Station (ISS) Science Data". In: *NASA Global Hydrology Resource Center DAAC: Huntsville, AL, USA*. URL: https://doi.org/10.5067/LIS/.

Blakeslee, R. J. et al. (2020). "Three years of the Lightning Imaging Sensor onboard the International Space Station: Expanded global coverage and enhanced applications". In: *Journal of Geophysical Research: Atmospheres* 125.16, e2020JD032918. DOI: 10.1029/2020JD032918.

Bozem, H. et al. (2014). "Influence of corona discharge on the ozone budget in the tropical free troposphere: a case study of deep convection during GABRIEL". In: *Atmospheric Chemistry and Physics* 14.17, pp. 8917–8931. DOI: 10.5194/acp-14-8917-2014.

Brandvold, D. K., P. Martinez, and R. Hipsh (1996). "Field measurements of O_3 and N_2O produced from corona discharge". In: *Atmospheric Environment* 30.6, pp. 973–976. DOI: 10.1016/1352-2310(95)00234-0.

Brune, W. H. et al. (2021). "Extreme oxidant amounts produced by lightning in storm clouds". In: *Science* 372, pp. 711–715. DOI: 10.1126/science.abg0492.

Cecil, D. J., D. E. Buechler, and R. J. Blakeslee (2014). "Gridded lightning climatology from TRMM-LIS and OTD: Dataset description". In: *Atmospheric Research* 135, pp. 404–414. DOI: 10.1016/j.atmosres.2012.06.028.

Celestin, S. and V. P. Pasko (2011). "Energy and fluxes of thermal runaway electrons produced by exponential growth of streamers during the stepping of lightning leaders and in transient luminous events". In: *Journal of Geophysical Research: Space Physics* 116, A03315, A03315. DOI: 10.1029/2010JA016260.

Černák, M. and T. Hosokawa (1991). "Complex form of current pulses in negative corona discharges". In: *Physical Review A* 43.2, p. 1107. DOI: 10.1103/PhysRevA.43.1107.

Cernak, M., T. Hosokawa, and I. Odrobina (1993). "Experimental confirmation of positive-streamer-like mechanism for negative corona current pulse rise". In: *Journal of Physics D: Applied Physics* 26.4, p. 607. DOI: 10.1088/0022-3727/26/4/013.

Černák, M and J. Skalnỳ (1984). "Influence of ozone ingredient in air on negative corona characteristics—contribution to the study of mechanism for trichel pulses". In: *Czechoslovak Journal of Physics B* 34.9, pp. 926–931. DOI: doi.org/10.1007/BF01589822.

Černák, M. et al. (1998). "Streamer mechanism for negative corona current pulses". In: *Journal of applied physics* 83.11, pp. 5678–5690. DOI: 10.1063/1.367422.

Chanrion, O. et al. (2016). "Profuse activity of blue electrical discharges at the tops of thunderstorms". In: *Geophysical Research Letters* 44.1, pp. 496–503. DOI: doi.org/10.1002/2016GL071311.

Chanrion, O. et al. (2019). "The Modular Multispectral Imaging Array (MMIA) of the ASIM payload on the International Space Station". In: *Space Science Reviews* 215.4, p. 28. DOI: 10.1007/s11214-019-0593-y.

Chou, J. K. et al. (2011). "Optical emissions and behaviors of the blue starters, blue jets, and gigantic jets observed in the Taiwan transient luminous event ground campaign". In: *Journal of Geophysical Research: Space Physics* 116.A7. DOI: 0.1029/2010JA016162.

Chou, J. K. et al. (2018). "ISUAL-Observed Blue Luminous Events: The Associated Sferics". In: *Journal of Geophysical Research: Space Physics* 123.4, pp. 3063–3077. DOI: doi.org/10.1002/2017JA024793.

Christian, H. J., R. J. Blakeslee, and S. J. Goodman (1989). "The detection of lightning from geostationary orbit". In: *Journal of Geophysical Research: Atmospheres* 94.D11, pp. 13329–13337. DOI: doi.org/10.1029/JD094iD11p13329.

Christian, H. J. et al. (2003). "Global frequency and distribution of lightning as observed from space by the Optical Transient Detector". In: *Journal of Geophysical Research: Atmospheres* 108.D1, ACL–4. DOI: doi.org/10.1029/2002JD002347.

Cooray, V. (2003). "Mechanism of Electrical Discharges". In: *The Lightning Flash*. Ed. by V. Cooray. IEE Power Series. Institution of Engineering and Technology. ISBN: 9780852967805.

Cooray, V. et al. (2020). "Modeling compact intracloud discharge (CID) as a streamer burst". In: *Atmosphere* 11.5, p. 549. DOI: doi.org/10.3390/atmos11050549.

Donohoe, K. G., F. H. Shair, and O. R. Wulf (1977). "Production of O_3, NO, and N_2O in a pulsed discharge at 1 atm". In: *Industrial & Engineering Chemistry Fundamentals* 16.2, pp. 208–215. DOI: doi.org/10.1021/i160062a006.

Dowdy, A. J. and A. Pepler (2018). "Pyroconvection risk in Australia: Climatological changes in atmospheric stability and surface fire weather conditions". In: *Geophysical Research Letters* 45.4, pp. 2005–2013. DOI: doi.org/10.1002/2017GL076654.

Dwyer, J. R. (2003). "A fundamental limit on electric fields in air". In: *Geophysical Research Letters* 30, 2055, p. 2055. DOI: 10.1029/2003GL017781.

— (2007). "Relativistic breakdown in planetary atmospheres". In: *Physics of Plasmas* 14.4, p. 042901. DOI: 10.1063/1.2709652.

— (2012). "The relativistic feedback discharge model of terrestrial gamma ray flashes". In: *Journal of Geophysical Research: Space Physics* 117, A02308, A02308. DOI: 10.1029/2011JA017160.

Dwyer, J. R. and M. A. Uman (2014). "The physics of lightning". In: *Physics Reports* 534, p. 147. DOI: 10.1016/j.physrep.2013.09.004.

Dwyer, J. R. et al. (2005). "X-ray bursts associated with leader steps in cloud-to-ground lightning". In: *Geophys. Res. Lett.* 32, L01803, p. L01803. DOI: 10.1029/2004GL021782.

Ebert, U. et al. (2010). "Review of recent results on streamer discharges and discussion of their relevance for sprites and lightning". In: *Journal of Geophysical Research: Space Physics* 115, A00E43. DOI: 10.1029/2009JA014867. arXiv: 1002.0070.

Edens, H. E. (2011). "Photographic and lightning mapping observations of a blue starter over a New Mexico thunderstorm". In: *Geophysical Research Letters* 38.17. DOI: doi.org/10.1029/2011GL048543.

Finney, D. L. et al. (2016). "The impact of lightning on tropospheric ozone chemistry using a new global lightning parametrisation". In: *Atmospheric Chemistry and Physics* 16.12, pp. 7507–7522. DOI: doi.org/10.5194/acp-16-7507-2016.

Fromm, M. et al. (2010). "The untold story of pyrocumulonimbus". In: *Bulletin of the American Meteorological Society* 91.9, pp. 1193–1210. DOI: doi.org/10.1175/2010BAMS3004.1.

Gallimberti, I., J. K. Hepworth, and R. C. Klewe (1974). "Spectroscopic investigation of impulse corona discharges". In: *Journal of Physics D: Applied Physics* 7, p. 880. DOI: 10.1088/0022-3727/7/6/315.

Giao, T.N. and J.B. Jordan (1970). "Trichel streamers and their transition into the pulseless glow discharge". In: *Journal of Applied Physics* 41.10, pp. 3991–3999. DOI: doi.org/10.1063/1.1658400.

Goldman, M., A. Goldman, and R. S. Sigmond (1985). "The corona discharge, its properties and specific uses". In: *Pure and Applied Chemistry* 57.9, pp. 1353–1362. DOI: doi.org/10.1351/pac198557091353.

Gordillo-Vázquez, F. J. (2008). "Air plasma kinetics under the influence of sprites". In: *Journal of Physics D: Applied Physics* 41.23, p. 234016. DOI: 10.1088/0022-3727/41/23/234016.

Gordillo-Vázquez, F. J. and Z. Donkó (2009). "Electron energy distribution functions and transport coefficients relevant for air plasmas in the troposphere: impact of humidity and gas temperature". In: *Plasma Sources Science and Technology* 18.3, p. 034021. DOI: 10.1088/0963-0252/18/3/034021.

Gordillo-Vázquez, F. J., A. Luque, and M. Simek (2011). "Spectrum of sprite halos". In: *J. Geophys. Res. (Space Phys)* 116, A09319. DOI: 10.1029/2011JA016652.

— (2012a). "Near infrared and ultraviolet spectra of TLEs". In: *Journal of Geophysical Research: Space Physics* 117, A05329. DOI: doi.org/10.1029/2012JA017516.

— (2012b). "Near infrared and ultraviolet spectra of TLEs". In: *J. Geophys. Res. (Space Phys)* 117, A05329, A05329. DOI: 10.1029/2012JA017516.

Gordillo-Vázquez, F. J. and F. J. Pérez-Invernón (2021). "A review of the impact of transient luminous events on the atmospheric chemistry: Past, present, and future". In: *Atmospheric Research*, p. 105432. DOI: doi.org/10.1016/j.atmosres.2020.105432.

Gordillo-Vázquez, F. J. et al. (2018). "High spectral resolution spectroscopy of sprites: A natural probe of the mesosphere". In: *Journal of Geophysical Research: Atmospheres* 123.4, pp. 2336–2346. DOI: doi.org/10.1002/2017JD028126.

Gordillo-Vázquez, F. J. et al. (2019). "Comparison of six lightning parameterizations in CAM5 and the impact on global atmospheric chemistry". In: *Earth and Space Science* 6.12, pp. 2317–2346. DOI: doi.org/10.1029/2019EA000873.

Grum, F. and L. F. Costa (1976). "Spectral emission of corona discharges". In: *Applied Optics* 15.1, pp. 76–79. DOI: 10.1364/AO.15.000076.

Gurevich, A. V., G. M. Milikh, and R. Roussel-Dupre (1992). "Runaway electron mechanism of air breakdown and preconditioning during a thunderstorm". In: *Physical Letters. A* 165, p. 463. DOI: 10.1016/0375-9601(92)90348-P.

Gurevich, A. V. and K. P. Zybin (2001). " Runaway breakdown and electric discharges in thunderstorms". In: *Physics Uspekhi* 44, p. 1119. DOI: 10.1070/PU2001v044n11ABEH000939.

Halanda, J. et al. (2012). "Chemical aspects of streamer mechanism for negative corona discharges". In: *Chem. Listy* 106, s1447–s1449.

Hale, G.M. and M.R. Querry (1973). "Optical constants of water in the 200-nm to 200-μm wavelength region". In: *Applied Optics* 12.3, pp. 555–563.

Heumesser, M. et al. (2021). "Spectral observations of optical emissions associated with terrestrial gamma-ray flashes". In: *Geophysical research letters* 48.4, 2020GL090700. DOI: 10.1029/2020GL090700.

Hiraki, Y. (2010). "The phase transition theory of sprite halo". In: *Journal of Geophysical Research: Space Physics* 115, A00E20. DOI: 10.1029/2009JA014384.

Hoder, T et al. (2016). "Radially and temporally resolved electric field of positive streamers in air and modelling of the induced plasma chemistry". In: *Plasma Sources Science and Technology* 25.4, p. 045021. DOI: 10.1088/0963-0252/25/4/045021.

Hoder, T. et al. (2020). "Emerging and expanding streamer head in low-pressure air". In: *Plasma Sources Science and Technology* 29.3, 03LT01. DOI: 10.1088/1361-6595/ab7087.

Holden, D. N., C. P. Munson, and J. C. Devenport (1995). "Satellite observations of transionospheric pulse pairs". In: *Geophysical Research Letters* 22.8, pp. 889–892. DOI: doi.org/10.1029/95GL00432.

Hu, Y. and Y. Yang (2020). "Ozone Emission and Electric Characters of Wire-plate Corona Discharge". In: *2020 IEEE 1st China International Youth Conference on Electrical Engineering (CIYCEE)*. IEEE, pp. 1–6. DOI: 10.1109/CIYCEE49808.2020.9332609.

Huang, A., S. A. Cummer, and Y. Pu (2021). "Lightning Initiation from Fast Negative Breakdown is Led by Positive Polarity Dominated Streamers". In: *Geophysical Research Letters*, e2020GL091553. DOI: doi.org/10.1029/2020GL091553.

Husbjerg, L. S. et al. (2022). "Observations of Blue Corona Discharges in Thunderclouds". In: *Geophysical Research Letters*, e2022GL099064. DOI: 10.1029/2022GL099064.

Jacobson, A. R. and M. J. Heavner (2005). "Comparison of narrow bipolar events with ordinary lightning as proxies for severe convection". In: *Monthly Weather Review* 133, p. 1144. DOI: 10.1175/MWR2915.1.

Jacobson, A. R. and T. E. L. Light (2012). "Revisiting" Narrow Bipolar Event" intracloud lightning using the FORTE satellite". In: *Annales Geophysicae*. Vol. 30. 2. Copernicus GmbH, p. 389. DOI: doi.org/10.5194/angeo-30-389-2012.

Jacobson, A. R. et al. (2013). "Joint radio and optical observations of the most radio-powerful intracloud lightning discharges". In: *Annales Geophysicae*. Vol. 31. 3. Copernicus GmbH, pp. 563–580. DOI: doi.org/10.5194/angeo-31-563-2013.

Jenkins, J. M., W. H. Brune, and D. O. Miller (2021). "Electrical Discharges Produce Prodigious Amounts of Hydroxyl and Hydroperoxyl Radicals". In: *Journal of Geophysical Research: Atmospheres* 126.9, e2021JD034557.

Köhn, C. et al. (2020). "The emission of terrestrial gamma ray flashes from encountering streamer coronae associated to the breakdown of lightning leaders". In: *Geophysical Research Letters* 47.20, e2020GL089749.

Koshak, W. J. et al. (1994). "Diffusion model for lightning radiative transfer". In: *Journal of Geophysical Research: Atmospheres* 99.D7, pp. 14361–14371. DOI: doi:10.1029/94JD00022.

Krapivsky, P.L., S. Redner, and E. Ben-Naim (2010). *A Kinetic View of Statistical Physics*. Cambridge University Press. ISBN: 9781139493345.

Krehbiel, P. R. et al. (2008). "Upward electrical discharges from thunderstorms". In: *Nature Geoscience* 1, p. 233. DOI: 10.1038/ngeo162.

Kudu, K., I. H. Lågstad, and R. S. Sigmond (1998). "Positive point-to-plane corona discharge forms in O2-N2 mixtures". In: *Czechoslovak Journal of Physics* 48.10, pp. 1180–1192. DOI: doi.org/10.1023/A:1022858001493.

Kuo, C. L., H. T. Su, and R. R. Hsu (2015). "The blue luminous events observed by ISUAL payload on board FORMOSAT-2 satellite". In: *Journal of Geophysical Research: Space Physics* 120.11, pp. 9795–9804. DOI: doi.org/10.1002/2015JA021386.

Kuo, C.-L. et al. (2005). "Electric fields and electron energies inferred from the ISUAL recorded sprites". In: *Geophysical Research Letters* 32, p. L19103. DOI: 10.1029/2005GL023389.

Kutsyk, I. M., L. . Babich, and E. N. Donskoi (2011). "Self-sustained relativistic-runaway-electron avalanches in the transverse field of lightning leader as sources of terrestrial gamma-ray flashes". In: *JETP letters* 94.8, pp. 606–609. DOI: doi.org/10.1134/S0021364011200094.

Le Vine, D. M. (1980). "Sources of the strongest RF radiation from lightning". In: *Journal of Geophysical Research: Oceans* 85.C7, pp. 4091–4095. DOI: doi.org/10.1029/JC085iC07p04091.

Leal, A. F. R., Vladimir A Rakov, and Brigida RP Rocha (2019). "Compact intracloud discharges: New classification of field waveforms and identification by lightning locating systems". In: *Electric Power Systems Research* 173, pp. 251–262. DOI: doi.org/10.1016/j.epsr.2019.04.016.

Li, D. et al. (2019). "The Propagation Effect of NBEs by Using FDTD Model and Compare with Ground-based Measurements at Different Distances". In: *AGU Fall Meeting 2019*. AGU. DOI: doi.org/10.1029/2018JD030014.

Li, D. et al. (2020). "On the Accuracy of Ray-Theory Methods to Determine the Altitudes of Intracloud Electric Discharges and Ionospheric Reflections: Application to Narrow Bipolar Events". In: *Journal of Geophysical Research: Atmospheres* 125.9, e2019JD032099.

Li, D. et al. (2021). "Blue Flashes as Counterparts to Narrow Bipolar Events: the Optical Signal of Shallow In-Cloud Discharges". In: *Journal of Geophysical Research: Atmospheres*, e2021JD035013.

Li, D. et al. (2022). "Multi-pulse corona discharges in thunderclouds observed in optical and radio bands". In: *Geophysical Research Letters*, e2022GL098938.

Light, T. E. et al. (2001). "Simulations of lightning optical waveforms as seen through clouds by satellites". In: *Journal of Geophysical Research: Atmospheres* 106, p. 17. DOI: 10.1029/2001JD900051.

Light, T. E. L. and A. R. Jacobson (2002). "Characteristics of impulsive VHF lightning signals observed by the FORTE satellite". In: *Journal of Geophysical Research: Atmospheres* 107.D24. DOI: doi.org/10.1029/2001JD001585.

Lin, J. W. B. (2012). "Why Python is the next wave in earth sciences computing". In: *Bulletin of the American Meteorological Society* 93.12, pp. 1823–1824. DOI: doi.org/10.1175/BAMS-D-12-00148.1.

Liu F.and Zhu, B. et al. (2021). "Meteorological and electrical conditions of two midlatitude thunderstorms producing blue discharges". In: *Journal of Geophysical Research: Atmospheres*, e2020JD033648.

Liu, C., E. J. Zipser, and S. W. Nesbitt (2007). "Global distribution of tropical deep convection: Different perspectives from TRMM infrared and radar data". In: *Journal of Climate* 20.3, pp. 489–503. DOI: 10.1175/JCLI4023.1.

Liu, F. et al. (2018). "Observations of blue discharges associated with negative narrow bipolar events in active deep convection". In: *Geophysical Research Letters* 45.6, pp. 2842–2851. DOI: doi.org/10.1002/2017GL076207.

Liu, F. et al. (2021a). "Optical emissions associated with narrow bipolar events from thunderstorm clouds penetrating into the stratosphere". In: *Nature communications* 12.1, pp. 1–8. DOI: doi.org/10.1038/s41467-021-26914-4.

Liu, N. et al. (2019). "Understanding the radio spectrum of thunderstorm narrow bipolar events". In: *Journal of Geophysical Research: Atmospheres* 124.17-18, pp. 10134–10153. DOI: doi.org/10.1029/2019JD030439.

Liu, Y. et al. (2021b). "Lightning Enhancement in Moist Convection with Smoke-laden Air Advected from Australian Wildfires". In: *Geophysical Research Letters* 48.11, e2020GL092355.

Loeb, L. B. (1965). *Electrical coronas*. Univ of California Press.

López, J. A. et al. (2022). "Initiation of lightning flashes simultaneously observed from space and the ground: Narrow bipolar events". In: *Atmospheric Research* 268, p. 105981. DOI: doi.org/10.1016/j.atmosres.2021.105981.

Luque, A. and U. Ebert (2009). "Emergence of sprite streamers from screening-ionization waves in the lower ionosphere". In: *Nature Geoscience* 2, p. 757. DOI: 10.1038/ngeo662.

— (2010). "Sprites in varying air density: Charge conservation, glowing negative trails and changing velocity". In: *Geophysical Research Letters* 37, p. L06806. DOI: 10.1029/2009GL041982.

Luque, A. and F. J. Gordillo-Vázquez (2011). "Modeling and analysis of $N_2(B^3\Pi_g)$ and $N_2(C^3\Pi_u)$ vibrational distributions in sprites". In: *J. Geophys. Res. (Space Phys)* 116, A02306. DOI: 10.1029/2010JA015952.

Luque, A. et al. (2016). "Sprite beads and glows arising from the attachment instability in streamer channels". In: *Journal of Geophysical Research: Space Physics* 121.3, pp. 2431–2449. DOI: doi.org/10.1002/2015JA022234.

Luque, A. et al. (2020). "Modeling lightning observations from space-based platforms (CloudScat. jl 1.0)". In: *Geoscientific Model Development* 13.11, pp. 5549–5566. DOI: doi.org/10.5194/gmd-13-5549-2020.

Lyons, W. A. et al. (2003). "Characteristics of Sprite-Producing Positive Cloud-to-Ground Lightning during the 19 July 2000 STEPS Mesoscale Convective Systems". In: *Monthly Weather Review* 131, p. 2417. DOI: 10.1175/1520-0493(2003)131<2417:COSPCL>2.0.CO;2.

Lyons, W. A. et al. (2003). "Upward Electrical Discharges From Thunderstorm Tops." In: *Bulletin of the American Meteorological Society* 84, p. 445. DOI: 10.1175/BAMS-84-4-445.

Lyu, F. et al. (2019). "Lightning initiation processes imaged with very high frequency broadband interferometry". In: *Journal of Geophysical Research: Atmospheres* 124.6, pp. 2994–3004. DOI: doi.org/10.1029/2018JD029817.

Malagón-Romero, A. and A. Luque (2019). "Spontaneous emergence of space stems ahead of negative leaders in lightning and long sparks". In: *Geophysical Research Letters* 46.7, pp. 4029–4038. DOI: 10.1029/2019GL082063.

Minschwaner, K et al. (2008). "Observation of enhanced ozone in an electrically active storm over Socorro, NM: Implications for ozone production from corona discharges". In: *Journal of Geophysical Research: Atmospheres* 113.D17. DOI: doi.org/10.1029/2007JD009500.

Miyamoto, H et al. (2021). "Simulations studies for the Mini-EUSO detector". In: *arXiv preprint arXiv:2112.12150*.

Montanyà, J. et al. (2016). "Global distribution of winter lightning: a threat to wind turbines and aircraft". In: *Natural Hazards and Earth System Sciences* 16.6, pp. 1465–1472. DOI: doi.org/10.5194/nhess-16-1465-2016.

Montanyà, J. et al. (2021). "A Simultaneous Observation of Lightning by ASIM, Colombia-Lightning Mapping Array, GLM, and ISS-LIS". In: *Journal of Geophysical Research: Atmospheres* 126.6, e2020JD033735.

Myhre, G., D. Shindell, and J. Pongratz (2014). "Anthropogenic and Natural Radiative Forcing". In: *Climate change 2013 : the physical science basis; Working Group 1 contribution to the fifth assessment report of the Intergovernmental Panel on Climate Change*. Ed. by Thomas Stocker. Cambridge: Cambridge University Press, pp. 659–740.

Neubert, T. et al. (2019). "The ASIM Mission on the International Space Station". In: *Space Science Reviews* 215.2, p. 26. DOI: doi.org/10.1007/s11214-019-0592-z.

Neubert, T. et al. (2021). "Observation of the onset of a blue jet into the stratosphere". In: *Nature* 589.7842, pp. 371–375. DOI: doi.org/10.1038/s41586-020-03122-6.

Offroy, M. et al. (2015). "Temporal and radiometric statistics on lightning flashes observed from space with the ISUAL spectrophotometer". In: *Journal of Geophysical Research: Atmospheres* 120.15, pp. 7586–7598. DOI: doi.org/10.1002/2015JD023263.

Parra-Rojas, F. C., A. Luque, and F. J. Gordillo-Vázquez (2013). "Chemical and electrical impact of lightning on the Earth mesosphere: The case of sprite halos". In: *Journal of Geophysical Research: Space Physics* 118, pp. 1–25. DOI: 10.1002/jgra.50449.

— (2015). "Chemical and thermal impact of sprite streamers in the Earth mesosphere". In: *Journal of Geophysical Research: Space Physics*. DOI: 10.1002/2014JA020933.

Parra-Rojas, F. C. et al. (2013). "Spectroscopic diagnosis of laboratory air plasmas as a benchmark for spectral diagnosis of TLEs". In: *Journal of Geophysical Research: Space Physics* 118, pp. 4649–4661. DOI: 10.1002/jgra.50433.

Pasko, V. P., U. S. Inan, and T. F. Bell (1998). "Spatial structure of sprites". In: *Geophys. Res. Lett.* 25, p. 2123. DOI: 10.1029/98GL01242.

Passas, M. et al. (2014). "Transient Upper Atmospheric Plasmas: Sprites and Halos". In: *IEEE Trans. Plasma Sci.* 42, pp. 2664–2665. DOI: 10.1109/TPS.2014.2329320.

Pérez-Invernón, F. J., F. J. Gordillo-Vázquez, and A. Luque (2016). "On the electrostatic field created at ground level by a halo". In: *Geophysical Research Letters* 43.13, pp. 7215–7222. DOI: doi.org/10.1002/2016GL069590.

Pérez-Invernón, F. J., A. Luque, and F. J. Gordillo-Vázquez (2018). "Modeling the chemical impact and the optical emissions produced by lightning-induced electromagnetic fields in the upper atmosphere: the case of halos and elves triggered by different lightning discharges". In: *Journal of Geophysical Research: Atmospheres* 123.14, pp. 7615–7641. DOI: doi.org/10.1029/2017JD028235.

Pérez-Invernón, F. J. et al. (2019). "Global occurrence and chemical impact of stratospheric Blue Jets modeled with WACCM4". In: *J. Geophys. Res - Atmos.* DOI: https://doi.org/10.1029/2018JD029593.

Pérez-Invernón, F. J. et al. (2020). "The contribution of sprite streamers to the chemical composition of the mesosphere-lower thermosphere". In: *Geophysical Research Letters* 47.14, e2020GL088578.

Rison, W. et al. (2016). "Observations of narrow bipolar events reveal how lightning is initiated in thunderstorms". In: *Nature Communications* 7, p. 10721. DOI: doi.org/10.1029/92JD00719.

Robusto, C.C. (1957). "The cosine-haversine formula". In: *The American Mathematical Monthly* 64.1, pp. 38–40. DOI: 10.2307/2309088.

Said, R. K., M. B. Cohen, and U. S. Inan (2013). "Highly intense lightning over the oceans: Estimated peak currents from global GLD360 observations". In: *Journal of Geophysical Research: Atmospheres* 118, p. 6905. DOI: 10.1002/jgrd.50508.

Schumann, U. and H. Huntrieser (2007). "The global lightning-induced nitrogen oxides source". In: *Atmospheric Chemistry and Physics* 7.14, pp. 3823–3907. DOI: 10.5194/acp-7-3823-2007. URL: https://www.atmos-chem-phys.net/7/3823/2007/.

Schwartz, M. J. et al. (2020). "Australian New Year's PyroCb Impact on Stratospheric Composition". In: *Geophysical Research Letters* 47.24, e2020GL090831.

Sentman, D. D. et al. (2008). "Plasma chemistry of sprite streamers". In: *J. Geophys. Res - Atmos.* 113, p. D11112. DOI: 10.1029/2007JD008941.

Shlanta, A and C.B Moore (1972). "Ozone and point discharge measurements under thunderclouds". In: *Journal of Geophysical Research* 77.24, pp. 4500–4510. DOI: doi.org/10.1029/JC077i024p04500.

Sigmond, R. S. (1997). "The oscillations of the positive glow corona". In: *Le Journal de Physique IV* 7.C4, pp. C4–383. DOI: 10.1051/JP4:1997431.

Simek, M. (2002). "The modelling of streamer-induced emission in atmospheric pressure, pulsed positive corona discharge: N_2 second positive and NO-γ systems". In: *J. Phys. D* 35, p. 1967. DOI: 10.1088/0022-3727/35/16/311.

Smith, D. A. et al. (1999). "A distinct class of isolated intracloud lightning discharges and their associated radio emissions". In: *Journal of Geophysical Research: Atmospheres* 104.D4, pp. 4189–4212. DOI: doi.org/10.1029/1998JD200045.

Smith, D. A. et al. (2004). "A method for determining intracloud lightning and ionospheric heights from VLF/LF electric field records". In: *Radio Science* 39.1. DOI: doi.org/10.1029/2002RS002790.

Soler, S et al. (2020). "Blue optical observations of narrow bipolar events by ASIM suggest corona streamer activity in thunderstorms". In: *Journal of Geophysical Research: Atmospheres* 125.16, e2020JD032708.

Soler, S. et al. (2021). "Global frequency and geographical distribution of nighttime streamer corona discharges (BLUEs) in thunderclouds". In: *Geophysical Research Letters* 48.18, e2021GL094657.

Stenbaek-Nielsen, H. C. et al. (2010). "Sprite initiation altitude measured by triangulation". In: *Journal of Geophysical Research: Space Physics* 115, A00E12. DOI: 10.1029/2009JA014543.

Suszcynsky, D. M. and M. J. Heavner (2003). "Narrow Bipolar Events as indicators of thunderstorm convective strength". In: *Geophysical Research Letters* 30.17. DOI: doi.org/10.1029/2003GL017834.

Takahashi, T. (1978). "Riming Electrification as a Charge Generation Mechanism in Thunderstorms". In: *Journal of the Atmospheric Sciences* 35, 1536–1548. DOI: doi.org/10.1175/1520-0469(1978)035<1536:REAACG>2.0.CO;2.

Tan, Z. et al. (2019). "Evaluation of cloud top height retrievals from China's next-generation geostationary meteorological satellite FY-4A". In: *Journal of Meteorological Research* 33.3, pp. 553–562. DOI: doi.org/10.1007/s13351-019-8123-0.

Thomason, L. W. and E. P. Krider (1982). "The Effects of Clouds on the Light Produced by Lightning." In: *Journal of Atmospheric Sciences* 39, p. 2051. DOI: 10.1175/1520-0469(1982)039<2051:TEOCOT>2.0.CO;2.

Tilles, J. N. et al. (2019). "Fast negative breakdown in thunderstorms". In: *Nature Communications* 10.1, p. 1648. DOI: doi.org/10.1038/s41467-019-09621-z.

Ukkonen, P. and A. Mäkelä (2019). "Evaluation of machine learning classifiers for predicting deep convection". In: *Journal of Advances in Modeling Earth Systems* 11.6, pp. 1784–1802. DOI: doi.org/10.1029/2018MS001561.

Van der Hulst, H.C. (1981). *Light Scattering by Small Particles*. Dover Books on Physics. Dover Publications. ISBN: 9780486642284.

Warren, S. G. and R. E. Brandt (2008). "Optical constants of ice from the ultraviolet to the microwave: A revised compilation". In: *Journal of Geophysical Research: Atmospheres* 113.D14. DOI: doi.org/10.1029/2007JD009744.

Wescott, E. M. et al. (1995). "Preliminary results from the Sprites94 aircraft campaign: 2. Blue jets". In: *Geophysical Research Letters* 22, p. 1209. DOI: 10.1029/95GL00582.

Wescott, E. M. et al. (1996). "Blue starters: Brief upward discharges from an intense Arkansas thunderstorm". In: *Geophysical Research Letters* 23, p. 2153. DOI: 10.1029/96GL01969.

Wescott, E. M. et al. (2001). "New evidence for the brightness and ionization of blue starters and blue jets". In: *Journal of Geophysical Research* 106, p. 21549. DOI: 10.1029/2000JA000429.

Wiens, K. C. et al. (2008). "Relationships among narrow bipolar events,"total" lightning, and radar-inferred convective strength in Great Plains thunderstorms". In: *Journal of Geophysical Research: Atmospheres* 113.D5. DOI: doi.org/10.1029/2007JD009400.

Williams, E. et al. (2012). "Resolution of the sprite polarity paradox: The role of halos". In: *Radio Science* 47.2. DOI: 10.1029/2011RS004794.

Williams, E. R. et al. (1992). "A radar and electrical study of tropical "hot towers"". In: *Journal of Atmospheric Sciences* 49.15, pp. 1386–1395. DOI: doi.org/10.1175/1520-0469(1992)049<1386:ARAESO>2.0.CO;2.

Wilson, C. T. R. (1925). "The electric field of a thundercloud and some of its effects". In: *Proc. Phys. Soc. London* 37, p. 32D. DOI: 10.1088/1478-7814/37/1/314.

Wu, T. et al. (2011). "Comparison of positive and negative compact intracloud discharges". In: *Journal of Geophysical Research: Atmospheres* 116.D3. DOI: doi.org/10.1029/2010JD015233.

Wu, T. et al. (2014). "Lightning-initiator type of narrow bipolar events and their subsequent pulse trains". In: *Journal of Geophysical Research: Atmospheres* 119.12, pp. 7425–7438. DOI: doi.org/10.1002/2014JD021842.

Yang, J. et al. (2017). "Introducing the new generation of Chinese geostationary weather satellites, Fengyun-4". In: *Bulletin of the American Meteorological Society* 98.8, pp. 1637–1658. DOI: doi.org/10.1175/BAMS-D-16-0065.1.

Zahn, A. et al. (2002). "Electrical discharge source for tropospheric "ozone-rich transients"". In: *Journal of Geophysical Research: Atmospheres* 107.D22, ACH–16. DOI: doi.org/10.1029/2002JD002345.

Zhang, P. et al. (2018). "General comparison of FY-4A/AGRI with other GEO/LEO instruments and its potential and challenges on non-meteorological applications". In: *Frontiers in Earth Science* 6, p. 224. DOI: doi.org/10.3389/feart.2018.00224.

Zhu, Y. et al. (2022). "Upgrades of the Earth Networks Total Lightning Network in 2021". In: *Remote Sensing* 14.9, p. 2209. DOI: 10.3390/rs14092209.

SERGIO SOLER

Researcher - Physics & Data Science

CONTACT

s.soler@tutanota.com

INTERESTS

- **Meteorology & Climate**
- **Data Science & Data Analytics**
- **Geosciences**
- **Model Simulations**

PROGRAMMING SKILLS

- **Python** — Main
- **R**
- **MatLab**
- **Java**
- **LATEX**

LANGUAGES

- **Spanish** — Native
- **English**
- **Valencian** — Native

EDUCATION

Ph. D. - Physics & Space Science — **2018 - Jan 2023**
IAA-CSIC, Universidad de Granada - Granada, (Spain)

Masters - Data Science — **2017 - 2018**
Universidad de Cantabria & Universidad Internacional Menéndez Pelayo - Santander, (Spain)

Bachelor - Physics — **2013 - 2017**
Universidad de Cantabria - Santander, (Spain)

WORK EXPERIENCE

PhD researcher — **2018 - 2022**
Instituto de Astrofísica de Andalucía (IAA), Granada (Spain)

Research on BLUE discharges (in-cloud coronas) with ASIM

Internship — **2017 - 2018**
Instituto de Física de Cantabria (IFCA), Santander (Spain)

Research support on measuring surface parameters in water reservoir using Google Earth Engine

Internship — **Jun 16 - Jul 16**
Instituto de Física de Cantabria (IFCA), Santander (Spain)

Predicting temperature trends using time series with R

FIRST AUTHOR PUBLICATIONS

Global Distribution of Key Features of Streamer Corona Discharges in Thunderclouds — **JGR Atmospheres**
S. Soler, F. J. Gordillo-Vázquez, F. J. Pérez-Invernón, A. Luque, D. Li, T. Neubert, O. Chanrion, V. Reglero, J. Navarro-González and N. Østgaard

JGR Atmospheres (doi: 10.1029/2022JD037535) Vol 127, Issue 24, 2022

Global Frequency and Geographical Distribution of Nighttime Streamer Corona Discharges (BLUEs) in Thunderclouds — **GRL**
S. Soler, F. J. Gordillo-Vázquez, F. J. Pérez-Invernón, A. Luque, D. Li, T. Neubert, O. Chanrion, V. Reglero, J. Navarro-González and N. Østgaard

Geophysical Research Letters (doi: 10.1029/2021GL094657) Vol 48, Issue 18, 2021

Blue Optical Observations of Narrow Bipolar Events by ASIM Suggest Corona Streamer Activity in Thunderstorms **JGR Atmospheres**

S.Soler, F. J. Pérez-Invernón, F. J. Gordillo-Vázquez, A. Luque, D. Li, A. Malagón-Romero, T. Neubert, O. Chanrion, V. Reglero, J. Navarro-González, G. Lu, H. Zhang, A. Huang, N. Østgaard

JGR Atmospheres (doi: 10.1029/2020jd032708) Vol 125, Issue 16, 2020 (Editor's Highlights)

OTHER PUBLICATIONS

Quantification of lightning-produced NOx over the Pyrenees and the Ebro Valley by using different TROPOMI-NO2 and cloud research products **AMT**

F. J. Pérez-Invernón, H. Huntrieser, T. Erbertseder, D. Loyola, P. Valks, S. Liu, D. J. Allen, K. E. Pickering, E. J. Bucsela, P. Jöckel, J. van Geffen, H. Eskes, **S. Soler**, F. J. Gordillo-Vázquez and J. Lapierre

Atmos. Meas. Tech., 15, 3329–3351 (2022) doi: 10.5194/amt-15-3329-2022

Lightning-ignited wildfires and long continuing current lightning in the Mediterranean Basin: preferential meteorological conditions **ACP**

F. J. Pérez-Invernón, H. Huntrieser, **S.Soler**, F. J. Gordillo-Vázquez, N. Pineda, J. Navarro-González, V. Reglero, J. Montanyà, O. van der Velde, and N. Koutsias

Atmos. Chem. Phys., 21, 17529–17557 (2021) doi: 10.5194/acp-21-17529-2021

Influence of the COVID-19 lockdown on lightning activity in the Po Valley **AR**

F. J. Pérez-Invernón, H. Huntrieser, F. Gordillo-Vázquez, **S. Soler**

Atmospheric Research, 263 (2021) doi: 10.1016/j.atmosres.2021.105808

Modeling lightning observations from space-based platforms (CloudScat.jl 1.0) **GMD**

A. Luque, F. J. Gordillo-Vázquez, D. Li, A. Malagón-Romero, F. J. Pérez-Invernón, A. Schmalzried, **S.Soler**, O. Chanrion, M. Heumesser, T. Neubert et al.

Geosci. Model Dev., 13, 5549–5566 (2020) doi: 10.5194/gmd-13-5549-2020

PROJECTS

PID2019-109269RB-C43 **2020-2023**

Title: Contribución del IAA a la explotación científica de ASIM: experimentos, observaciones desde el suelo, análisis de datos y modelización

Funding Agency: Ministerio de Ciencia e Innovación

ESP2017-86263-C4-4-R **2018-2020**

Title: Contribución del IAA a la explotación científica de ASIM: observaciones desde el suelo y análisis de datos

Funding Agency: Ministerio de Ciencia e Innovación

WORKSHOPS & CONFERENCES

SAINT SUMMER SCHOOL & WORKSHOPS, Toulouse, France — June 2019
Participation with an oral presentation

EGU19 General Assembly, Vienna, Austria — April 2019
Participation with a poster

SAINT WINTER SCHOOL & WORKSHOP, Leiden, Netherlands — February 2019
Participation with a poster

SAINT SUMMER SCHOOL & WORKSHOP, Barcelona, Spain — June 2018